POLITECNICO DI MILANO
Corso di Laurea Magistrale in Ingegneria delle Telecomunicazioni
Dipartimento di Elettronica Informazione e Bioingegneria

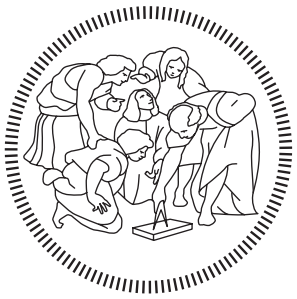

Exploitation of an innovative few-mode fiber for high-capacity advanced communication networks

Supervisor: Prof. Pierpaolo Boffi
Co-Supervisor: Dott. Ing. Alberto Gatto

Master thesis by:
Veronica Villa
ID Number 920322

Academic Year 2019-2020

Exploitation of an innovative few-mode fiber for high-capacity advanced communication networks

Veronica Villa

Academic Year 2019-2020

Abstract

The growing capacity demand for optical communication has motivated the development of fibers supporting the transmission of multiple propagating modes to enable Mode Division Multiplexing (MDM). Recently, a new fiber that supports 9 Linearly Polarized (LP) modes, corresponding to 15 spatial modes, with low Mode-Group Division Multiplexing (MGDM) has been proposed in the literature and now it is available on the market. This innovative Few-Mode Fiber (FMF) can be exploited to increase the optical system's potential both in the case of medium-long distance transmissions and in short-range applications, even if the intermodal crosstalk strongly limits the performance, both in terms of the maximum reachable distance and the achievable capacity. The main goal of this work is to propose possible solutions to design high-capacity communication networks based on the exploitation of this innovative FMF. In particular, considering mode groups, we focused on MGDM to propose sustainable solutions in terms of complexity, which exceed the strong limits imposed by intermodal crosstalk. The presented solutions use special mode multiplexers/demultiplexers based on Multi-Plane Light Conversion (MPLC), already available on the market. For medium-long transmission systems, characterized by the use of complex modulation formats supported by coherent detection and the presence of network nodes, an analytical simulator has been used to assess the impact of linear and nonlinear effects on performance in a MGDM network exploiting the considered FMF with 5 different mode groups. In particular, performance has been analyzed for different combinations of groups and modulation formats to achieve Tb/s capacity for each wavelength, even over hundreds of km, minimizing the effects of intermodal crosstalk introduced by fiber propagation and by the use of realistic mode multiplexers/demultiplexers. For short-range systems typical of intra and inter-datacenter connections, where low-cost and reduced complexity are required, the direct detection of simple modulation formats such as On-Off Keying (OOK) and 4-Pulse-Amplitude Modulation (PAM) has been considered. Thanks to appropriate simulations

in the MATLAB® environment, the limits and the potential of MGDM propagation have been systematically analyzed. In this context, the main penalties introduced by chromatic dispersion and intermodal crosstalk have been partially compensated by using a Decision Feedback Equalizer (DFE). Transmission capacity of 100 Gb/s can be reached over distances of $10-15$ km, taking advantage of an appropriate combination of mode groups. Finally, wavelength interleaving between groups of modes has been proposed to further reduce the cost of optical components used in this particular application field.

Sommario

La crescente richiesta di capacità nelle comunicazioni ottiche ha motivato lo sviluppo di fibre capaci di supportare la trasmissione di più modi di propagazione per abilitare la multiplazione a divisione di modo (MDM). Recentemente, una nuova fibra che supporta 9 modi Linearly Polarized (LP), corrispondenti a 15 modi spaziali, con basso Differential Mode Group Delay (DMGD) è stata proposta in letteratura e messa a disposizione sul mercato. Questa innovativa Few-Mode Fiber (FMF) può essere sfruttata per aumentare le potenzialità del sistema ottico sia nel caso di trasmissioni di media-lunga distanza e sia in applicazioni a corto raggio, anche se il crosstalk intermodale limita fortemente le prestazioni, sia a livello di massima distanza raggiunta che di capacità trasportata. Lo scopo principale di questo lavoro è quello di proporre possibili soluzioni implementative per progettare reti di comunicazione ad alta capacità, basate sull'utilizzo di questa innovativa FMF. In particolare, considerando gruppi di modi, ci si è concentrati sull'utilizzo della multiplazione a divisione di gruppo (MGDM) per proporre soluzioni sostenibili in termini di complessità, che superino i forti limiti imposti dal crosstalk intermodale. Le soluzioni presentate utilizzano particolari multiplatori/demultiplatori modali basati su Multi-Plane Light Conversion (MPLC), ormai disponibili sul mercato. Per le applicazioni in reti a media-lunga distanza, caratterizzate dall'utilizzo di formati di modulazione complessi supportati da rivelazione coerente e dall'attraversamento di nodi di rete, un simulatore analitico è stato impiegato per valutare l'impatto degli effetti lineari e non-lineari sulle prestazioni in una rete di tipo MGDM, che utilizzando la FMF considerata ha la possibilità di gestire 5 differenti gruppi di modi. In particolare, si sono analizzate le prestazioni per diverse combinazioni di gruppi e formati di modulazione, al fine di raggiungere capacità dell'ordine dei Tb/s per lunghezza d'onda, anche su centinaia di km, minimizzando gli effetti del crosstalk intermodale, sia introdotto dalla propagazione in fibra, sia dall'utilizzo di multiplatori/demultiplatori modali realistici. Per collegamenti a corto raggio tipici di connessioni intra e inter-datacenter, per cui il costo e

la ridotta complessità sono mandatori, si è considerata la rivelazione diretta di formati di modulazione semplici quali On-Off Keying (OOK) e 4-Pulse-Amplitude Modulation (PAM). Grazie a opportune simulazioni in ambiente MATLAB® sono stati analizzati sistematicamente i limiti e le potenzialità della propagazione MGDM nella fibra considerata. In questo contesto, le principali penalità introdotte dalla dispersione cromatica e dal crosstalk intermodale sono state parzialmente compensate dall'uso di un Decision Feedback Equalizer (DFE). Capacità di trasmissione pari a 100 Gb/s sono raggiungibili su distanze intorno a $10 - 15$ km, sfruttando un'opportuna combinazione di gruppi modali. Infine, si è proposto di utilizzare l'interleaving in lunghezza d'onda tra i gruppi di modi per ridurre ulteriormente i costi dei componenti ottici impiegati in questo particolare ambito applicativo.

Contents

List of Figures

List of Tables

Acronyms

ADC	Analogic-To-Digital Converter
ASE	Amplified Spontaneous Emission
AWG	Arrayed Waveguide Grating
AWGN	Additive White Gaussian Noise
B2B	Back-To-Back
BER	Bit Error Rate
DAC	Digital-To-Analog Converter
DEMUX	Demultiplexer
DFB	Distributed Feedback
DFE	Decision Feedback Equalizer
DMGD	Differential Mode Group Delay
DSP	Digital Signal Processing
EVM	Error Vector Magnitude
FEC	Forward Error Correction
FIR	Finite Impulse Response
FM	Few Mode
FMF	Few-Mode Fiber
FWM	Four-Wave Mixing
GD	Group Delay
GN	Gaussian Noise
ISI	Intersymbol Interference
LMS	Least Mean Square
LP	Linearly Polarized
LPG	Long-Period Grating

MAN	Metropolitan Area Network
MDM	Mode Division Multiplexing
MDMUX	Mode-Demultiplexer
MGDM	Mode-Group Division Multiplexing
MIMO	Multiple-Input Multiple-Output
MMF	Multi-Mode Fiber
MMUX	Mode-Multiplexer
MPLC	Multi-Plane Light Conversion
MUX	Multiplexer
NLI	Nonlinear Interference
NLT	Nonlinear Threshold
OOK	On-Off Keying
OSNR	Optical Signal-To-Noise Ratio
PAM	Pulse-Amplitude Modulation
PCVD	Plasma Chemical Vapor Decomposition
PD	Photodiode
PDM	Polarization Division Multiplexing
PSD	Power Spectral Density
QAM	Quadrature Amplitude Modulation
QPSK	Quadrature Phase Shift Keying
RMS	Root-Mean-Squared
SDM	Space Division Multiplexing
SLD	Super Luminescent Diode
SLM	Spatial Light Modulator
SMF	Single-Mode Fiber
SNR	Signal-To-Noise Ratio
UT	Uncompensated Transmission
VCSEL	Vertical Cavity Surface Emitting Laser
VS	Volterra Series
WDM	Wavelength Division Multiplexing

Introduction

Over the last ten years, the capacity demand of a telecommunication system has grown dramatically due to the exponential increment of data traffic. As the transmission bandwidth of single-mode optical fibers has been almost fully exploited, multiplexing techniques are used to transmit data at higher bit rates. The most common one is Wavelength Division Multiplexing (WDM). Most recently, Space Division Multiplexing (SDM) has been required for a further substantial increase of transmission capacities over both short and long distances. Taking advantage of the spatial dimension has been possible by producing optical fibers supporting multiple spatial modes or containing multiple cores exploited as parallel independent data channels.

This work will deal with the variant of SDM called Mode Division Multiplexing (MDM). This solution exploits the possibility to propagate multiple modes in a single core fiber, but it is strongly limited by intermodal coupling. Usually, the use of Multiple-Input Multiple-Output (MIMO) Digital Signal Processing (DSP) is required together with the coherent detection technique at the receiver. On the other hand, the complexity of the MIMO increases dramatically with the number of modes propagating into the fiber. Thus, it would be difficult to utilize an electrical MIMO equalizer with a large number of modes.

One of the most recent challenges is to design a Few-Mode Fiber (FMF) with low Differential Mode Group Delay (DMGD) so that all modes can be simultaneously MIMO processed with as low complexity as possible. In particular, we focus on an innovative FMF, produced by Prysmian Group, in which 9 Linearly Polarized (LP) modes, i.e. 15 spatial modes, can propagate together. Ideally, exploiting this promising fiber, the transmission capacity could be multiplied by a factor 30 which is the total number of modes per wavelength, considering also Polarization Division Multiplexing (PDM).

The main goal of this work is to find possible solutions to design high-capacity MDM communication systems based on the challenging FMF de-

scribed before, reducing their overall complexity. In particular, Mode-Group Division Multiplexing (MGDM) is considered to propagate the 5 mode groups supported by the 9-LP FMF.

The MDM propagation into a single transmission line requires also a Mode-Multiplexer (MMUX)/Mode-Demultiplexer (MDMUX) technology to combine/separate the several supported modes. Recently, Cailabs has developed a promising MMUX/MDMUX by exploiting a new emerging technique called Multi-Plane Light Conversion (MPLC). This works focuses on a particular 15-mode-selective MMUX to excite carefully and independently modes, now already available on the market.

Two totally different applications of this innovative FMF have been analyzed highlighting its potential in increasing the transmission capacity in optical communications.

Firstly, the possibility to employ this fiber into a system covering long and medium distances. In particular, a reconfigurable mesh network such as a Metropolitan Area Network (MAN), full of nodes in the middle, which menages distances of about hundreds of kilometers is considered. In this scenario, it has been explored the use of coherent detection with MIMO equalizers applied to groups of LP-modes independently, compensating intermodal effects between modes of the same group. Only some group combinations can be excited according to the distance to be covered, to propagate together into the fiber due to the effect of intermodal crosstalk.

Several analytic simulations have been presented to evaluate the achievable performance, with high-speed modulation formats, of MGDM propagation in medium/long-haul transmission systems underlying the impacts of linear and nonlinear effects. This study supports project FIRST (Fiber Infrastructure for Research on Space-Division Multiplexed Transmission) founded by MIUR PRIN in 2017. FIRST targets demonstrating the effectiveness and viability of SDM and its higher performance compared to standard Single-Mode Fiber (SMF) technology used today. Thus, this analysis considers field trials with a pioneer MDM network exploiting the already deployed 9-LP-mode fiber rings installed in L'Aquila city.

Secondly, the employment of this FMF fiber to design intra/inter data center point-to-point connections with large capacity and low complexity has been proposed. With the aim of finding a low-cost solution for short communication systems, simple modulation formats, such as On-Off Keying (OOK) and 4-Pulse-Amplitude Modulation (PAM), and direct detection have been implemented. The main drawback of this particular choice is that the effect of chromatic dispersion cannot be removed, as it happened in case of coherent detection. Over the years, there are several methods proposed to

mitigate these propagation impairments. In particular, this work focuses on nonlinear Decision Feedback Equalizer (DFE), which can partly compensate for lost spectral information by making decision thresholds dependent on past decisions made in the receiver. It will be proved that the signal quality can be significantly improved, even in the presence of intermodal crosstalk.

In order to evaluate system performance, a simulator developed in MATLAB® has been used to our requirements. Some simulations are reported to understand the potentiality of MGDM transmission over short distances by pointing out the effects of dispersion and mode coupling. System capabilities have been individuated in terms of maximum reachable distances, capacity and spectral efficiency.

At the end, to further reduce the cost of optical components in short-range applications, the wavelength interleaving between mode groups has been investigated. Thus, the WDM channel spacing on a single group is reduced enabling more common and simpler Arrayed Waveguide Grating (AWG). Several solutions have been proposed to find, also in this case, a right trade-off between system complexity and performance.

This thesis is articulated in 4 chapters as follows.

CHAPTER 1 The state-of-art of MDM is introduced, first focusing on the theory of modes in an optical waveguide. Then, the additional impairments occurring in multimode propagation are described. Finally, the last part of the chapter is dedicated to the concept of MGDM.

CHAPTER 2 It gives a detailed description of the key optical elements exploited in the presented communication systems. In particular: the design of the 9-LP-mode fiber produced by Prysmian Group and the 15-mode-selective MMUX/MDMUX optimized for this specific fiber by Cailabs.

CHAPTER 3 The study of the impact of MDM propagation based on the 9-LP modes FMF in a long-medium haul scenario. Initially, the simulation approach and system architecture exploiting MGDM are introduced. Then, the main simulations are reported to point out the capabilities and limits of the proposed solutions.

CHAPTER 4 This chapter shows the performance and the main limitations of MDM propagation based on the 9-LP modes FMF in a short-range communication system. Two different implementations of the MGDM technique are reported. A general overview of the used simulator and system structure are presented.

Chapter 1

Mode Division Multiplexing theory

This chapter is focused on the concept of MDM, a particular SDM technique to efficiently enhance the capacity of optical networks. The idea is using different guided modes of a Multi-Mode Fiber (MMF) for independent transmission channels. The modes inside a fiber are possible patterns of the electromagnetic field that propagate along the fiber. In this chapter we analyze the solutions of the wave equation into an optical waveguide. Then, the the major limiting factors of the multimode propagation are described in detail. At the end, the concept of MGDM is introduced.

1.1 General theory of modes in optical fibers

In this section is reported a simple method for determining the modes of an optical waveguide with a cladding refractive index n_{cl} that differs only slightly from the maximum refractive index of the core n_{co}. This method, called the $n_{co} \cong n_{cl}$ method, has been introduced by Snyder and Young in 1978 and it's normally used to obtain the propagating modes of a generic optical waveguide of arbitrary cross section and arbitrary profile grading [1]. Snyder's treatment focuses on the propagation constants β of the higher-order modes and their stability during propagation in a cylindrical waveguide and in an elliptical space using simple symmetry considerations.

The $n_{co} \cong n_{cl}$ method synthesizes the vector modal fields from linear combinations of solutions to the scalar wave equation. The appropriate linear combinations are dictated by properties of the $\nabla\epsilon$ terms in the vector wave equation, where $\epsilon(x, y, z)$ is the permittivity of the waveguide and ∇ is the

operator expressed by

$$\nabla = \frac{\partial}{\partial x}\hat{\mathbf{x}} + \frac{\partial}{\partial y}\hat{\mathbf{y}} + \frac{\partial}{\partial z}\hat{\mathbf{z}}. \tag{1.1}$$

where $\hat{\mathbf{x}}, \hat{\mathbf{y}}$ and $\hat{\mathbf{z}}$ are unit vectors in the x, y, z directions. Failure to account for the $\nabla\epsilon$ terms, however small, will in general lead to "pseudo-modes" with the property that their cross sectional intensity and polarization pattern changes as the modes propagates [2].

Firstly, it's important to review several fundamental concepts required for the following analysis: when the permittivity $\epsilon(x, y)$ of the medium has cylindrical (not necessary circular) symmetry the modal electric $\mathbf{E}$ and magnetic $\mathbf{H}$ vector fields have the form

$$\mathbf{E}(x, y, z) = \mathbf{e}(x, y)\exp(i\beta z) = (\mathbf{e}_t + \mathbf{e}_z)\exp(i\beta z), \tag{1.2a}$$

$$\mathbf{H}(x, y, z) = \mathbf{h}(x, y)\exp(i\beta z) = (\mathbf{h}_t + \mathbf{h}_z)\exp(i\beta z), \tag{1.2b}$$

assuming an $\exp(-i\omega t)$ time dependence. The fields $\mathbf{e}_t$ are solutions of the reduced wave equation

$$\nabla_t^2\mathbf{e}_t + (k^2 + \beta^2)\mathbf{e}_t = -\nabla_t(\mathbf{e}_t \cdot \nabla_t \ln\epsilon), \tag{1.3}$$

where

$$\nabla_t = \nabla - \hat{\mathbf{z}}\left(\frac{\partial}{\partial z}\right), \tag{1.4}$$

∇_t^2 is the transverse vector Laplacian [3], $k(x, y) = 2\pi n(x, y)/\lambda$, $\epsilon = \epsilon_0 n^2$ and ϵ_0 is the permittivity of free space. The remaining field components are determined from $\mathbf{e}_t$ using Maxwell's equations. The allowed values of β result by demanding only that solutions of equation (1.3) be bounded, since effects of any discontinuity in ϵ are fully contained within the $\nabla_t(\ln\epsilon)$ term. For bound modes β is real and restricted to the range [4, 5]

$$k_{cl} \leq \beta \leq k_{co} \tag{1.5}$$

where $k_{cl} = 2\pi n_{cl}/\lambda$, $k_{co} = 2\pi n_{co}/\lambda$, n_{co} is the maximum refractive index of the core and n_{cl} is the refractive index of the cladding. Because of the $\nabla_t \ln\epsilon$ terms in vector wave equation, the modal fields are in general hybrid, possessing both $\mathbf{e}_z$ and $\mathbf{h}_z$ components.

1.1.1 The $\mathbf{n_{co}} \cong \mathbf{n_{cl}}$ method for deriving modes

In this section are derived the approximations for modal fields and their propagation constants on waveguides with $n_{co} \cong n_{cl}$. This approximation

is based on the calculus of the modes of a $n_{co} = n_{cl}$ waveguide (paragraph 1.1.1.1), that are the "building blocks" needed for obtaining the approximated results for a generalized $n_{co} \cong n_{cl}$ waveguides (paragraph 1.1.1.2). In the following sections the fields of optical waveguides will be expressed in terms of the parameters:

$$\sin\theta_c = \left(1 - \frac{n_{cl}^2}{n_{co}^2}\right)^{1/2} \cong \theta_c \tag{1.6a}$$

$$V = R(k_{co}^2 - k_{cl}^2)^{1/2} = k_{co} R \sin\theta_c \tag{1.6b}$$

where the first is the critical angle θ_c, the second is the well-known dimensionless waveguide parameter V and R is the characteristic dimension of the waveguide cross section, i.e. the core radius for circularly symmetric waveguides.

1.1.1.1 TEM modes of the $n_{co} = n_{cl}$ waveguide (LP modes)

Snyder and Young begin by finding the modes of optical waveguides in the artificial limit when the maximum refractive index of the core is equal to the cladding refractive index, i.e. when $n_{co} = n_{cl}$. By itself, this condition would appear to assume that the medium is homogeneous and incapable of guiding energy. However, to avoid the trivial consequences of this assumption, it's imposed the constraint that the guiding properties of the structure remain unchanged, i.e. the waveguide parameter V be an arbitrary constant [6]. Because bound modes are restricted to the range of values in equation (1.5), the limit $n_{co} = n_{cl} = n$ demands that

$$\beta = k_{co} = k_{cl} = k = \frac{2\pi n}{\lambda}. \tag{1.7}$$

This condition is satisfied only by a z-directed transverse electromagnetic (TEM) wave, i.e. by a wave for which the electric and magnetic field vectors lie in a plane that is transverse to the axis of the waveguide. Accordingly, the modal fields components on the $n_{co} = n_{cl}$ waveguide are

$$\tilde{\mathbf{h}}_z = \tilde{\mathbf{e}}_z = 0 \tag{1.8a}$$

$$\tilde{\mathbf{h}}_t = \left(\frac{\epsilon}{\mu}\right)^{1/2} \hat{\mathbf{z}} \times \tilde{\mathbf{e}}_t \tag{1.8b}$$

where μ is the magnetic permeability of the medium and the $\tilde{}$ is used to indicate quantities to be associated with the scalar wave equation.

Because $n_{co} = n_{cl}$, all polarization-dependent properties of the structure are removed. Since the $\nabla_t \ln\epsilon$ term in the vector wave equation (1.3) is solely

responsible for the polarization properties of modes, it is omitted solving for the $\tilde{\mathbf{e}}$ fields of the $n_{co} = n_{cl}$ waveguide. In other words, the $n_{co} = n_{cl}$ fields are solutions to the scalar wave equation. These vector modal fields can then be expressed in rectangular coordinates as

$$\tilde{\mathbf{e}}_x = \psi\hat{\mathbf{x}},\ \tilde{\mathbf{e}}_y = \psi\hat{\mathbf{y}}, \tag{1.9}$$

where ψ is a solution of

$$(\nabla_t^2 + k^2 - \tilde{\beta}^2)\psi = 0. \tag{1.10}$$

The solutions ψ must be bounded everywhere and have the property of the scalar wave equation that ψ and its normal derivative are everywhere continuous. These constraint lead to an eigenvalue equation from which the allowed values of $\tilde{\beta}$ are found, where $\tilde{\beta}$ is distinguished from β being an eigenvalue of equation (1.10) rather than equation (1.3).

It's important to underline that the $n_{co} = n_{cl}$ waveguide is an unphysical condition. Nevertheless, as shown in the next sections, the fields of the $n_{co} = n_{cl}$ waveguide are the building blocks for the $n_{co} \cong n_{cl}$ waveguide. The modal fields of step profile waveguides with circular symmetry are often called LP or uniformly polarized modes.

In the next section is shown how the solutions of the scalar wave equation $\tilde{\mathbf{e}}$ and $\tilde{\beta}$ can be used to construct accurate representation of $\mathbf{e}$ and β, which are themselves solutions of the vector wave equation (1.3).

1.1.1.2 Modes on the $\mathbf{n_{co}} \cong \mathbf{n_{cl}}$ waveguide

The significant consequence of having n_{co} different from n_{cl} is that the waveguide has polarization properties. The polarization properties are contained within the $\nabla_t\epsilon$ term of the wave equation. The modes of such a waveguide must exhibit these properties and, therefore, they must be solution of the vector equation (1.3). However, since the term $\nabla_t(\mathbf{e}_t \cdot \nabla_t \ln\epsilon)$ is zero when $n_{co} = n_{cl}$, it must have a small, but nevertheless a very important effect for $n_{co} \cong n_{cl}$. The modes of the $n_{co} \cong n_{cl}$ waveguide can then be approximated by linear combinations of the modal fields $\tilde{\mathbf{e}}$ of the $n_{co} = n_{cl}$ waveguide. The proper linear combinations are dictated by the symmetries of the waveguide which are fully contained within the $\nabla_t\epsilon$ term of the vector wave equation. The method of constructing the linear combination introduced by Snyder and Young is reported in section 1.1.2.

Because $\beta \cong k$ on the $n_{co} \cong n_{cl}$ waveguide, the transverse fields obey the approximate relationship

$$\mathbf{h}_t \cong \left(\frac{\epsilon}{\mu}\right)^{1/2} \hat{\mathbf{z}} \times \mathbf{e}_t. \tag{1.11}$$

The longitudinal fields are then found from Maxwell's divergence equations, leading to

$$\mathbf{h}_z = \frac{i}{\beta}\nabla_t \cdot \mathbf{h}_t \tag{1.12a}$$

$$\mathbf{e}_z = \frac{i}{\beta}[\nabla_t \cdot \mathbf{e}_t + (\nabla_t \ln \epsilon) \cdot \mathbf{e}_t] \cong \frac{i}{\beta}\nabla_t \cdot \mathbf{e}_t \tag{1.12b}$$

The propagation constant β for the $n_{co} \cong n_{cl}$ modes nearly equals $\tilde{\beta}$ determined from equation (1.10). To include small polarization effects one uses a standard method presented in [1], leading to

$$\beta - \tilde{\beta} \cong \frac{\beta^2 - \tilde{\beta}^2}{2k} = \frac{\int_{A_\infty} \tilde{\mathbf{e}}_t \cdot \nabla_t (\mathbf{e}_t \cdot \nabla_t \ln \epsilon) dA}{2k \int_{A_\infty} \tilde{\mathbf{e}}_t \cdot \mathbf{e}_t dA}, \tag{1.13}$$

where $k = 2\pi n/\lambda$, $\tilde{\beta}$ and $\tilde{\mathbf{e}}_t$ are defined by equations (1.9) and (1.10), $\mathbf{e}_t$ and β are defined by equations (1.3) and A_∞ is the infinite cross section. The small correction to $\tilde{\beta}$ obtained by equation (1.13) is necessary to separate the erroneous degenerate $\tilde{\beta}$'s found by solving the scalar wave equation rather than the vector wave equation. For example, equation (1.13) includes the small polarization dependent effects necessary to distinguish the β of a TM from a TE wave.

1.1.2 Vector modal fields

In this section is reported the method of constructing approximations of the vector modal fields by linearly combining the $n_{co} = n_{cl}$ fields. The philosophy of the method is based on the fact that modal fields must satisfy the symmetry properties of the waveguide. These symmetry properties are contained within the $\nabla_t \epsilon$ term of the vector wave equation and therefore they are automatically included in solutions of this equation. However, it is often possible to guess the appropriate symmetry conditions without solving the vector wave equation (1.3). In particular, paragraph 1.1.2.1 and paragraph 1.1.2.1 report respectively the examples of circularly symmetric waveguide and a waveguide with two preferred axes of symmetry.

1.1.2.1 Waveguides with circular simmetry

The $n_{co} = n_{cl}$ modes are given by equation (1.9) in terms of the scalar function ψ. By virtue of the circular symmetry, there are in general two solutions of the scalar wave equation (1.10) for each allowed value of $\tilde{\beta}$. One solution, ψ_e, has even symmetry, while the other, ψ_o, has odd symmetry:

$$\psi_e(\rho, \phi) = f_\ell(\rho) \cos \ell\phi, \;\; \psi_o(\rho, \phi) = f_\ell(\rho) \sin \ell\phi. \tag{1.14}$$

In equation (1.14), ϕ is the azimuthal coordinate and $f_\ell(\rho)$ is a solution of

$$\left(\frac{d^2}{d\rho^2} + \frac{1}{\rho}\frac{d}{d\rho} + k^2(\rho) - \tilde{\beta}^2 - \frac{\ell^2}{\rho^2}\right) f_\ell(\rho) = 0 \tag{1.15}$$

and, for an optical fiber with a step profile of the refractive index, it assumes the form

$$f_\ell(\rho) = \frac{J_\ell(\tilde{U}\rho/R)}{J_\ell(\tilde{U})} \qquad \rho \leq R \tag{1.16a}$$

$$f_\ell(\rho) = \frac{K_\ell(\tilde{W}\rho/R)}{K_\ell(\tilde{W})} \qquad \rho \geq R \tag{1.16b}$$

where the notation $\tilde{}$ indicates that they are derived from the scalar wave equation, J_ℓ is a Bessel function and K_ℓ is a modified Hankel function and $\tilde{U}$ and $\tilde{W}$ are related to the parameter V of equation (1.6b) by $V^2 = \tilde{U}^2 + \tilde{W}^2$.

Thus, the $n_{co} = n_{cl}$ waveguide of paragraph 1.1.1.1 has four modes for each allowed value of $\tilde{\beta}$, i.e.

$$\tilde{\mathbf{e}}_{xe} = f_\ell(\rho)\cos(\ell\phi)\hat{\mathbf{x}} \tag{1.17a}$$

$$\tilde{\mathbf{e}}_{xo} = f_\ell(\rho)\sin(\ell\phi)\hat{\mathbf{x}} \tag{1.17b}$$

$$\tilde{\mathbf{e}}_{ye} = f_\ell(\rho)\cos(\ell\phi)\hat{\mathbf{y}} \tag{1.17c}$$

$$\tilde{\mathbf{e}}_{yo} = f_\ell(\rho)\sin(\ell\phi)\hat{\mathbf{y}} \tag{1.17d}$$

When $\ell = 0$, there are only two $n_{co} = n_{cl}$ modes, $\tilde{\mathbf{e}}_{xe}$ and $\tilde{\mathbf{e}}_{ye}$. These fields exist at all frequencies and depend only by the radial coordinate ρ. By virtue of the circular symmetry, any linear combination of these two fields must be a modal field on the $n_{co} \cong n_{cl}$ waveguide. Also, from circular symmetry, the $n_{co} \cong n_{cl}$ waveguide has two fundamental modes with equal $\tilde{\beta}$'s. We can take one mode to be polarized in the x direction ($\mathbf{e}_x$) and the other to be polarized in the y direction ($\mathbf{e}_y$):

$$\mathbf{e}_x = f_0(\rho)\hat{\mathbf{x}},\ \mathbf{e}_y = f_0(\rho)\hat{\mathbf{y}} \tag{1.18}$$

where $f_0(\rho)$ is the solution of equation (1.15) with $\ell = 0$.
The two fundamental modes of the circular symmetric $n_{co} \cong n_{cl}$ waveguide are exceptional in that they are the same as the fundamental modes on the $n_{co} = n_{cl}$ waveguide, i.e. they are uniformly polarized throughout the cross section and have the same β's.

Unlike the fundamental modes, none of the $n_{co} = n_{cl}$ fields for $\ell \geq 1$ are individually modal fields of the $n_{co} \cong n_{cl}$ waveguide. This can be proved from symmetry considerations together with equation (1.13) [1]. Thus, we

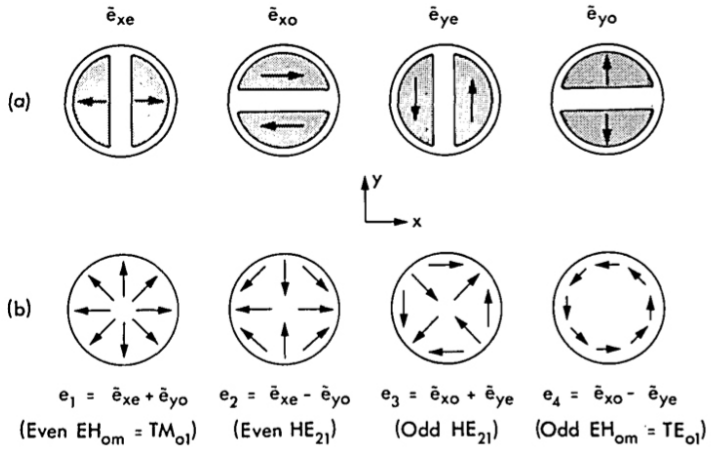

Figure 1.1. First-order modes. (a) The $n_{co} = n_{cl}$ or LP modes for $\ell = 1$. The $\tilde{\mathbf{e}}_{xe}$ and $\tilde{\mathbf{e}}_{yo}$ are symmetric under reflections in the x and y axes, while $\tilde{\mathbf{e}}_{xo}$ and $\tilde{\mathbf{e}}_{ye}$ are antisymmetric. If any one of the above fields is rotated through an arbitrary angle it transforms into a linear combination of all four. (b) The $n_{co} \cong n_{cl}$ modes for $\ell = 1$. Under an arbitrary reflection and rotation, $\mathbf{e}_1$ and $\mathbf{e}_4$ are unchanged, while either $\mathbf{e}_2$ and $\mathbf{e}_3$ transform into linear combinations of $\mathbf{e}_2$ and $\mathbf{e}_3$ themselves.

require linear combinations of $\tilde{\mathbf{e}}_{xe}$, $\tilde{\mathbf{e}}_{xo}$, $\tilde{\mathbf{e}}_{ye}$ and $\tilde{\mathbf{e}}_{yo}$ to form the higher-order modes.

To form the correct linear combinations, we combine those modes which have the same properties under a rotation of 90° and under reflections in the x and y axes. It may help to consider the specific example of $\ell = 1$ modes shown in Figure 1.1(a). Thus, $\tilde{\mathbf{e}}_{xe}$ is combined with $\tilde{\mathbf{e}}_{yo}$ because one rotates into the other, while $\tilde{\mathbf{e}}_{xo}$ is combined with $\tilde{\mathbf{e}}_{ye}$ because one rotates into minus the other. Taking symmetric and antisymmetric combinations lead to the 4 modes of the $n_{co} \cong n_{cl}$ waveguide:

$$\mathbf{e}_{t1} = \tilde{\mathbf{e}}_{xe} + \tilde{\mathbf{e}}_{yo} \tag{1.19a}$$

$$\mathbf{e}_{t2} = \tilde{\mathbf{e}}_{xe} - \tilde{\mathbf{e}}_{yo} \tag{1.19b}$$

$$\mathbf{e}_{t3} = \tilde{\mathbf{e}}_{xo} + \tilde{\mathbf{e}}_{ye} \tag{1.19c}$$

$$\mathbf{e}_{t4} = \tilde{\mathbf{e}}_{xo} - \tilde{\mathbf{e}}_{ye} \tag{1.19d}$$

Using conventional nomenclature [7, 8] modes 1-4 refer to the even $EH_{(\ell-1,m)}$, even $HE_{(\ell+1,m)}$, odd $HE_{(\ell+1,m)}$ and odd $EH_{(\ell-1,m)}$ modes respectively. Figure 1.1(b) illustrates the modes for $\ell = 1$. These combinations can be shown

to be consistent with the symmetry properties of the waveguide. By placing $\mathbf{e}_{t1}$ in equation (1.13) for $\mathbf{e}_t$ and $\tilde{\mathbf{e}}_{xe}$ for $\tilde{\mathbf{e}}_t$ we obtain β for mode 1 and similarly for the other three modes. In general, the β's of the EH and HE modes differ from one another. This difference gives rise to a beat phenomenon causing a rotation of the $n_{co} = n_{cl}$ or LP patterns as the mode advances. The stability of the LP mode patterns is set by the difference $|\beta_{HE} - \beta_{EH}|$ in the propagation constant of the two different mode types that form an LP pattern. If $\beta_{HE} = \beta_{EH}$, the $n_{co} = n_{cl}$ modes could be also modes of the $n_{co} \cong n_{cl}$ waveguide. However, the LP modes are not modes of a $n_{co} \neq n_{cl}$ waveguide. The reason is that each LP mode is formed by combining two proper modes, an $HE_{(\ell+1,m)}$ and $EH_{(\ell-1,m)}$ modes, and these proper modes have different propagation constants, β_{HE} and β_{EH}. Because of the beat phenomenon, when $|\beta_{HE} - \beta_{EH}| \neq 0$, the modes appear to rotate or fade into each other [9].The greater $|\beta_{HE} - \beta_{EH}|$, the shorter the beat length and hence more rapidly the LP modes fade into one another. As explained by Snyder and Young [1], the condition $|\beta_{HE} - \beta_{EH}| \neq 0$ is always satisfied by modes with $\ell \geq 2$: these LP modes are never modes of the circularly symmetric waveguide. Furthermore, the greater ℓ, the greater $|\beta_{HE} - \beta_{EH}|$, so the less stable the LP modes. It's important to notice that, apart from $\ell = 1$, the four modes can be divided into two couples of modes, HE and EH. The modes of each set have the same propagation constant, i.e. the even and odd HE modes have the same β_{HE}, while the even and odd EH modes have the same β_{EH}. The situation for $\ell = 1$ is more complicated, because the EH modes are the TE and TM modes that present different propagation constants β_{TE} and β_{TM}, while the HE modes share the same constant β_{HE}. The relation between these two propagation constants and β_{HE} are shown in Figure 1.2.

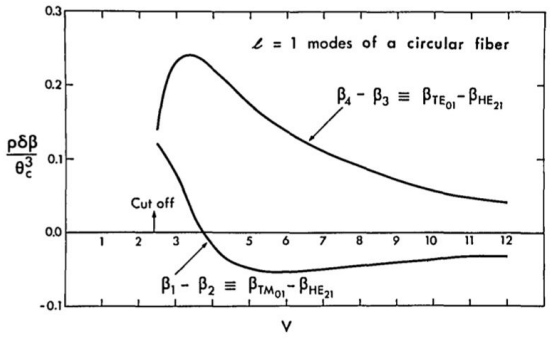

Figure 1.2. The difference in $\tilde{\beta}$'s for $\ell = 1$ modes of the circular symmetric, step profile waveguide.

1.1.2.2 Waveguides with two preferred axes of simmetry

Many structures of practical interest have a pair of preferred orthogonal axes of symmetry, i.e. the ellipse that can represent the core of a real optical fiber characterized by birefringence. When $n_{co} \cong n_{cl}$, the modes of these waveguides can be formed by linear combinations of the $n_{co} = n_{cl}$ modal fields.

It's intuitive that the fundamental modes, which propagate for all values of frequency, have electric fields that are polarized along one of these two axes of symmetry. Thus, the $n_{co} = n_{cl}$ modal fields are the proper approximations of the fundamental fields of the $n_{co} \cong n_{cl}$ waveguide only if the $\hat{\mathbf{x}}$ and $\hat{\mathbf{y}}$ directions of equation (1.9) are aligned with the direction of the symmetry axes. Therefore the fundamental mode has vector fields of the form

$$\mathbf{E}_x = \mathbf{e}_x \exp(i\beta_x z) = \psi \exp(i\beta_x z)\hat{\mathbf{x}} \tag{1.20a}$$

$$\mathbf{E}_y = \mathbf{e}_y \exp(i\beta_y z) = \psi \exp(i\beta_y z)\hat{\mathbf{y}} \tag{1.20b}$$

where ψ is the fundamental solution of the scalar wave equation (1.10). The modal propagation constants β_x and β_y are found by substituting into equation (1.13) $\mathbf{e}_t = \tilde{\mathbf{e}}_t = \mathbf{e}_x$ and $\mathbf{e}_t = \tilde{\mathbf{e}}_t = \mathbf{e}_y$ respectively. It's important to notice that in an elliptical space $\beta_x \neq \beta_y$, i.e. the two fundamental modes have different phase velocity. So, if the fiber is illuminated by linearly polarized light at 45° to the optical or symmetry axes, then both fundamental modes are excited equally and the wave becomes elliptically polarized as it propagates. Because of the beat phenomenon, the $\mathbf{E}$ vector appears to rotate. The length of a 360° rotation is $2\pi|\beta_x - \beta_y|^{-1}$.

The fields of higher-order modes, instead, are more complicated than the fundamental modes. It is clear that for a sufficiently large eccentricity the field of any particular $n_{co} \cong n_{cl}$ mode is represented by equation (1.20), so that the only difference between it and a fundamental mode is in the values of ψ and β. However, it is equally clear that for a sufficiently small eccentricity, the same mode resembles a modal field of a circular symmetric waveguide, with $\hat{\mathbf{x}}$ and $\hat{\mathbf{y}}$ parallel to the symmetry axes of the ellipse. This transition is depicted in Figure 1.3. We can associate each ellipse mode with the fields of a distorted circle mode. For example, the ellipse mode that corresponds to distorting either $\mathbf{e}_{t1}$ or $\mathbf{e}_{t2}$ of Figure 1.1 is formed by a linear combination of $\tilde{\mathbf{e}}_{xe}$ and $\tilde{\mathbf{e}}_{yo}$, where these $\tilde{\mathbf{e}}$'s are now solutions to the scalar wave equation in elliptical geometry. Consequently, the fields of the ellipse modes $\mathbf{e}_{t1}$ and $\mathbf{e}_{t2}$ are

$$\mathbf{e}_{ti} = a_i\psi_e\hat{\mathbf{x}} + b_i\psi_o\hat{\mathbf{y}} = a_i\tilde{\mathbf{e}}_{xe} + b_i\tilde{\mathbf{e}}_{yo} \tag{1.21}$$

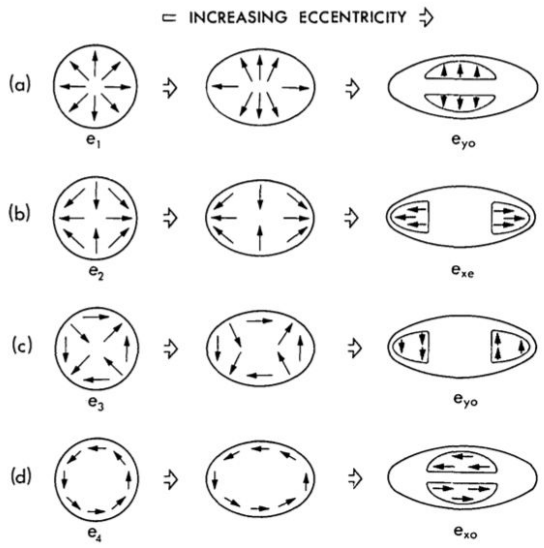

Figure 1.3. Transition from circle to ellipse modes for $\ell = 1$ modes. An electric field vector maintains its orientation to the interface, i.e. if it was initially perpendicular it remains perpendicular, as the eccentricity increases. Using this heuristic principle one can anticipate the way in which a particular circle mode changes as the eccentricity increases.

where $i = 1$ or 2, ψ_e and ψ_o are solutions of the scalar wave equation in elliptical geometry and are analogous to ψ_e and ψ_o given by equation (1.14) for the scalar wave equation in circular cylindrical geometry. Figure 1.4 provides an example of ψ_e and ψ_o. The propagation constants associated with ψ_e and ψ_o are denoted $\tilde{\beta}_e$ and $\tilde{\beta}_o$ respectively. These $\tilde{\beta}$'s are different; the difference increases as eccentricity increases.

At the end of paragraph 1.1.2.1, it has been stated that the rate that LP modes rotate into one another depends upon $|\beta_{HE} - \beta_{EH}|$, where β_{HE}, β_{EH} are the β's of the circular waveguide. When this difference is zero, the LP modes are stable, i.e. they are proper modes of the $n_{co} \cong n_{cl}$ waveguide. The stability of circle modes on an ellipse depends upon $(\tilde{\beta}_e - \tilde{\beta}_o)$, where $\tilde{\beta}_e, \tilde{\beta}_o$ are the $\tilde{\beta}$'s for the ellipse determined from the scalar wave equation. Consequently, the parameter Λ is influential in determining the limiting behavior of ellipse fields, where

$$\Lambda = \frac{(\tilde{\beta}_e - \tilde{\beta}_o)}{(\beta_{EH} - \beta_{HE})}, \tag{1.22}$$

where $\beta_{EH} = \beta_1$ and $\beta_{HE} = \beta_2$ for the particular ellipse modes $\mathbf{e}_{t1}$ and $\mathbf{e}_{t2}$ given by equation (1.21). When $|\Lambda| \gg 1$, the fields of the ellipse are uniformly polarized, while when $|\Lambda| \ll 1$ the ellipse modal fields are the fields of modes

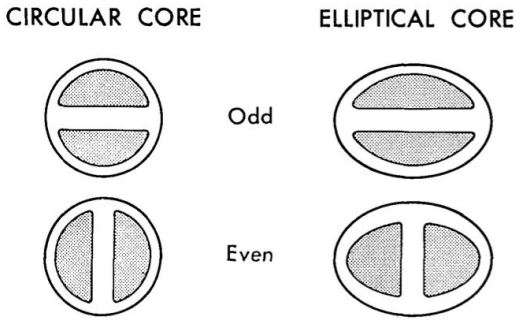

Figure 1.4. An example of a solution of the scalar wave equation corresponding to the $\ell = 1$ mode. The $\tilde{\beta}$'s of the even and odd circle modes are identical unlike the $\tilde{\beta}$'s for the even and odd modes of the elliptical core.

of a circularly symmetric waveguide.

1.2 The main limiting factors in MDM systems

On the one hand, the signal propagation into a fiber with multiple modes is subjected to the physical phenomena that impact the transmission also in case of a typical SMF. These intramodal effects are usually classified into two categories said "linear effects" and "nonlinear effects" [10]. The linear transmission effects are: attenuation, chromatic dispersion, differential group delay and polarization mode dispersion. Instead, the dominant nonlinearieties are caused by the so called Kerr-effect. On the other hand, because of interactions between modes co-propagating into the core of the same optical fiber, the transmission performance are bound by additional limiting effects described in the following sections [10].

1.2.1 Intermodal crosstalk

Intermodal crosstalk describes linear interactions between signals modulated on different propagation modes and, if signals are modulated on the same wavelength, it can be modeled as in-band crosstalk [11]. More in detail, crosstalk can be defined as energy transferred from one mode to an other, called mode coupling.

This thesis focuses on transmission systems, where a channel i suffers crosstalk from multiple co-propagating channels. Thus, the total crosstalk on channel i is simply described as the sum over the transferred powers to channel i coming from each interfering channel respect to the power of the signal propagating on channel i. Accordingly, the general crosstalk definition

is

$$Crosstalk_i = \frac{\sum_j P_{j->i}}{P_{signal_i}}. \tag{1.23}$$

In addiction, crosstalk can be divided in two different types. A "concentrate" mode coupling takes place at discrete points in the transmission systems where light propagation condition changes quickly. This can be the case in the MMUX and MDMUX, in splices/connectors between different fiber sections or in the amplifiers. On the other hand, during propagation through the fiber itself, imperfections and mechanical stress can cause a kind of "distributed" mode coupling. In this work, crosstalk will be analyzed in terms of in-fiber contributions and contributions from the MMUX/MDMUX.

As described in detail in the following, intermodal crosstalk is one of the main limiting factors of MDM transmission. Thus, it is of great interest to know its impact on performance. Accordingly, Winzer [11] recently proposed a model to estimate penalties in terms of Signal-To-Noise Ratio (SNR) from in-band crosstalk on higher-order modulation formats. Figure 1.5(a) shows the back-to-back Bit Error Rate (BER) curves for the three measured formats and compares them to their theoretical limits. At a BER of 10^{-3}, the experimental performance of Quadrature Phase Shift Keying (QPSK) (i.e. 4-Quadrature Amplitude Modulation (QAM)), 16-QAM, and 64-QAM at 21.4 $GBaud$ is 0.9, 1.8, and 4.0 dB off their theoretical limits. The corresponding crosstalk penalties at a BER of 10^{-3} are shown in Figure 1.5(b). Because the SNR-penalties also depend on the relative phase between measured and interfering channel, Figure (1.5) represents separately the case of an undispersed interferer (with a random phase respect to the signal) and the other case of a dispersed interferer. As expected, introducing dispersion into the interferer increases crosstalk penalties due to the larger peak-to-average power of the interfering signal, resulting in more severe crosstalk-induced reductions of the minimum symbol distance compared to a well-confined, undispersed interfering constellation. The solid black curves represent the (phase-aligned) simulation results, with an excellent match to the experimental results [11]. As possible to see, the experimental 64-QAM format shows less robustness to crosstalk compared to the other two formats because the transmitter-induced dispertions are larger for this high-order and high-speed format. Moreover, can be notice that a crosstalk penalty of 1 dB is allowed for average crosstalk levels of about -16, -24, and -32 dB for QPSK, 16-QAM, and 64-QAM, respectively. Especially the latter value puts stringent requirements on the crosstalk performance of optical network elements and on coupling in spatially multiplexed systems.

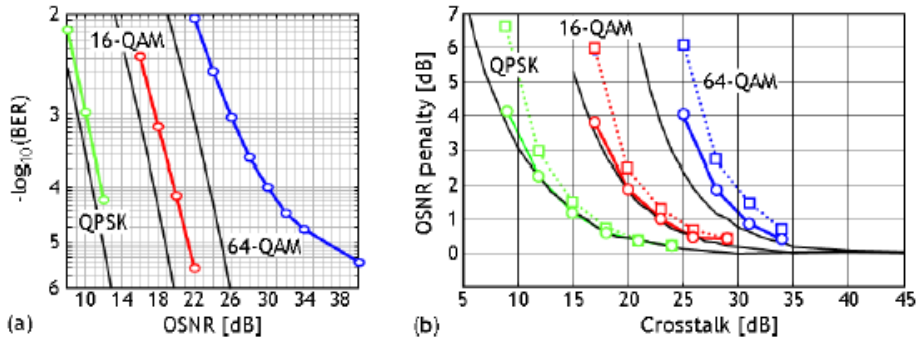

Figure 1.5. (a) Back-to-back BER for different modulation formats and the corresponding theoretical limits; (b) OSNR penalties from in-band crosstalk at BER=10^{-3} vs. crosstalk for different modulation formats with undispersed (circles) and dispersed (squares) interferer. The solid curves represent the results obtained from Monte Carlo simulations for phase-aligned interference [11].

1.2.2 Differential Mode Group Delay

DMGD is defined as the difference in group velocity between two modes of a MMF resulting in mode dependent group delays for a given length. DMGD is an intrinsic property of a given fiber and can be mesured as the difference between the maximum and the minimum group delay of short signal pulse propagating on different spatial modes. On the one hand, the amount of DMGD increases linearly with the transmission distance, indeed it is often specified in picoseconds per kilometer (ps/km), and on the other hand, it's inversely proportional to the mode coupling during fiber propagation. DMGD can substantially depend on fiber design and on considered modes, but realizing MMF with small DMGD is quite challenging. As we will see in section 2.2, graded-index fibers can be optimized for having small DMGD which however is usually achieved only within a quite limited wavelength range.

1.2.3 Intermodal nonlinear effects

As already mentioned, over single mode transmissions, nonlinearities are mainly caused by the so called Kerr-effect. To better understand, they can be divided into several subcategories including nonlinear interactions of a frequency tributary with itself (Self Phase Modulation), between different frequency carriers in a WDM system (Cross Phase Modulation) and between signals in the two orthogonal polarization axes (Cross Polarization Modulation).

In a MDM communication system, additional intermodal nonlinear effects have been identified as nonlinear interactions between signals modulated on different spatial modes. In general, these intermodal effects can be only observed when the input power is sufficiently high and the transmission distance are sufficiently long. However, it's difficult to achieve both conditions because the transmission distance is mainly limited by intermodal crosstalk. A theoretical model for a first evaluation of intermodal nonlinear effects, taking into account two spatial modes, has been developed as reported in [12]. This model and the derived results have been reported below in order to understand how intermodal nonlinearities could impact on the performance of a MDM system.

1.2.3.1 Theoretical model

The nonlinear interaction between two propagating modes p and q depend on the overlap integral

$$f_{pq} = \frac{\int\int |F_p(x,y)|^2 |F_q(x,y)|^2}{\int\int |F_p(x,y)|^2 dxdy \int\int |F_q(x,y)|^2 dxdy}, \tag{1.24}$$

where $F_p(x,y)$ and $F_q(x,y)$ are the mode functions describing the spatial distribution of these two modes. For p=q, f_{pq} is defined as the inverse of the effective area ($A_{eff,p}$) and it describes how the energy is distributed along the fiber cross-section. Consequently, the general definition for all combinations of spatial modes is

$$f_{pq} = \frac{1}{A_{eff,pq}}. \tag{1.25}$$

If p≠q, $A_{eff,pq}$ is denoted as the intermodal effective area between two propagation modes. $A_{eff,p}$ and $A_{eff,p}$ values of two nondegenerate spatial modes vary without any evident rule, otherwise the intermodal effective area between two degenerate modes (es. p=LP_{11a} and q=LP_{11b}) can be calculated as

$$A_{eff,pq} = 3 \cdot A_{eff,p}. \tag{1.26}$$

In addiction to intermodal effective area, an other relevant parameter to evaluate the intermodal effects is the DMGD. It induces a decorrelation between the signals on the different spatial modes leading to a mitigation of intermodal nonlinear effects.

1.2.3.2 Impact of intermodal nonlinear effects on MDM system performance

Following the model reported above, Koebele [12] classified the intermodal nonlinear effects in two categories: firstly, nonlinear effects between two degenerate modes and secondly, nonlinear effects between two nondegenerate modes. The former, because of having almost the same propagation constant β, are characterized by DMGD almost equal to 0 and the intermodal effective area is three times the effective area of one of interacting modes. The latter show a value of DMGD in order of magnitude of some ns/km and the intermodal effective area follows no simple rule. In particular, simulation results reported in [12] have been obtained by modeling a step-index fiber which would allow 30 spatial modes. Figure 1.6 shows the Q^2-factor after propagation as a function of the input power per channel and per spatial mode for the degenerate spatial modes with the lowest (LP_{13} mode, $A_{eff} = 300\mu m$) and the highest effective area (LP_{23} mode, $A_{eff} = 450\mu m$). As possible to see, the difference between the solid curves, where only one spatial mode is transmitted, and the dashed curves, where both degenerate modes propagate together, is around 0.2 dB. This value represents the penalties of maximum Q^2-factor caused by intermodal non linear effects of two degenerate propagation modes. Moreover, in Figure 1.7 penalties due to intermodal nonlinearities are

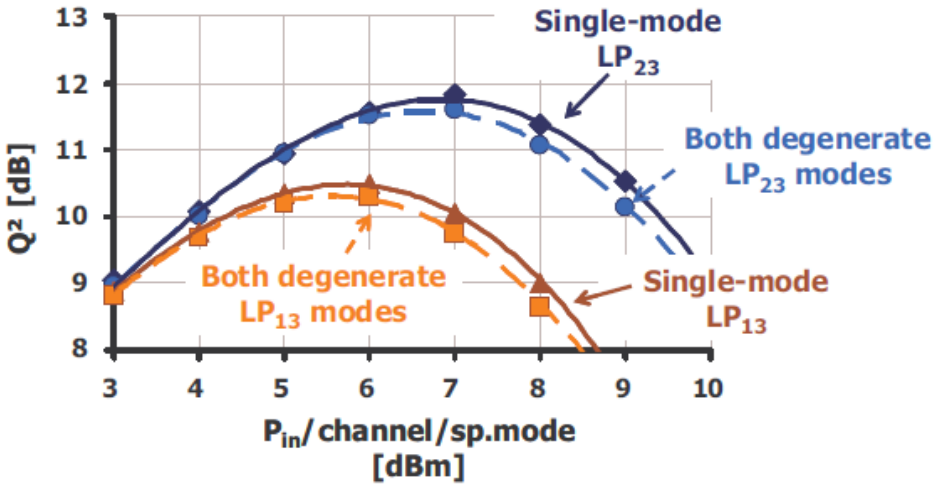

Figure 1.6. Q^2-factor as a function of input power for degenerate modes with highest (LP_{23} mode, A_{eff}=450μm) and lowest (LP_{13} mode, A_{eff}=300μm) effective area in the emulated fiber [12].

depicted in terms of Nonlinear Threshold (NLT) which is the input power at the maximum Q^2-factor. In particular, NLT is plotted as a function of

the effective area. The two visible straight lines, referring respectively to every single spatial mode at a time and to every pair of degenerate spatial modes at a time, are superposed. Thus, it means that intermodal nonlinear effects remain negligible for all couples of degenerate modes. In the case of

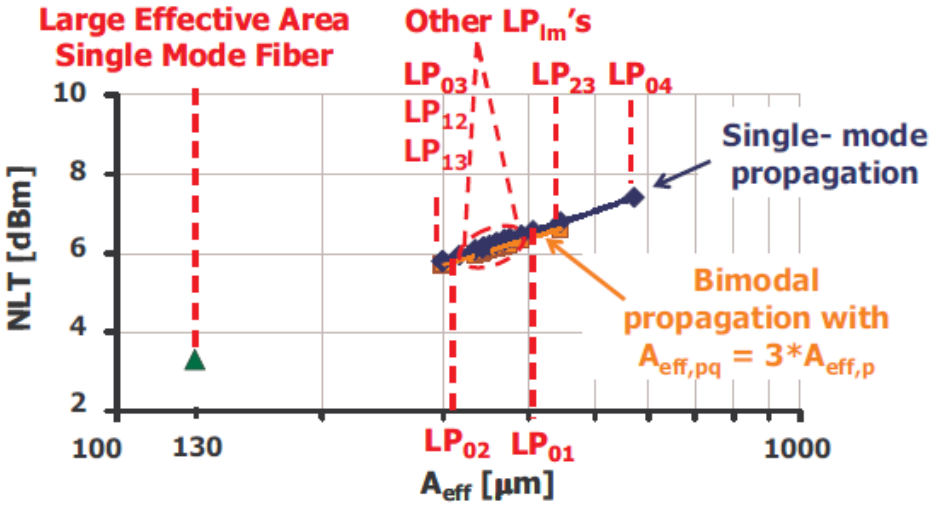

Figure 1.7. Nonlinear threshold after single-mode PDM propagation of all spatial modes and after bimodal PDM propagation of all degenerate spatial modes [12].

two nondegenerate modes, the mitigation of intermodal nonlinear effects is made by the occuring DMGD because the intermodal effective area $A_{eff,pq}$ can be significantly lower than $3 \cdot A_{eff,p}$. Figure 1.8(a) presents some results obtained applying the worst case in which $A_{eff,pq} = A_{eff,p} = A_{eff,q}$. It's possible to see how penalties of maximum Q^2-factor can be totally neglected when the DMGD is higher than 50ps/km. In order to understand if it is possible to fulfill this condition in practice, all DMGD values for 17 modes with different β have been calculated. Results plotted in Figure 1.8(b) shows that all DMGD values for pairs of occurring propagation modes are quite larger than the defined threshold.

According to what presented in this paragraph and taking into account that intermodal nonlinearieties can be effectiveness only for high powers and long distances, it has been decided to neglect them in my simulations. Only intramodal nonlinear effects will be considered.

1.3 Mode Group Division Multiplexing

For simplicity, in this thesis we will deal with the so called LP modes which are, as mentioned in section 1.1.1, an approximate solution in case of

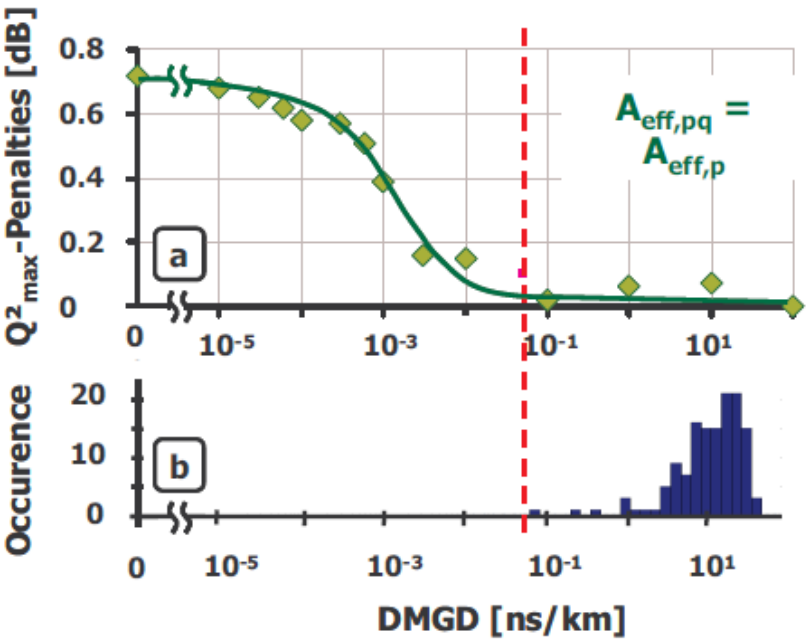

Figure 1.8. (a) Penalties on maximum Q^2-factor due to intermodal nonlinear effects as a function of DMGD between two spatial modes with 100% overlap (theoretical worst case). (b) Distribution of all DMGD values in simulated 17-mode-fiber [12].

weak guidance condition when $n_{co} \cong n_{cl}$. Linear polarized $LP_{l\mu}$ modes are determined by an azimuthal order l and a radial order μ. Each $LP_{0\mu}$ family of modes, with azimuthal index $l = 0$ and an arbitrarily fixed radial index μ contains one spatial mode with two possible orthogonal polarizations along the horizontal and vertical directions, that is a total of two orthogonal modes. Whereas each $LP_{l\mu}$ family of modes with fixed integer indices $l \geq 1$ and $\mu \geq 1$ contains two "degenerate" spatial modes, named respectively a and b, with two possible orthogonal polarizations, that is a total of four orthogonal modes.

As mentioned in [13], all modes with the mode number m fulfilling the equation $m = l + 2\mu + 1$ have approximately the same propagation constant β and group delay. Table 1.1 summarizes the principal mode groups of a fiber supporting 15 spatial modes. Accordingly, groups which are named A,B,C,D and E in explanation of my work correspond respectively to modes with mode numbers equal to 3, 4, 5, 6 and 7. As possible to see, the number of modes per mode group increases with the increasing number of groups, so that even with a high number of modes the number of groups remains relatively small [13]. The MGDM is a particular multiplexing technique

m	modes	group
3	LP01	A
4	LP11a, LP11b	B
5	LP02, LP21a, LP21b	C
6	LP12a, LP12b, LP31a, LP31b	D
7	LP03, LP22a, LP22b, LP41a, LP41b	E

Table 1.1. Principal mode groups of a FMF supporting 15 spatial modes.

where these mode groups are used as independent transmission channels. In general, MDM using one mode per channel requires coherent detection in conjunction with digital MIMO processing for signal separation. Thus, exploiting a fiber with 15 spatial modes, a 30x30 MIMO receiver is needed to recover signals transmitted along different polarization modes. Otherwise, if all modes inside a group are considered part of the same channel, a further simplification of the MDM system is possible by avoiding the use of the inter-mode group MIMO receiver. With this solution, the full-MIMO processing is reduced to independent and parallel MIMO equalizers among the members of each group (paragraph 2.1). The possibility of MGDM implementation for long-haul transmission systems in a metro network scenario is widely analyzed in chapter 3.

Chapter 2

Key elements of the analyzed MDM optical transmission system

This second chapter is dedicated to a fully description of the MDM key elements considered in this thesis. Firstly, a general introduction about the typical components of a MDM optical transmission system has been done following what mentioned in [10]. In particular, this thesis focuses on the exploitation of an innovative FMF, realized by Prysmian Group, which supports 9 different LP modes, i.e. 15 spatial modes. Here, the fiber state-of-art and practical characteristics of its design and realization have been reported in order to understand its advantages in a MDM scenario [14]. Moreover, to get a clear idea of the system components used, a section has been dedicated to describe the MMUX and MDMUX produced by Cailabs and optimized for 9-LP graded-index fiber from Prysmian.

2.1 MDM system overview

The main idea of MDM is to use a single core optical fiber which allows the propagation on different modes as separate transmission channels. As a consequence of fiber modes orthogonality, theoretically it's possible to modulate signals on different guided modes and, after propagation, to recover the original transmitted data without losses. Thus, the capacity of the transmission system can be multiplied by the number of spatial modes.

The basic elements for a MDM transmission are shown in Figure 2.1. This picture depicts a typical scheme of an optical system in which WDM and MDM techniques are combined together in order to enhance the transmission

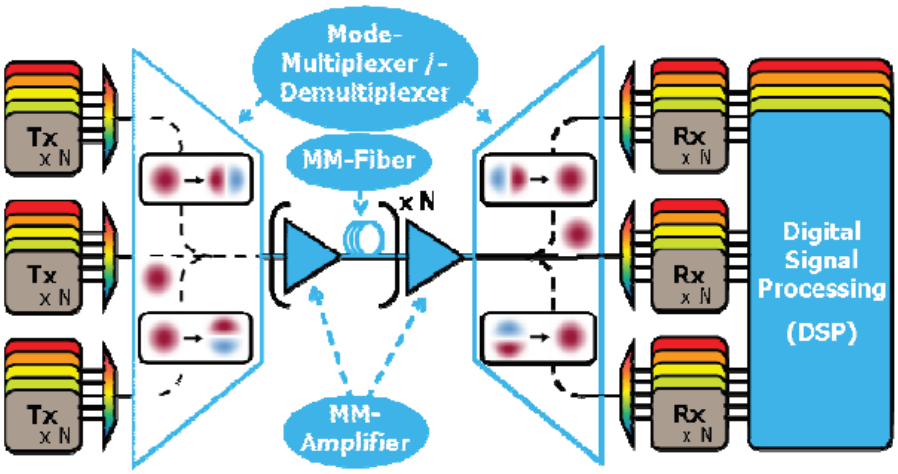

Figure 2.1. General architecture of a MDM optical system [10].

capacity. On the transmitter side, signals modulated on different wavelengths are multiplexed and then injected into a MMUX. The MMUX converts the incoming signals arrived through fundamental modes of SMFs into different guided modes of the MMF. Typically, the propagation occurs with MMFs, which have a relatively small number of guided modes and are so called FMFs. In order to amplify signals during propagation on different spatial channels, a new type of amplifier can be used. The so called Few Mode (FM) amplifier enables to amplify signals without separating the modes. Recently, two different type of FM amplifiers have been described, based either on erbium doped fiber amplification [15] or on distributed Raman amplification [16]. At the receiver side, signals enters the MDMUX where the different spatial modes are separated and reinserted into a SMF each. There, the different WDM channels are demultiplexed and sent into optical receivers.

In this thesis, coherent receiver and consequently DSP is considered only for communication over long distances.The peculiarity of this receiver for MDM reception is that it enables the decoupling of spatial modes lowering the effects of intermodal crosstalk. To allow mode separation, MIMO processing has to be generalized to the order N, with N being 2 times the number of processed spatial modes. The main drawback of full-MIMO DSP used with high number of modes is the increasing calculation complexity, as mentioned in the following section. One of my goals is to assess the possibility of exploiting the MIMO technology for groups of LP-modes based on MGDM concept described in paragraph 1.3. Otherwise, in order to greatly reduce system costs and receiver complexity in short transmission systems, coherent detection

is substituted with direct one taking into account the main performance limitation due to this particular choice. This last solution will be analyzed in chapter 4.

2.1.1 MIMO DSP complexity

The MIMO receiver in MDM transmission systems can be used not only to decouple the two polarizations but also the spatial modes. The main principle is that each MIMO input is injected into N Finite Impulse Response (FIR) filters, then summing up the N FIR filters outputs, one coming from each input, the N MIMO outputs can be formed. The filter taps of the FIR filters are continuously updated in order to adapt them to dynamic changes of the transmission channel along the link, such as polarization rotations and coupling between degenerate modes [17]. In addiction, MIMO processing can be also used to separate spatial modes that are nondegenerate. The main drawback of increasing the number of spatial modes, i.e. the system capacity, and consequently the order N of the MIMO processing is the substantial increase in computational complexity. In particular, the number of FIR filters scales quadratically with the MIMO order N. For example, a 2x2 MIMO receiver requires 4 FIR filters, 4x4 MIMO requires 16 FIR filters and so on. Thus, the number of FIR filters equal to N^2 can be considered as the parameter to evaluate the calculation complexity of the MIMO DSP. Assuming the 2x2 MIMO receiver with $N^2 = 4$ as the simplest one, its computational complexity is fixed to 1. Accordingly, the complexity of higher order MIMO receivers can be evaluated as $N^2/4$. Referring to a FMF which supports 15 spatial modes, the full-MIMO to recover the two polarizations of all the spatial modes has the order $N = 30$ so its complexity is equal to $30^2/4 = 225$ which is extremely greater than 1.

Moreover, the required minimum filter length, i.e. the number of filter taps, is proportional to the highest accumulated DMGD between the jointly processed modes [18]. Thus it increases linearly with the transmission distances and the DMGD value between two modes. Because the DMGD between two modes of different order is generally higher then the DMGD between two degenerate modes, the MIMO processing between two nondegenerate modes leads to an additional increase in filter length [10].

Considering the MGDM technique already explained in paragraph 1.3, the full-MIMO receiver is replaced with parallel MIMO equalizers for each group of propagating modes. Figure 2.2 compares these two structures of the coherent receiver in case of the exploitation of a fiber supporting the groups reported in Table 1.1. As it is possible to see, the required independent DSP

for groups A, B, C, D and E are respectively 2x2, 4x4, 6x6, 8x8 and 10x10 MIMO equalizers. With this second solution, the complexity of the MDM receiver is greatly reduced. On the one hand, the number of FIR filters, evaluated as reported before, decreases from 225 ($N = 30$) to a maximum of 25 ($N = 10$). On the other, since modes of a different order are no longer processed together, the required minimum filter length can be shorter than a full-MIMO equalizer.

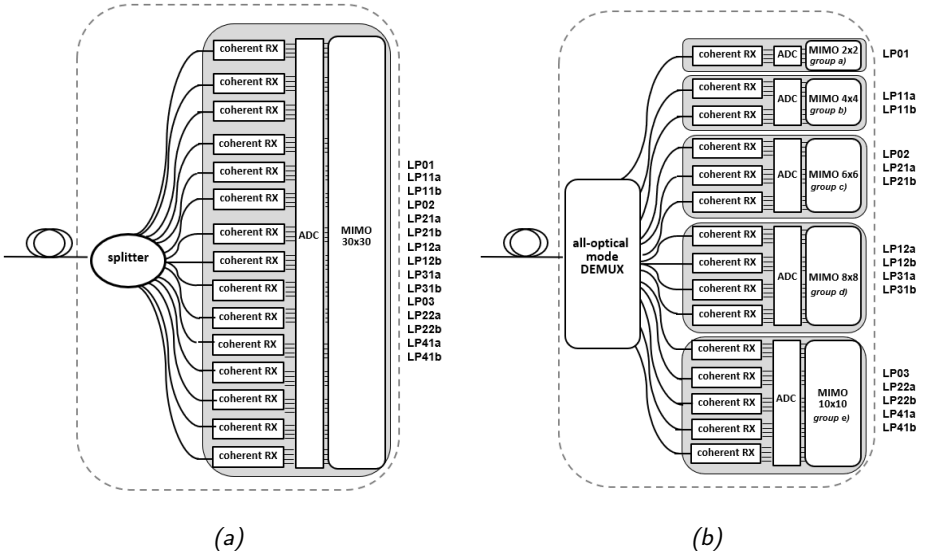

Figure 2.2. Structure of coherent receiver with full-MIMO (a) and with MIMO for mode groups (b) used to recover signals propagating on the supported LP-modes.

2.2 Low-DMGD 9-LP-Mode fiber

One of the main problems of a MDM system is that random mode crosstalk and modal dispersion in FMFs distort signals after propagation. In order to recover independent data channels at the receiver, MIMO technology is utilized. The increasing complexity of MIMO equalization, as discussed in 2.1.1, leads to higher power consumption for MDM receiver. To relive this problem, Sillard [14] recently proposed a solution to optimize and fabricate 9-LP-mode fibers with low DMGDs ($< 155\ ps/km$), low attenuations ($< 0.22\ dB/km$), large effective areas ($\geq 95\ \mu m$) and low bend losses at 1550 nm.

2.2.1 Design

For 9-LP-mode fibers, the normalized frequency V is set at 11.8, which is the highest possible value that allows the first nine LP modes to be guided. Then, the core radius, the *Alpha* which is the exponent of the graded-index shape core, and the trench are optimized to get the smallest possible DMGDs. An optimized profile, depicted in Figure 2.3, is obtained for a core radius of $14\mu m$, yielding a core-cladding index difference of $14.9 \cdot 10^{-3}$ for $V = 11.8$ at 1550 nm, an *Alpha* of 1.94 and a trench at 0.91 μm from the core and with a volume of 0.38 μm^2. The nine LP modes of the optimized profile

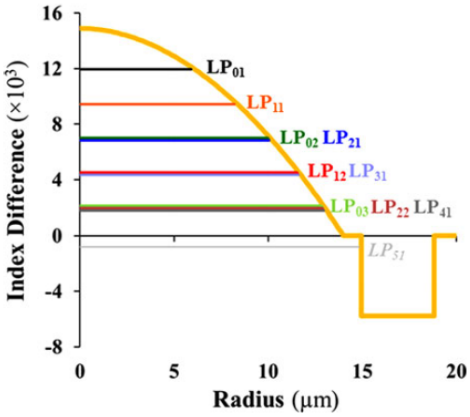

Figure 2.3. Theoretical index profile of the optimized 9-LP-mode fiber and effective indexes of the nine guided LP modes and of the most robust leaky LP_{51} mode [14].

can be divided into five mode groups, following what mentioned in 1.3. Its main characteristics are defined in [14]. In particular, it can be notice that the effective index differences between the guided mode groups are higher than $2.5 \cdot 10^{-3}$, which prevents from undesired coupling. Moreover, the maximum value of DMGD ($Max|DMGD|$) between the nine guided LP modes is as low as 24.4 ps/km, the chromatic dispersions are between 19.3 and 20.6 $ps/nm/km$ and the effective areas (A_eff) are above 100 μm^2 (from 104 μm^2 for the fundamental LP_{01} mode to 311 μm^2 for the LP_{03} mode), which limit intramode nonlinearity.

The core-cladding index difference of the 9-LP-mode fiber is only $\sim 0.2 \cdot 10^{-3}$ higher than that of standard $50\mu m$-diameter-core multimode fibers. Thus, the practical realization of the optimized 9-LP-mode fibers is possible using trench-assisted bend-insensitive multimode preforms appropriately scaled to reach a core radius of 14.1 μm in order to ensure $V = 11.8$. This

is done by targeting a preform diameter that is 1.77 times larger than that of the standard multimode preforms. As possible to see in Figure 2.4(a), the rescaled profile is very close to the optimized 9-LP-mode profile except for the trench. It is more closed to the core which causes a degradation in DMGDs, and its volume is smaller respect to the optimized one. The $Max|DMGD|$ moves from 24.4 to 138.2 ps/km, an extremely higher value but still acceptable [14]. Lastly, the A_{eff} and the chromatic dispersion are almost unchanged.

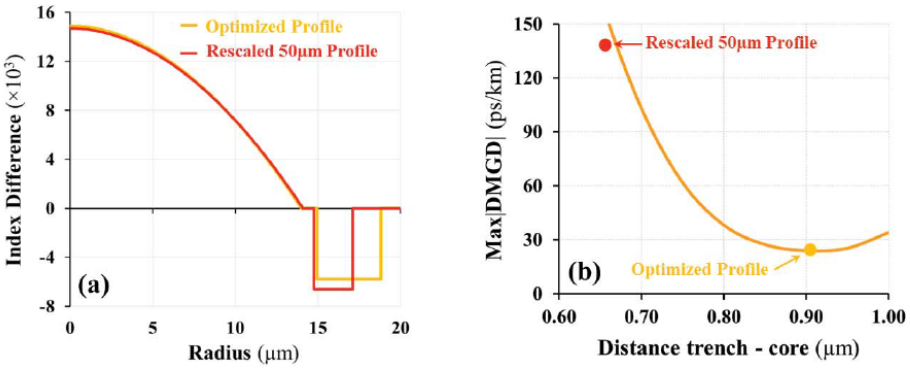

Figure 2.4. Index profiles of the optimized 9-LP-mode fiber and of the rescaled $50\mu m$*-diameter-core multimode fiber with* $V = 11.8$ *and core radius* $\sim 14\mu m$ *(a);* $Max|DMGD|$ *at* $1550nm$ *vs. distance of the trench from the core (b) [14].*

2.2.2 Fabrication and characterization

This 9-LP-mode fiber has been fabricated using a standard bend-intensive multimode perform with *Alpha* of 1.94 made with the Plasma Chemical Vapor Decomposition (PCVD) technique. Thanks to the accuracy of this process, the experimental index profile, shown in Figure 2.5(a), is very close to the rescaled one. The chromatic dispersion and A_{eff} of the fundamental LP01 mode has been experimental calculated respectively at 18 $ps/nm/km$ and 95 μm^2 and the attenuation for this germanium-doped-core structure was at 0.219 dB/km. The DMGDs have first been measured with the standard multimode DMGD setup using an input pulse duration of 50 ps. In Figure 2.5(b) can be seen that the $Max|DMGD|$ is 153 ps/km at 1550 nm. Note that only four peaks, regarding five mode groups, are depicted because the DMGD of mode groups B and C are almost identical.

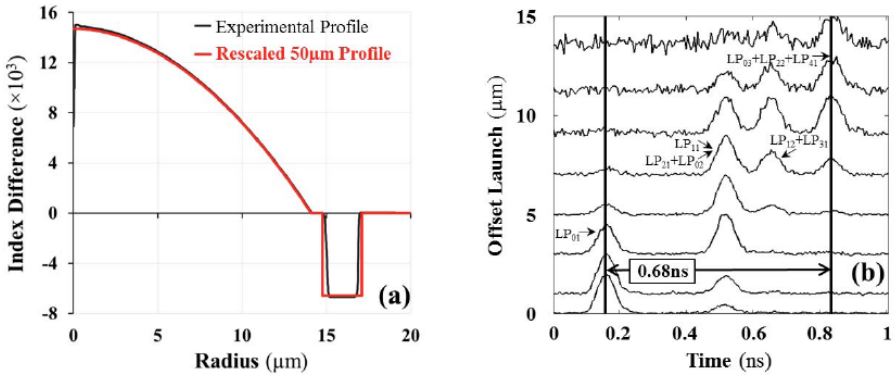

Figure 2.5. Experimental and theoretical rescaled 50μm-diameter-core multimode index profiles of 9-LP-mode fibers (a); DMGD plot of the rescaled multimode fiber at $1550nm$ *(b) [14].*

2.2.3 Further practical solutions to reduce DMGD into a 9-LP-mode fiber

As reported in Section 2.2.2, the theoretical low values of DMGDs cannot be reached in practice due to the sensitivity to profile variations during the manufacturing process. Thus, new improvements are needed in order to further reduce the complexity of MIMO receiver. In particular, two possible solutions, also combined together, can be implemented in order to compensate this sensibility effect. Firstly, an additional improvement in DMGD values is obtained by slightly adjusting the trench position of the bend-insensitive $50\mu m$-diameter-core multimode preform before rescaling [14]. Secondly, DMGD can be compensated using a concatenation of fibers with modes characterized by DMGDs with opposite signs [19].

Moreover, an other promising method to reduce Group Delay (GD) spread, recently proposed in [20], is the strong mode coupling. In fact, when modes in a FMF are weakly coupled, the GD spread increase linearly with transmission distance, otherwise it increases only with the square root of the transmission distance when modes are strongly coupled. This is due to the fact that, in strongly coupled conditions each MDM signal would have a nearly equal probability of traveling on different modes. Strong mode coupling, unlike weak mode coupling that occurs randomly in FMF, can be introduced intentionally using a typical structure called Long-Period Grating (LPG). Usually, a different grating is required for each pair of modes leading however to additional complexity and losses. For the first time, the possibility of using a series of uniform mechanical LPG with only one grating period has been experimentally demonstrated in [20] in order to couple all

modes in the 9-LP-mode graded-index FMF presented before. This solution can be implemented because the effective indices are nearly equally spaced thanks to the nearly-parabolic graded-index profile. Figure 2.6 shows the Root-Mean-Squared (RMS) pulse width, which represents the GD spread, in function of the measured loss as the force applied by LPG increases. As possible to see, the RMS width was reduced significantly while LPG induced loss remains negligibly. Moreover, it's important to underline that a reduction of RMS width consequently leads to smaller GD spread in the FMF and than to a lower complexity of MIMO DSP.

However, this problem will be not analyzed in this work, since we have assumed the use of MGDM technique (paragraph 1.3). As previously explained, each mode belonging to the same group is considered part of the same channel that allows the reception of different groups with independent MIMO equalizers. Therefore, the DMGD between modes of different order can be neglected.

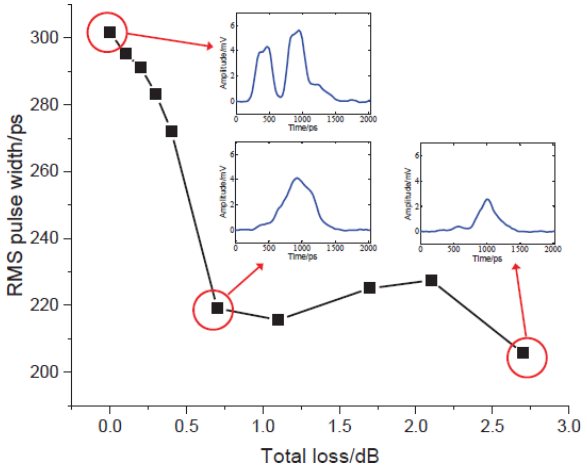

Figure 2.6. RMS pulse width as a function of measured loss inducted by 11 *LPGs. Three waveforms corresponding to different losses are represented [20].*

2.2.4 Mode coupling effects

The signal propagation is affected by imperfections and mechanical stress of the fiber which can cause the so-called mode coupling in MMFs and FMFs; their cumulative effects may become important after a long propagation length, so that they need to be taken into account.

Over the years, several models have been proposed to evaluate how propagation is affected by random variations of the optical and geometrical properties of the fibers. The most common approach is to derive and solve

the coupled power equations describing the evolution of the average optical power carried by the propagating modes [21]. Within appropriate limits, the coupling process can be ideally described in terms of a diffusion equation in which the mode number is treated as a continuous variable [22, 23]. In a recent paper, a new contribution to the diffusion approach has been presented for TE modes propagation in round fibers with a parabolic graded-index profile [24]. All these models take into account that coupling is caused by random imperfections or random fluctuations of the refraction index. Despite the advanced and sophisticated methods for manufacturing graded-index MMF, these small impairments are impossible to avoid. Thus, the presence of intermodal crosstalk due to mode coupling during in-fiber propagation must be considered for our simulations.

However, specific information about propagation mode coupling of the presented graded-index 9-LP-mode fiber is not available in the literature. Thus, the values that will be used for our simulations have been derived from some crosstalk measures related to FMFs with a lower number of modes [25, 26, 27]. In particular, the integrated propagation crosstalk between all modes of a 4-LP-mode fiber, always realized by Prysmian Group, results to be $-23\ dB$ after 10 km span, i.e. $-33\ dB/km$ [26]. With the hypothesis that coupling is dominated by transitions between nearest guided modes [25], it has been decided to approximate the propagation crosstalk equal to $-25\ dB/km$ and $-40\ dB/km$ between modes belonging to first-neighbouring and second-neighbouring groups, respectively. These are reasonable values considering that having an higher number of modes in a fiber core leads to a smaller effective refractive index difference between the guided mode groups. Therefore, even small index fluctuations could cause a higher mode coupling. However, the propagation crosstalk between modes inside more distant groups is still negligible since the difference between the indexes is much greater than $2.5 \cdot 10^{-3}$ (paragraph 2.2.1). Table 2.1 lists the considered crosstalk values in dB/km for each mode supported in the 9-LP-mode fiber.

2.3 Mode-MUX and Mode-DEMUX

In order to realize a full mode multiplexed transmission system with a FMF is required the use of MMUX and MDMUX. Over the years several design strategies have been proposed to build a MMUX. A conventional solution is to use binary phase plates to convert single mode LP01 from a SMF to a higher order LP mode [28]. Each mode is generated with a specific phase plate and all the generated LP modes are superposed together into the FMF fiber with a succession of beam splitters. The main drawback of this

	LP01	LP11a	LP11b	LP21a	LP02	LP21b	LP31a	LP12a	LP12b	LP31b	LP41a	LP22a	LP03	LP22b	LP41b
LP01	N.A.	-25	-25	-40	-40	-40	-inf	-inf	-inf	-inf	-inf	-inf	-inf	-inf	-inf
LP11a	-25	N.A.	N.A.	-25	-25	-25	-40	-40	-40	-40	-inf	-inf	-inf	-inf	-inf
LP11b	-25	N.A.	N.A.	-25	-25	-25	-40	-40	-40	-40	-inf	-inf	-inf	-inf	-inf
LP21a	-40	-25	-25	N.A.	N.A.	N.A.	-25	-25	-25	-25	-40	-40	-40	-40	-40
LP02	-40	-25	-25	N.A.	N.A.	N.A.	-25	-25	-25	-25	-40	-40	-40	-40	-40
LP21b	-40	-25	-25	N.A.	N.A.	N.A.	-25	-25	-25	-25	-40	40	-40	-40	-40
LP31a	-inf	-40	-40	-25	-25	-25	N.A.	N.A.	N.A.	N.A.	-25	-25	-25	-25	-25
LP12a	-inf	-40	-40	-25	-25	-25	N.A.	N.A.	N.A.	N.A.	-25	-25	-25	-25	-25
LP12b	-inf	-40	-40	-25	-25	-25	N.A.	N.A.	N.A.	N.A.	-25	-25	-25	-25	-25
LP31b	-inf	-40	-40	-25	-25	-25	N.A.	N.A.	N.A.	N.A.	-25	-25	-25	-25	-25
LP41a	-inf	-inf	-inf	-40	-40	-40	-25	-25	-25	-25	N.A.	N.A.	N.A.	N.A.	N.A.
LP22a	-inf	-inf	-inf	-40	-40	-40	-25	-25	-25	-25	N.A.	N.A.	N.A.	N.A.	N.A.
LP03	-inf	-inf	-inf	-40	-40	-40	-25	-25	-25	-25	N.A.	N.A.	N.A.	N.A.	N.A.
LP22b	-inf	-inf	-inf	-40	-40	-40	-25	-25	-25	-25	N.A.	N.A.	N.A.	N.A.	N.A.
LP41b	-inf	-inf	-inf	-40	-40	-40	-25	-25	-25	-25	N.A.	N.A.	N.A.	N.A.	N.A.

Table 2.1. Values of propagation crosstalk [dB/km] for all 15 spatial modes propagating into 9-LP-mode fiber.

design is that the intrinsic splitting loss scales up with the number of modes.

Another technique is to use a photonic lantern [29], where N input SMF are adiabatically transformed into a single FMF. On one hand, this method enables to have very low insertion loss and mode dependent loss, but on the other, the crosstalk between modes is still too high [30]. Thus, this last type of Multiplexer (MUX) is mainly implemented for strongly coupled approach.

Focusing on weakly coupled solutions, recently, Cailabs company have developed a new type of MMUX based on MPLC. This particular technique is able to achieve multiplexing to any set of spatial modes, with low intrinsic loss whatever the number of modes while achieving a very low level of crosstalk, for a broad wavelength range from 1530 to 1565 nm [31]. Firstly it can be useful to see how MPLC works because the MDM system described in this thesis exploits a 15-mode-selective MUX, designed by Cailabs and based on this particular technique.

2.3.1 Multi-Plane Light Conversion technique

MPLC is a multiplexing technique which allows to perform any unitary spatial transform. In particular, spatial multiplexing converts N separate input beams into N orthogonal propagation modes of a FMF. Theoretically, the Multi-Plane Light Converter is a succession of transverse phase plates profiles, generally built using phase plates or Spatial Light Modulator (SLM),

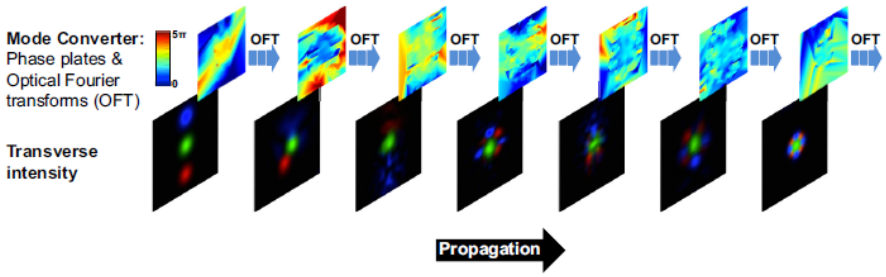

Figure 2.7. MPLC as spatial multiplexing technique. Top line shows the succession of transverse phase profiles and optical Fourier transforms and the second line the evolution of the transverse intensity in the plane of the phase plate [31].

separated by optical Fourier transforms. Figure 2.7 reports an example of unitary transform between an input and an output plane. The full theoretical decomposition of a unitary transform into a succession of phase profiles in general requires an unpractical number of elements, on the order of $17(N^2-N)$, where N is the number of pixels chosen in the transform description [32]. On the other hand, as empirically demonstrated in [32], when practical situations are considered, with K number of inputs and outputs, the number of phase profiles can be approximated to $2K+1$. Since the phase plates, unlike the conventional beam splitters, are lossless elements, one of the advantages is that the losses are caused only by imperfections of optical elements.

Practically, the MPLC is implemented using a multipass cavity, where the successive transverse phase profiles are all printed on a single reflective phase plate and the optical Fourier transforms are obtained by propagation and reflections on a spherical mirror. The mirror and the phase plate forms the cavity allowing to perform successive phase profiles and optical transforms. As shown in Figure 2.8 which reports an example of experimental setup with 3 reflections, the phase plates are generated on a reflective liquid crystal on silicon. As possible to see, three SMF are connected to a fiber array creating a bundle of fibers, than at the output, the microlens array is used to collimate the three beams in free space. Subsequently, the beams are sent to the multipass cavity and at the output a D-shaped mirror is used to extract the final beam. As demonstrated in [31], the spatial MUX and Demultiplexer (DEMUX) based on MPLC achieve high mode selectivity ($> 23\ dB$) with a coupling loss on the order of other mode selective MUXes ($< 4.1\ dB$) across the full C-band. With this technique the highest losses are the optical ones which could be decreased with better coatings on the optical elements, whereas the insertion losses are lower than $1.2\ dB$. Finally,

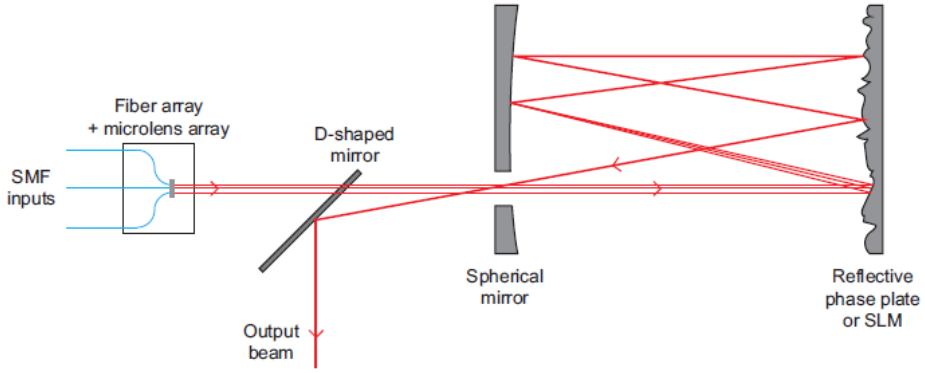

Figure 2.8. Experimental setup of the MPLC in a multipass cavity with three reflections on the phase plate [31].

MPLC is able to address any spatial mode profile with high fidelity, and can be applied to multiplex a higher number of spatial modes by increasing the number of reflections in the multipass cavity.

2.3.2 Characterization of a mode-selective 15-mode spatial multiplexer

According to the description of MPLC reported in the previous section, Cailabs presented in [33] the characterization of two multiplexers supporting the first 15 spatial modes of a conventional graded-index MMF with 50μm-core-diameter. Each one of the 15 input SMFs is converted by the multipass cavity into one of the modes of the MMF. Figure 2.9 shows the converted output spatial modes in free space before coupling into a MMF when using a Super Luminescent Diode (SLD) centered at 1570 nm as light source and captured by a near-infrared camera with Indium Gallium Arsenide sensor. By measuring the input power and the matrix of output powers, the coupling efficiency and the modal crosstalk are evaluated for all modes. The obtained results have demonstrated that the two multiplexers show highest reported mode selectivity (average 23 dB) and good insertion losses (average 4.4 dB) over the full C+L band.

More recently, Cailabs produced a pair of spatial MUX supporting the first 15 Hermite-Gaussian modes (Proteus-C-15) optimized at 1550nm for 9-LP graded-index fiber from Prysmian previous described in 2.2. The first 15 Hermite-Gaussian modes have a direct correspondence with the first LP modes showed in Figure 2.9. The characterization of the 15-mode multiplexers has been done by measuring the transmission matrix of a Back-To-Back (B2B) system comprising a Proteus MUX, the FMF and a Proteus

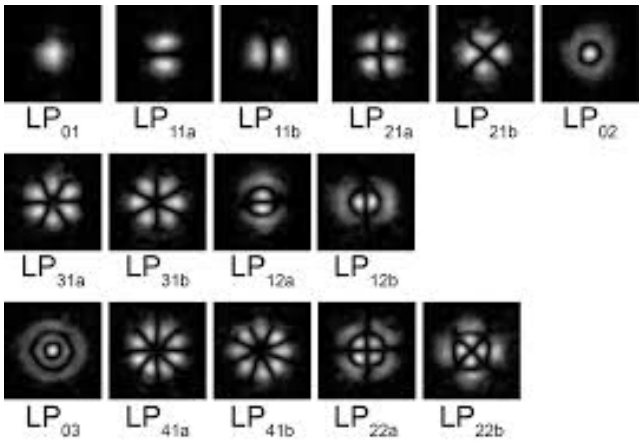

Figure 2.9. Free space output of the 15-mode MUX using a SLD source [33].

	LP01	LP11a	LP11b	LP21a	LP02	LP21b	LP31a	LP12a	LP12b	LP31b	LP41a	LP22a	LP03	LP22b	LP41b
LP01	N.A.	-19.5684	-19.5684	-28.6598	-28.6598	-28.6598	-29.9507	-29.9507	-29.9507	-29.9507	-36.9543	-36.9543	-36.9543	-36.9543	-36.9543
LP11a	-20.4549	N.A.	N.A.	-22.7925	-22.7925	-22.7925	-25.4747	-25.4747	-25.4747	-25.4747	-28.4723	-28.4723	-28.4723	-28.4723	-28.4723
LP11b	-22.1158	N.A.	N.A.	-22.3318	-22.3318	-22.3318	-25.0898	-25.0898	-25.0898	-25.0898	-26.6983	-26.6983	-26.6983	-26.6983	-26.6983
LP21a	-28.3349	-23.7276	-23.7276	N.A.	N.A.	N.A.	-20.7495	-20.7495	-20.7495	-20.7495	-25.929	-25.929	-25.929	-25.929	-25.929
LP02	-29.8714	-21.1174	-21.1174	N.A.	N.A.	N.A.	-21.664	-21.664	-21.664	-21.664	-26.0483	-26.0483	-26.0483	-26.0483	-26.0483
LP21b	-30.933	-20.9869	-20.9869	N.A.	N.A.	N.A.	-22.6237	-22.6237	-22.6237	-22.6237	-25.858	-25.858	-25.858	-25.858	-25.858
LP31a	-31.3908	-25.893	-25.893	-22.6545	-22.6545	-22.6545	N.A.	N.A.	N.A.	N.A.	-19.9746	-19.9746	-19.9746	-19.9746	-19.9746
LP12a	-31.3694	-24.3285	-24.3285	-20.8584	-20.8584	-20.8584	N.A.	N.A.	N.A.	N.A.	-20.9702	-20.9702	-20.9702	-20.9702	-20.9702
LP12b	-28.3814	-25.0107	-25.0107	-22.8401	-22.8401	-22.8401	N.A.	N.A.	N.A.	N.A.	-21.0181	-21.0181	-21.0181	-21.0181	-21.0181
LP31b	-27.9723	-26.511	-26.511	-23.9736	-23.9736	-23.9736	N.A.	N.A.	N.A.	N.A.	-21.9862	-21.9862	-21.9862	-21.9862	-21.9862
LP41a	-28.7289	-26.8682	-26.8682	-24.1764	-24.1764	-24.1764	-18.2444	-18.2444	-18.2444	-18.2444	N.A.	N.A.	N.A.	N.A.	N.A.
LP22a	-27.6197	-29.9933	-29.9933	-23.36	-23.36	-23.36	-18.7488	-18.7488	-18.7488	-18.7488	N.A.	N.A.	N.A.	N.A.	N.A.
LP03	-32.1326	-29.1223	-29.1223	-22.9289	-22.9289	-22.9289	-18.3549	-18.3549	-18.3549	-18.3549	N.A.	N.A.	N.A.	N.A.	N.A.
LP22b	-32.4406	-26,5269	-26,5269	-23,8763	-23,8763	-23.8763	-19.0827	-19.0827	-19.0827	-19.0827	N.A.	N.A.	N.A.	N.A.	N.A.
LP41b	-32.1676	-24.1183	-24.1183	-23.963	-23.963	-23.963	-20.5975	-20.5975	-20.5975	-20.5975	N.A.	N.A.	N.A.	N.A.	N.A.

Table 2.2. B2B crosstalk performance for 15 modes with full MMUX + MDMUX (Proteus).

Modes	LP01	LP11a	LP11b	LP21a	LP02	LP21b	LP31a	LP12a	LP12b	LP31b	LP41a	LP22a	LP03	LP22b	LP41b
B2B coupling efficiency	-7.67	-7.27	-7.15	-7.54	-7.34	-7.23	-7.84	-7.48	-7.03	-7.79	-8.48	-9.16	-8.51	-8.55	-8.59

Table 2.3. B2B coupling efficiency for 15 spatial modes for a pair of Proteus.

DEMUX. The crosstalk is measured sending power sequentially to each of the MUX inputs and for each of them evaluating the output power at each of DEMUX outputs. Table 2.2 reports the measured crosstalk matrix for a B2B system using the SLD source, and 2.3 shows the insertion losses of each channel. The average B2B crosstalk value is $-22.8\ dB$ and the average insertion loss is 7.80 dB. Such performances enable lower DSP complexity in MDM transmission systems over a large number of modes.

Chapter 3

MDM transmission for long-medium haul optical networks

This third chapter is dedicated to the performance analysis of an MDM system exploiting the use of the considered 15-spatial modes (5 groups) FMF and the other optical components, fully described in Chapter 2, in a long-medium haul scenario. Because of the complexity of the full-MIMO at the receiver, the possibility of MGDM has been investigated taking the advantage of simpler MIMO equalizers (paragraph 1.3). Thus, the maximum reachable distance for different groups combinations and M-QAM modulation formats has been calculated by highlighting the impact of intermodal crosstalk on the system performance. As mentioned in section 1.2.1, crosstalk will be evaluated in terms of two different contributions: the "propagation crosstalk" accumulated during signals propagation over multiple modes into the FMF and "node crosstalk" due to the presence of pairs of MMUX and MDMUX at the nodes and the transmitter and receiver sides in the traveled distance. First of all, the used analytical simulator is described in detail in order to understand under which hypothesis the reported results have been observed.

3.1 Simulator description

The analytical model, on which the simulations developed in this thesis are based, assumes that mode crosstalk and Kerr fiber nonlinearities can be considered as an Additive White Gaussian Noise (AWGN).

3.1.1 Gaussian Noise model for intramodal nonlinear effects

The Nonlinear Interference (NLI) due to Kerr effect is one of the main limitation of the long-haul transmission systems. Over the years, several approximated models have been proposed in order to describe NLI in a simple but accurate way. In particular, as discussed in [34], the signal propagating on Uncompensated Transmission (UT) links appears to be Gaussian due to the accumulated dispersion and, after the DSP, the received constellation points seem to follow a Gaussian statistical distribution. These two mentioned properties are the reason why nonlinearities are often modeled as a Gaussian noise that can be simply added to Amplified Spontaneous Emission (ASE) noise introduced by the optical amplifiers.

Two different perturbative approaches have been proposed to model nonlinear propagation in UT fiber links: the Volterra Series (VS) based on the truncated solution of the nonlinear Schroedinger equation (NLSE) and the Four-Wave Mixing (FWM) modeling of nonlinear beating during propagation. Recently, Poggiolini proposed a new FWM-like approach named Gaussian Noise (GN) model which is widely described in [35]. Its name remarks the fundamental assumptions of modeling the signal and NLI effects as GN. According to these hypothesis, the SNR can be expressed as

$$SNR = \frac{\overline{A^2}}{\sigma^2_{ASE} + \sigma^2_{NLI}}, \tag{3.1}$$

where $\overline{A^2}$ is the average of the squared distance of the noise-less signal constellation points from the origin, σ^2_{ASE} is the ASE noise variance about each point and σ^2_{NLI} represents the independent contribution of the NLI noise. This last term, as reported in [36], depends on the NLI noise Power Spectral Density (PSD), $G_{NLI}(f)$. After some analytical steps, [35] defines the final expression for the PSD of the dual-polarization NLI noise as

$$\begin{aligned} G_{NLI}(f) =& \frac{16}{27}\gamma^2 L^2_{eff} \int_{-\infty}^{\infty}\int_{-\infty}^{\infty} G_{WDM}(f_1) G_{WDM}(f_2) \\ & \cdot G_{WDM}(f_1 + f_2 - f) \cdot \rho(f_1, f_2, f) \cdot \chi(f_1, f_2, f) df_2 df_1, \end{aligned} \tag{3.2}$$

where γ is the fiber nonlinearity coefficient and L_{eff} is the effective length. This equation physically describes, through the FWM process, the beating of each spectral slice of the WDM signal with all others [35]. In fact, the factor $\rho(f_1, f_2, f)$ represents the normalized FWM efficiency of the beating of three pump frequencies $f_1, f_2, f = (f_1 + f_2 - f)$ and the integrand factor $G_{WDM}(f_1)G_{WDM}(f_2)G_{WDM}(f_1 + f_2 - f)$ represents the PSD that each of three pump carries. Finally, the phased array factor $\chi(f_1, f_2, f)$ takes into

account the coherent interference at the receiver location of the NLI produced at each span.

Equation (3.2) cannot be solved analytically so accurate approximations have been presented in [35]. In particular, the solution of the Nyquist-WDM case, over a single span, will be useful for the simulator modeling explained in the next paragraph. For this reason, the final expression to which we refer is

$$G_{NLI}(0) \approx \frac{8}{27} \frac{\gamma^2 G_{WDM}^3 L_{eff}^2}{\pi \beta_2 L_{eff,a}} asinh\left(\frac{\pi^2}{2} \beta_2 L_{eff,a} B_{WDM}^2\right), \tag{3.3}$$

where γ and L_{eff} are parameters already defined above, β_2 is the chromatic dispersion parameter, $L_{eff,a}$ is the asymptotic effective length in the limit of long span length, G_{WDM} is the average signal PSD over all the WDM bandwidth, B_{ch} is the bandwidth occupied by the signal in a single wavelength channel. In addiction, if $B_{ch} = \Delta f$ is imposed than

$$B_{WDM}^2 = B_{ch}^2 N_{ch}^{2\frac{B_{ch}}{\Delta f}}, \tag{3.4}$$

where N_{ch} is the number of WDM channels and Δf is the WDM frequency spacing.
Moreover if the link consists of a number N_s of identical spans, the equation (3.2) can be splits in two different contributions:

$$G_{NLI}(f) = G_{NLI}^{inc} + G_{NLI}^{cc}, \tag{3.5}$$

where the first term represents the incoherent noise accumulation expressed by

$$G_{NLI}^{inc}(f) = N_s \cdot G_{NLI}(f)|_{N_s=1} \tag{3.6}$$

and the second one is a sort of coherence correction which however can be neglected because relatively small respect to previous term. Thus, the final approximation consists of considering

$$G_{NLI}(f) \approx G_{NLI}^{inc}(f). \tag{3.7}$$

3.1.2 Analytical model of the simulator

The used simulator is based on an analytical model proposed in [37] allowing the calculation of the reaches for optically-amplified SDM medium-long distance coherent systems. The main goal is to evaluate the impairments due to the in-band crosstalk on SDM coherent transmission in terms of increase of the Error Vector Magnitude (EVM), defined as the root-mean-squared value of the difference between the received symbols and the reference

symbols. The following expression [38] can be used to approximate the BER, in case of ideal coherent detection of a square M-QAM format with Gray code bit mapping in presence of AWGN:

$$BER = 2\frac{\sqrt{M}-1}{\log_2 M\sqrt{M}} erfc\left(\sqrt{\frac{3\log_2 M}{2(M-1)}} SNR_{bit}\right), \tag{3.8}$$

where $M = 2^k$, with k even, is the number of symbols and SNR_{bit} is the SNR per bit, such that $SNR = k \cdot SNR_{bit}$. Starting from this equation, it is possible to express the BER as a function of the EVM by

$$BER = 2\frac{\sqrt{M}-1}{\log_2 M\sqrt{M}} erfc\left(\sqrt{\frac{3}{2(M-1)}} \frac{1}{EVM}\right). \tag{3.9}$$

Consequently, the target value of EVM_0 can be calculated in order to have a target BER_0 according this expression:

$$EVM_0 = \frac{\sqrt{\frac{3}{2(M-1)}}}{erfc^{-1}\left(\frac{\log_2 M\sqrt{M}}{2(\sqrt{M}-1)} BER_0\right)}. \tag{3.10}$$

The theoretical model, on which my simulations are based, is under the fundamental assumption of considering the equation (3.9) valid also in presence of crosstalk and Kerr fiber nonlinearities. Basically the effect of each of these two impairments is considered as an equivalent AWGN and so, the EVM in equation (3.9) is given by

$$EVM = \sqrt{\frac{1}{SNR} + \zeta^2 + \frac{\sigma^2_{NLI}}{P_s}}. \tag{3.11}$$

In particular, ζ^2 is the crosstalk parameter defined as the square root of the ratio between the average powers of the interferer and of the considered signal, and the P_s is the average power of each signal in a single wavelength, polarization and spatial mode. Moreover, the SNR after a number N_{spans} of spans can be calculated following the usual expression [39] for optically-amplified systems:

$$SNR = \frac{Ps}{h\nu FGR_s N_{span}}, \tag{3.12}$$

where h is the Plank's constant, ν is the optical frequency, F is the noise figure of the optical amplifier, G is the amplifier gain exactly compensating for the losses of each respective span and R_s is the symbol rate. Lastly, the σ^2_{NLI} parameter in equation (3.11) is the variance of the signal constellation

points due to the nonlinear interference modelled as AWGN according to the GN model discussed in the previous section. Under the hypotheses of incoherent noise sum, σ^2_{NLI} can be approximated as

$$\sigma^2_{NLI} \simeq G^{(span)}_{NLI}(0) N_{span} R_s, \tag{3.13}$$

where the $G^{(span)}_{NLI}(0)$ factor is evaluated by Equation 3.3.

Starting from equation (3.11) and from the reach calculation proposed in [37], a more accurate model has been developed in case of having two separate components of crosstalk such that $\zeta^2 = \zeta^2_{fix} + \zeta^2_{prop}$. The first term ζ^2_{fix} is the node crosstalk parameter and the second term ζ^2_{prop} represents the propagation crosstalk. According to this, equation (3.11) can be rewritten as

$$EVM = \sqrt{\frac{1}{SNR} + \zeta^2_{prop} + \frac{\sigma^2_{NLI}}{P_s} + \zeta^2_{fix}}. \tag{3.14}$$

Thus, the squared EVM is the sum of three terms directly proportional to the number of spans of the link and one term which depends only by the number n of nodes used in the fiber link. Consequently, it is possible to write the following relation for a single-span case not considering the latter parameter:

$$EVM^2_{span} = \frac{1}{SNR_{span}} \left(1 + \zeta^{2(span)}_{prop} + \frac{\sigma^{2(span)}_{NLI} SNR_{span}}{P_s} \right), \tag{3.15}$$

where the penalty factor due to propagation crosstalk and Kerr nonlinearity is evidenced by

$$Penalty_{prop} = \left(1 + \zeta^{2(span)}_{prop} + \frac{\sigma^{2(span)}_{NLI} SNR_{span}}{P_s} \right). \tag{3.16}$$

Taking into account a MDM system with a number N_{span} of spans and an optical amplifier at the end of each span, exactly compensating for the span losses, it is possible to analytically evaluate the reach for guaranteeing a target BER_0 and according to equation (3.9) a target EVM_0. In order to calculate the reach, it is necessary to find the maximum length L_{max} corresponding to the maximum number of span N_{max} for fulfilling the condition

$$EVM^2 = N_{span} EVM^2_{span} + n \cdot \zeta^{2(node)}_{fix} \leq EVM^2_0. \tag{3.17}$$

Moreover, a new penalty factor due to the node crosstalk can be defined as

$$Penalty_{fix} = \frac{1}{1 - n \frac{\zeta^{2(node)}_{fix}}{EVM^2_0}} \tag{3.18}$$

and, hence according to the previous equations and considering a proper margin factor, the reach can be calculated as

$$L_{max} = L_{span} N_{max} = L_{span} \left\lfloor \frac{EVM_0^2 \cdot SNR_{span}}{Margin \cdot Penalty_{prop} \cdot Penalty_{fix}} \right\rfloor, \quad (3.19)$$

where L_{max} is the length of each span.

3.2 Performance analysis of MDM transmission systems for a long-medium haul scenario

In this paragraph we analyze the performance which could be reach in a long-medium haul scenario exploiting MDM, and in particular MGDM. We propose several solutions to design high-capacity medium-long transmission systems with reduced DSP complexity. All the reported simulations are based on the analytical model previously described.

3.2.1 Simulation set-up

The transmission system architecture, which we refer to for this section, is depicted in Figure 3.1. The 15-mode-selective MUX is required to multiplex each spatial mode in a transmission line made by the 9-LP-mode fiber. We have analyzed several situations:

- point-to-point network with only mode-MUX at the transmitter and mode-DEMUX at the receiver;
- full-mesh network with a node at each fiber span;
- mesh network with a node in only some fiber spans;

Nodes include a pair of MMUX/MDMUX and are required to rout data traffic in a network. To compensate fiber attenuation, a FM amplifier is needed at each span. The fundamental optical component is the coherent receiver with DSP which allows compensating for chromatic dispersion and intermodal crosstalk.

In particular, we consider a structure of parallel MIMO equalizers for each supported mode groups to process jointly modes of the same order (paragraph 2.1.1). In order to simulate the signal propagation with different combinations of the 5 groups supported by the 9-LP-mode fiber, it is necessary to fix some parameters typical of the considered transmission system:

- R_s symbol rate = 28 *Gbaud*;

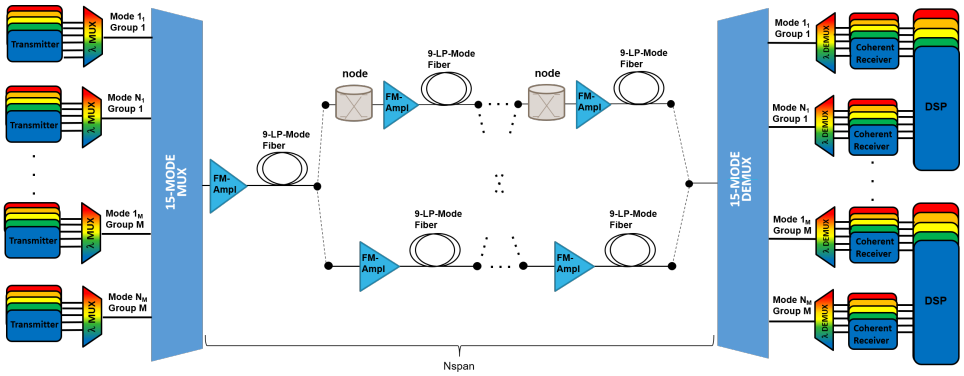

Figure 3.1. Schematic representation of the optical transmission system in a long-medium haul network scenario. In particular: λ-MUX/DEMUX, 15-mode MUX/DEMUX from Cailabs, the transmission line with 9-LP-Mode fiber span from Prysmian and FM amplifier, and coherent detection with DSP. At each fiber span, there may be nodes to route traffic.

- Δf frequency spacing = 37.5 GHz;
- N_{ch} number of WDM channel = 106 (whole C-band);
- α fiber attenuation = 0.22 dB/km;
- D chromatic dispersion = 16.7 $ps/nm/km$;
- A_{eff} effective area = $80\mu m^2$;
- F noise figure of optical amplifiers = $6dB$;
- possibility of three multiplexing technique combined together: WDM + PDM + MDM;
- modulation formats: 4-QAM, 16-QAM, 64-QAM;
- Hard-Forward Error Correction (FEC) with overhead of 7% which implies that the achievable bit rates with 4-QAM, 16-QAM and 64-QAM are 52.08, 104.16 and 156.24Gb/s, respectively.

The main goal is to evaluate the maximum reachable distances for having a target BER of $3.8 \cdot 10^{-3}$ by varying the order M of the QAM modulation and the length of the spans. As already mentioned, all simulations have been done considering only intramodal nonlinearities (intermodal nonlinearieties are neglected according what said in paragraph 1.2.3.2) and intermodal crosstalk caused by the presence of nodes and by the simultaneous propagation of

several modes into the fiber. The node crosstalk accumulated on each LP-mode has been calculated by using the measured real values concerning the Cailabs MMUX and MDMUX reported in Table 2.2. Instead, the propagation crosstalk has been approximated at $-25\ dB/km$ between pairs of modes of first neighbouring groups and at $-40\ dB/km$ between pairs of modes of second neighbouring groups (paragraph 2.2.4). These values are listed in Table 2.1.

3.2.2 Simulation results

First step has been to evaluate the performance obtained by means a 30x30 full-MIMO equalizer at the receiver in order to fully compensate the intermodal crosstalk. Under this hypothesis, the maximum reachable distance has been calculated by varying the transmitted power of two PDM signals between $-6\ dBm$ to $6\ dBm$ to find the optimal lunch power in case of different span lengths. Figure 3.2 reports respectively the calculation for 4-QAM, 16-QAM and 64-QAM. As possible to see, this ideal case allows to reach thousands of kilometers in the case of 4-QAM, but the maximum achievable distance decreases for higher order M. Nevertheless, also the case of 64-QAM remains in the order of hundreds of kilometres. In addiction, increasing the length of the span, maximum reach decreases due to lower SNR value after a span, i.e. higher noise. These first results show that the exploitation of a full-MIMO receiver could have a great potential in terms of transmission capacity. In fact, for each wavelength channel, it's possible to reach 1.56 , 3.12 and 4.69 $Tbit/s$ with 4-QAM, 16-QAM and 64-QAM respectively, and always covering very long transmission distances. However, having a 30x30 MIMO receiver is quite difficult today due to its high complexity (paragraph 2.1.1), so we looked for an alternative solution always trying to exploit multimode propagation to enhance the transmission capacity of the system. This is the case of MGDM that gives the possibility of choosing different combinations of the supported groups (A, B, C, D and E) exploiting at the receiver simpler MIMO equalizers to compensate only intermodal crosstalk between modes inside the same group (paragraph 1.3). The structure of the considered receiver is depicted in Figure 2.2 (b).

Initially, the maximum achievable distances have been calculated for a span length typical of metro networks, 80 km, by imposing its optimal launch power (0 dB for two polarizations) and always including intramodal nonlinearities. Table 3.1 shows respectively the non-null reach obtained for 4-QAM, 16-QAM and 64-QAM where several groups of LP-modes are considered. All the reported results have been evaluated in the case of

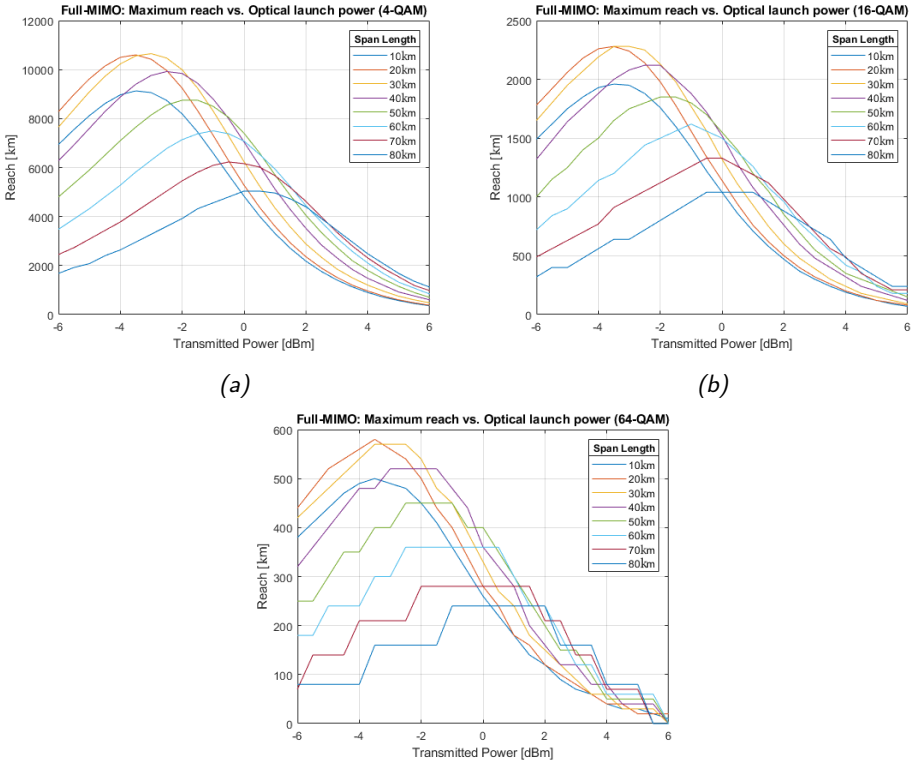

Figure 3.2. Maximum reach vs. optical transmitted power (PDM) with different span lengths for 4-QAM (a), 16-QAM (b) and 64-QAM (c) in case of full-MIMO

a point-to-point network with a MMUX at the transmitter and MDMUX at the receiver. For each combination of groups, the maximum achievable distances have been evaluated for each propagating mode. For example, in the case of combination $A + C$ with 4-QAM: mode LP01 (group A) can reach 400 km; instead, modes LP21a, LP02, LP21b (group C) can reach 1040 km. Obviously, the potential of mode LP01 is lower than the other excited modes because it is affected by a greater intermodal crosstalk. This is due to the fact that LP01 has three interfering modes, instead, LP21a, LP02, LP21b have only one. As we expect, the maximum reachable distances are reduced from the full-MIMO case. In addiction, we can said the intermodal crosstalk causes a substantial limitation on number of usable groups: only two or three mode groups could be use to exploit multimode propagation. As shown, reaching at least one span length is possible only with combinations of non-first neighbouring groups.

As already mentioned, in general a mesh network such as a MAN, presents

Point-to-point network (no crossed nodes) with Lspan = 80km					
Mode groups	**Maximum reach for each propagating group [km]**				
	LP01	**LP11a/LP11b**	**LP21a/LP02/LP21b**	**LP31a/LP12a/LP12b/ LP31b**	**LP41a/LP22a/LP02/ LP22b/LP41b**
4-QAM					
A+C	400	-	1040	-	-
A+D	4880	-	-	4960	-
A+E	4800	-	-	-	4960
B+D	-	240	-	560	-
B+E	-	4640	-	-	4880
C+E	-	-	160	-	400
A+C+E	400	-	160	-	400
16-QAM					
A+C	80	-	160	-	-
A+D	880	-	-	1040	-
A+E	880	-	-	-	1040
B+D	-	0	-	80	-
B+E	-	640	-	-	880
64-QAM					
A+D	80	-	-	240	-
A+E	80	-	-	-	240
B+E	-	0	-	-	80

Table 3.1. Point-to-point network with $80km$ span length: maximum reach (at $0dBm$ for PDM) for different groups combinations with 4-QAM, 16-QAM and 64-QAM.

several nodes required to route data traffic. Thus, it can be useful to see how system performance changes by adding a given number of nodes. Figure 3.3 shows the maximum reach varying with the number of nodes inserted in the link for some relevant cases. It's easy to understand that, for groups combinations with negligible propagation crosstalk ($A + D$, $A + E$, $B + E$), the maximum reach decreases linearly with the number of nodes. On the other hand, for the other combinations ($A + C$, $B + D$, $C + E$, $A + C + E$) the main limitation is propagation crosstalk since as the number of nodes increases, the traveled distances remains fairly constant.

According to this last consideration, it can be helpful to know the maximum cumulative propagation crosstalk, over a single span, in function of the number of link spans. In this way, it's possible to define in advance, knowing the propagation crosstalk parameters and the span length, which combination of groups choosing to cover a certain number of spans, always remembering that the reachable distances may vary according to the node crosstalk. Figure 3.4 shows the maximum propagation crosstalk supported at 0 dBm for two polarizations to cover a number of spans from 1 to 10 for the modulation formats previously considered. Furthermore, it can be said that, using the smallest order M, this limit is pretty equal for all lengths between 10 km and 80 km while, increasing the modulation order, it becomes more stringent for higher span lengths due to higher limitations of high-speed

modulation formats.

Afterwards we have tried to reduce the span length in order to enhance the system performance. As before, we have been evaluated the non-null reach obtained for 4-QAM, 16-QAM and 64-QAM using $-2\ dBm$ as transmission power for two polarizations (optimal value from Figure 3.2) and considering a point-to-point connection (MMUX at the transmitter and MDMUX at the receiver). We notice that the groups combinations covering at least one span length are the same of the 80 km span case. Thus, the maximum achievable capacities don't vary decreasing the span length because the effect of intermodal crosstalk is still to high. However, it's possible to have an improvement in the maximum reachable distances exploiting groups combinations with relatively small crosstalk values $(A+D, A+E, B+E)$. In fact, for these particular cases, the reachable distances are almost the same as what obtained in case of full-MIMO where only intramodal nonlinearieties impact on system performance. Figure 3.5 shows the maximum achievable capacities as function of reachable distances with $80km$ and $40km$ span lengths.

At the end, Table 3.2 and Table 3.3 summarize the obtained results with 80 km span in terms of maximum achievable capacities and maximum reach for a point-to-point interconnection and for a mesh network with a node for each span. As it is possible to notice, increasing the number of spatial modes leads to an higher transmission capacity. However, exploiting the MGDM, it's impossible to reach the same performance of a full-MIMO case due to the effect of intermodal crosstalk between modes belonging to different groups. Only some groups combinations can be excited to reach at least one span length. However, there are three combinations ($A+D$, $A+E$, $B+E$) which allows to reach more than 4500 km with at least 500 Gb/s (4-QAM) for each wavelength. They could be also a possible solution to design a mesh network with about ten nodes covering a total distance of at least 800 km with a capacity of 500 Gb/s. Increasing the order of the modulation allows to achieve 1 Tb/s but over shorter distances. As possible to notice, the 64-QAM modulation can be exploit only in a point-to-point connection reaching at most one span length. This is due to the fact that the node crosstalk is greater than the EVM target of this particular square format, a condition not allowed by the equation (3.18). In addiction, we have reported several solutions combining different modulation format for each group. In this way, the 64-QAM can be exploit in some cases also in a full-mesh network scenario. For example, it's possible to reach more than 150 km with combinations $A+D$ and $A+E$ using the 16-QAM, for group A which is the most affected by intermodal crosstalk, and the 64-QAM for the other mode group.

Point-to-point network with Lspan = 80km			
Mode groups	**Spatial modes**	**Total capacity [Gb/s]**	**Max reach [km]**
PDM-4QAM			
A	1	104.16	5040
A+C	4	416.64	400
A+D	5	520.80	4880
A+E	6	624.96	4880
B+D	6	624.96	240
B+E	7	729.12	4640
C+E	8	833.28	160
A+C+E	9	937.44	160
A+B+C+D+E (full-MIMO)	15	1562.40	5040
PDM-16QAM			
A	1	208.32	1040
A+C	4	833.28	80
A+D	5	1041.60	880
A+E	6	1249.92	880
B+E	7	1458.24	640
A+B+C+D+E (full-MIMO)	15	3124.80	1040
PDM-64QAM			
A	1	312.48	240
A+D	5	1562.40	80
A+E	6	1874.88	80
A+B+C+D+E (full-MIMO)	15	4687.20	240
PDM-Different modulation format for each mode group			
A(4QAM)+C(16QAM)	4	719.12	160
A(4QAM)+D(16QAM)	5	937.44	1040
A(16QAM)+D(64QAM)	5	1458.24	240
A(4QAM)+E(16QAM)	6	1145.76	1040
A(16QAM)+E(64QAM)	6	1770.72	240
B(4QAM)+D(16QAM)	6	1041.60	80
B(4QAM)+E(16QAM)	7	1249.92	880
B(16QAM)+E(64QAM)	7	1979.04	80

Table 3.2. Point-to-point network with $80km$ span: maximum achievable capacity (for each wavelength) and maximum reach for each combination of groups (at $0dBm$ for PDM).

Mesh network with Lspan = 80km				
Mode groups	**Spatial modes**	**Total capacity [Gb/s]**	**Crossed nodes**	**Max reach [km]**
PDM-4QAM				
A	1	104.16	62	5040
A+C	4	416.64	3	320
A+D	5	520.80	19	1600
A+E	6	624.96	18	1520
B+D	6	624.96	2	240
B+E	7	729.12	10	880
C+E	8	833.28	1	160
A+C+E	9	937.44	0	80
A+B+C+D+E (full-MIMO)	15	1562.40	62	5040
PDM-16QAM				
A	1	208.32	12	1040
A+C	4	833.28	0	80
A+D	5	1041.6	3	320
A+E	6	1249.92	3	320
B+E	7	1458.24	1	160
A+B+C+D+E (full-MIMO)	15	3124.8	12	1040
PDM-64QAM				
A	1	312.48	2	240
A+D	5	1562.40	0	80
A+E	6	1874.88	0	80
A+B+C+D+E (full-MIMO)	15	4687.20	2	240
PDM-Different modulation format for each mode group				
A(4QAM)+C(16QAM)	4	719.12	1	160
A(4QAM)+D(16QAM)	5	937.44	8	720
A(16QAM)+D(64QAM)	5	1458.24	1	160
A(4QAM)+E(16QAM)	6	1145.76	11	960
A(16QAM)+E(64QAM)	6	1770.72	2	240
B(4QAM)+E(16QAM)	7	1249.92	4	400

Table 3.3. Mesh network with $80km$ span (a node at each span): maximum achievable capacity (for each wavelength), maximum reach and number of crossed nodes for each combination of groups (at $0dBm$ with PDM).

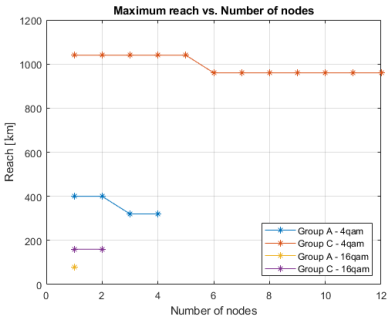

(a) A+C

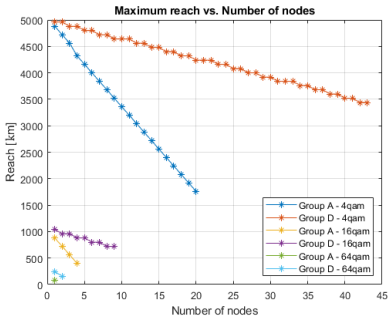

(b) A+D

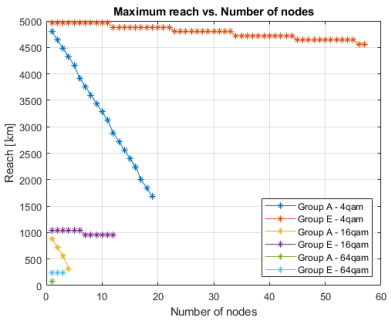

(c) A+E

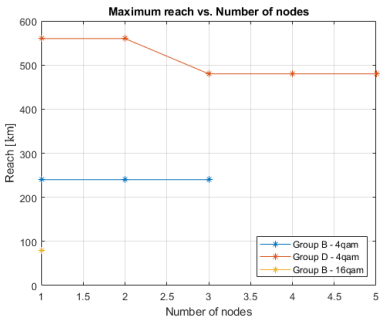

(d) B+D

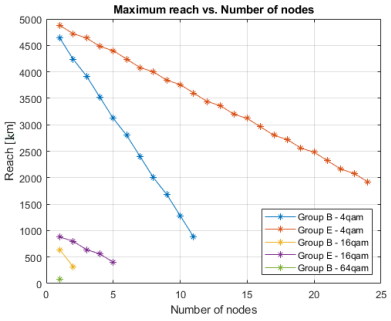

(e) B+E

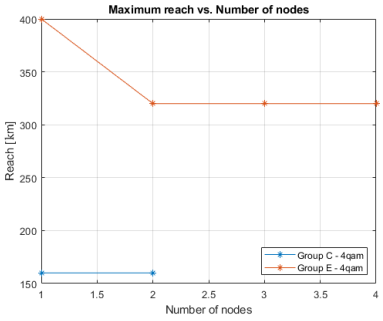

(f) C+E

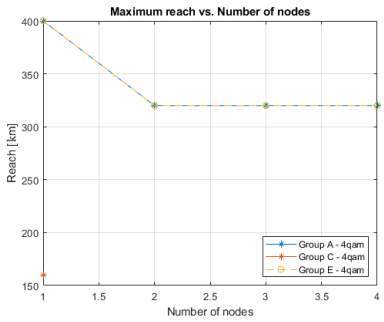

(g) A+C+E

Figure 3.3. Maximum reach vs. number of nodes in a network using $80km$ span length for different groups combinations.

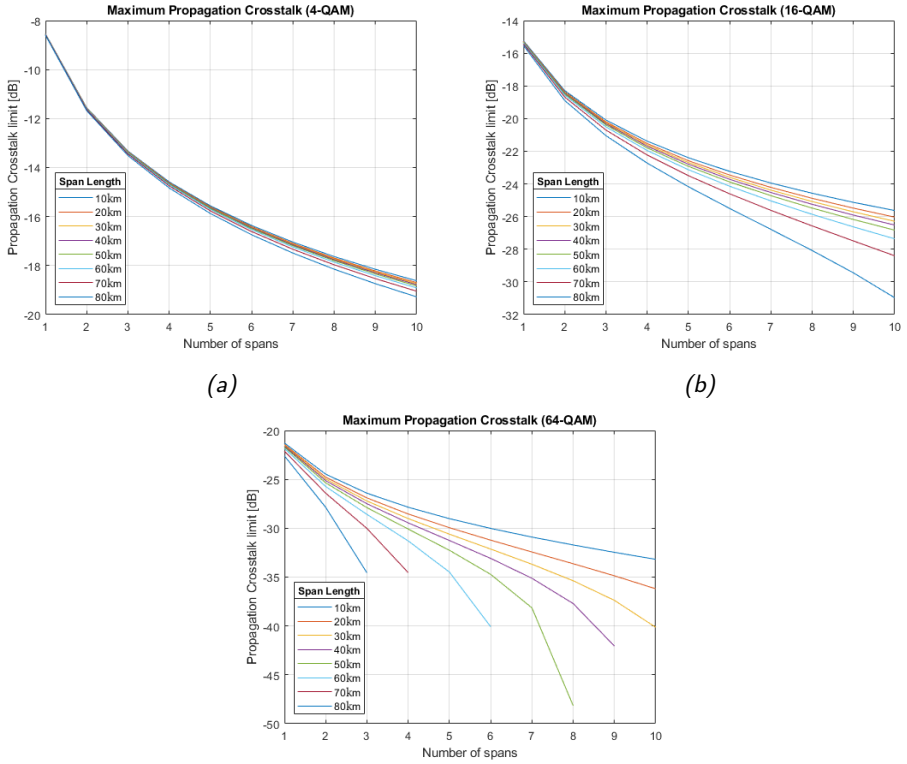

Figure 3.4. Maximum propagation crosstalk vs. number of spans with different lengths for 4-QAM (a), 16-QAM (b) and 64-QAM (c).

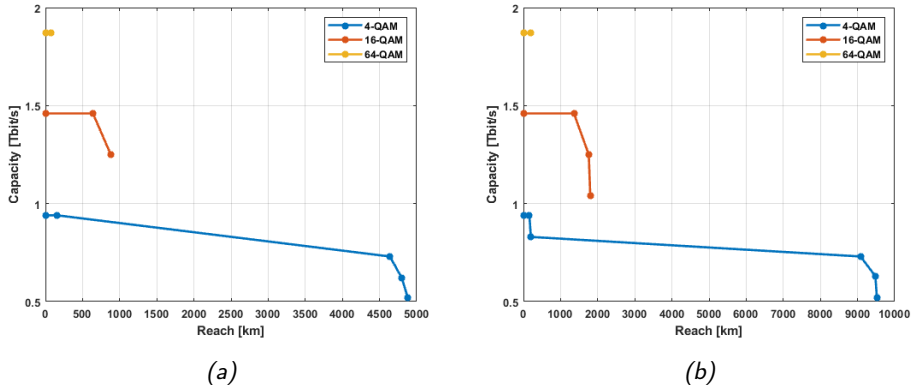

Figure 3.5. Maximum achievable capacities vs. reachable distances with 80km (a) and 40km (b) span length for 4-QAM, 16-QAM and 64-QAM.

3.2.2.1 System performance in case of a realistic MDM network

A MDM transmission system with the analyzed 9-LP-mode fiber has been already deployed in L'Aquila city in support of FIRST project which has the aim of demonstrating the effectiveness and the potential of SDM techniques. In particular, there is the possibility of testing the MDM propagation over installed fiber rings with spans of 6 km and 16 km. Thus, we have been evaluated the performance of this realistic network in the case of span lengths mentioned above. For each of them, two possible case are investigated: a point-to-point network (no crossed nodes) with MMUX in transmission and MDMUX in reception; a mesh network with a node for each span. The hypotheses and the parameters used for these particular simulations are the same as the previous ones.

As before, the first step has been to identify the optimal launch powers for the selected fiber lengths in case of 30x30 full-MIMO with only intramodal nonlinearities. They results to be -2.5 dBm, and -3.5 dBm (with two polarizations) respectively for 6 km and 16 km. Then, the maximum reachable distances with different mode groups combinations have been evaluated in order to exploit the MIMO technology to mitigate only the crosstalk between modes belonging to the same group. Thus, these simulations take into account, in addition to intramodal nonlinearities, the impairments due to node and propagation crosstalk between modes of different groups. On the one hand, Table 3.4 and Table 3.6 shows the case of a point-to-point network with 6 km and 16 km spans, respectively. On the other hand, Table 3.5 and Table 3.6 collects the obtained results in a full-mesh network with the same span length. Each of the tables shows the maximum achievable capacity and the maximum reachable distances specifying the corresponding groups of LP-modes with 4-QAM, 16-QAM and 64-QAM and with different modulation format for each group. The combinations of groups which allows to have a non-null reach are the same as before: the effect of intermodal crosstalk is still too high in the case of first neighbouring groups. However, the maximum reach in a point-to-point network with 4-QAM is more than 5000 km with $A + D$, $A + E$ and $B + D$. For the mesh network case, the number of crossed nodes is highlighted. Only with the 4-QAM modulation format it's possible to have at least 10 crossed nodes over hundreds of kilometers.

Observing these tables, the possibility of experimenting the increase in transmission capacity is highlighted by using particular combinations of groups in some possible topologies of a realistic MDM network. In particular, the maximum achievable capacities are in the order of Tb/s for each wavelength channel.

Point-to-point network with Lspan = 6km			
Mode groups	**Spatial modes**	**Total capacity [Gb/s]**	**Max reach [km]**
PDM-4QAM			
A	1	104.16	7830
A+C	4	416.64	426
A+D	5	520.80	7578
A+E	6	624.96	7554
B+D	6	624.96	306
B+E	7	729.12	7248
C+E	8	833.28	228
A+C+E	9	937.44	186
A+B+C+D+E (full-MIMO)	15	1562.40	7830
PDM-16QAM			
A	1	208.32	1686
A+C	4	833.28	84
A+D	5	1041.60	1434
A+E	6	1249.92	1416
B+D	6	1249.92	42
B+E	7	1458.24	640
C+E	8	1665.60	12
A+C+E	9	1874.88	6
A+B+C+D+E (full-MIMO)	15	3124.80	1686
PDM-64QAM			
A	1	312.48	426
A+C	4	1249.92	12
A+D	5	1562.40	174
A+E	6	1874.88	156
A+B+C+D+E (full-MIMO)	15	4687.20	426
PDM-Different modulation format for each mode group			
A(4QAM)+C(16QAM)	4	719.12	240
A(4QAM)+D(16QAM)	5	937.44	1626
A(16QAM)+D(64QAM)	5	1458.24	372
A(4QAM)+E(16QAM)	6	1145.76	1674
A(16QAM)+E(64QAM)	6	1770.72	414
B(4QAM)+D(16QAM)	6	1041.60	108
B(4QAM)+E(16QAM)	7	1249.92	1488
B(16QAM)+E(64QAM)	7	1979.04	228

Table 3.4. Point-to-point network with $6km$ span: maximum achievable capacity (for each wavelength) and maximum reach for each combination of groups (at $-2.5dBm$ for PDM).

Mesh network with Lspan = 6km				
Mode groups	**Spatial modes**	**Total capacity [Gb/s]**	**Crossed nodes**	**Max reach [km]**
PDM-4QAM				
A	1	104.16	1304	7830
A+C	4	416.64	24	150
A+D	5	520.80	30	180
A+E	6	624.96	27	168
B+D	6	624.96	8	54
B+E	7	729.12	12	78
C+E	8	833.28	4	30
A+C+E	9	937.44	4	30
A+B+C+D+E (full-MIMO)	15	1562.40	1304	7830
PDM-16QAM				
A	1	208.32	280	1686
A+C	4	833.28	4	30
A+D	5	1041.60	5	36
A+E	6	1249.92	5	36
B+D	6	1249.92	1	12
B+E	7	1458.24	1	12
C+E	8	1666.56	0	6
A+C+E	9	1874.88	0	6
A+B+C+D+E (full-MIMO)	15	3124.8	280	1686
PDM-64QAM				
A	1	312.48	70	426
A+C	4	1249.92	0	6
A+D	5	1562.40	0	6
A+E	6	1874.88	0	6
A+B+C+D+E (full-MIMO)	15	4687.20	70	426
PDM-Different modulation format for each mode group				
A(4QAM)+C(16QAM)	4	719.12	13	84
A(4QAM)+D(16QAM)	5	937.44	26	162
A(16QAM)+D(64QAM)	5	1458.24	5	36
A(4QAM)+E(16QAM)	6	1145.76	27	168
A(16QAM)+E(64QAM)	6	1770.72	5	36
B(4QAM)+E(16QAM)	7	1249.92	7	48

Table 3.5. Mesh network with $6km$ span (a node at each span): maximum achievable capacity (for each wavelength), maximum reach and number of crossed nodes for each combination of groups (at $-2.5dBm$ for PDM).

Point-to-point network with Lspan = 16km			
Mode groups	**Spatial modes**	**Total capacity [Gb/s]**	**Max reach [km]**
PDM-4QAM			
A	1	104.16	10224
A+C	4	416.64	432
A+D	5	520.80	9904
A+E	6	624.96	9872
B+D	6	624.96	304
B+E	7	729.12	9472
C+E	8	833.28	224
A+C+E	9	937.44	176
A+B+C+D+E (full-MIMO)	15	1562.40	10224
PDM-16QAM			
A	1	208.32	2192
A+C	4	833.28	80
A+D	5	1041.60	1862
A+E	6	1249.92	1840
B+D	6	1249.92	32
B+E	7	1458.24	1440
C+E	8	1666.56	16
A+B+C+D+E (full-MIMO)	15	3124.80	2192
PDM-64QAM			
A	1	312.48	560
A+D	5	1562.40	224
A+E	6	1874.88	208
A+B+C+D+E (full-MIMO)	15	4687.20	560
PDM-Different modulation format for each mode group			
A(4QAM)+C(16QAM)	4	719.12	240
A(4QAM)+D(16QAM)	5	937.44	2128
A(16QAM)+D(64QAM)	5	1458.24	480
A(4QAM)+E(16QAM)	6	1145.76	2176
A(16QAM)+E(64QAM)	6	1770.72	544
B(4QAM)+D(16QAM)	6	1041.60	112
B(4QAM)+E(16QAM)	7	1249.92	1936
B(16QAM)+E(64QAM)	7	1979.04	288

Table 3.6. Point-to-point network with $16km$ span : maximum achievable capacity (for each wavelength) and maximum reach for each combination of groups (at $-3.5dBm$ for PDM).

Mesh network with Lspan = 16km				
Mode groups	**Spatial modes**	**Total capacity [Gb/s]**	**Crossed nodes**	**Max reach [km]**
PDM-4QAM				
A	1	104.16	638	10224
A+C	4	416.64	15	256
A+D	5	520.80	28	464
A+E	6	624.96	27	432
B+D	6	624.96	6	112
B+E	7	729.12	13	208
C+E	8	833.28	3	64
A+C+E	9	937.44	3	64
A+B+C+D+E (full-MIMO)	15	1562.40	638	10224
PDM-16QAM				
A	1	208.32	136	2192
A+C	4	833.28	2	48
A+D	5	1041.60	5	96
A+E	6	1249.92	4	80
B+D	6	1249.92	0	16
B+E	7	1458.24	1	32
C+E	8	1666.56	0	16
A+B+C+D+E (full-MIMO)	15	3124.8	136	2192
PDM-64QAM				
A	1	312.48	34	560
A+D	5	1562.40	0	16
A+E	6	1874.88	0	16
A+B+C+D+E (full-MIMO)	15	4687.20	34	560
PDM-Different modulation format for each mode group				
A(4QAM)+C(16QAM)	4	719.12	8	144
A(4QAM)+D(16QAM)	5	937.44	23	384
A(16QAM)+D(64QAM)	5	1458.24	5	96
A(4QAM)+E(16QAM)	6	1145.76	26	432
A(16QAM)+E(64QAM)	6	1770.72	4	80
B(4QAM)+E(16QAM)	7	1249.92	7	128

Table 3.7. Mesh network with $16km$ span (a node at each span): maximum achievable capacity (for each wavelength) and maximum reach for each combination of groups (at $-3.5dBm$ for PDM).

3.2.3 Results discussion

All the reported results represent a satisfactory solution in trying to increase the transmission capacity of the optical system in a long-medium haul scenario and at the same time decreasing its computational complexity. The exploitation of MGDM has allowed to replace the full-MIMO equalizer with simpler MIMO receivers for supported mode groups. However, the impossibility of multiplying the transmission capacity by a factor 30 is due to the presence of node and propagation crosstalk between modes inside different groups; they are the main limiting effects in the absence of a full-MIMO DSP at the receiver. The mode coupling during fiber propagation between modes belonging to closest groups limits the usable groups combinations. We have noticed that in a point-to-point connection, for all the analyzed situations, it's possible to reach at least one span length only with non-first neighbouring groups. In addiction, when nodes are added to the network, the maximum reach decreases linearly due to the increase in node crosstalk.

We have proposed different solutions to design long-medium optical transmission systems with high potentialities. According to the capacity demand of the link, it's possible to select the best combination in terms of groups and modulation formats. Among all analyzed group combinations, the most promising solution is $A+D$. Table 3.8 shows the reachable distances and capacities in the case of a point-to-point connection or a full-mesh network. All studied span lengths and modulation formats are reported. As expected, in the case 80 km span, the covered distances by a point-to-point connection are always lower than 6 km and 16 km spans. This is a consequence of the typical propagation impairments in single mode fibers. However, in a full-mesh network, adding a node every 80 km allows to reach greater distances (node intermodal crosstalk has a lower impact). In general, 80 km is the typical span length exploited over long-medium transmission distances. However, the cases of 6 km and 16 km spans have been reported because obtained results could be experimentally validated by field trials in L'Aquila city. This particular group combination can allow to achieve 500 Gb/s, 1 Tb/s and 1.5 Tb/s with 4-QAM, 16-QAM and 64-QAM, respectively. Exploiting the use of different modulation format for each group, we can have a transmission capacity of 900 Gb/s with 4-QAM for A and 16-QAM for D or 1.4 Tb/s with 16-QAM for A and 64-QAM for D. These maximum reachable capacities are calculated for a single wavelength channel. In order to have the total achievable capacities for a transmission system exploiting WDM, PDM and MDM, these values must be multiplied by the number N_{ch} of employed wavelength channels. At the same time, the transmission of these selected 5

Group A+D			
Span length [km]	**Total capacity [Gb/s]**	**Maximum reach [km]**	
		Point-to-point network	**Mesh network**
PDM-4QAM			
6	520.80	7578	180
16	520.80	9904	464
80	520.80	4880	1600
PDM-16QAM			
6	1041.60	1434	36
16	1041.60	1862	96
80	1041.60	880	320
PDM-64QAM			
6	1562.40	174	0
16	1562.40	204	0
80	1562.40	80	0
PDM-4QAM(A)-16QAM(D)			
6	937.44	1626	162
16	937.44	2128	384
80	937.44	1040	720
PDM-16QAM(A)-64QAM(D)			
6	1458.24	372	36
16	1458.24	480	96
80	1458.24	240	160

Table 3.8. Maximum capacity and reach with $6km$, $16km$ and $80km$ span lengths: point-to-point transmission vs. full mesh network.

spatial modes allows to greatly reduce the DSP complexity: from 225 in the case of full-MIMO to a total of 17 (paragraph 2.1.1).

Chapter 4

MDM transmission for short-range applications

In this last chapter, we introduce the possibility of using the 9-LP-mode fiber for short-range communications.

On the one hand, we propose a low-cost solution that exploits MDM propagation to increase the transmission capacity to cover typical distances of inter and intra-datacenter connections. Thus, due to its high complexity, the coherent receiver has been replaced with the direct detection. This choice implies using easier modulation formats, i.e. OOK and 4-PAM. Without coherent detection, it is not possible to demultiplex the modes inside each group owing the lack of the necessary MIMO post-processing. Hence, only one mode with a single polarization inside the 5 supported groups can be excited to exploit multimode propagation. In addiction, we will see that the consequent lack of DSP in reception will cause also additional performance limitations due to the chromatic dispersion.

On the other hand, for the same application field, we propose to further reduce the cost of the optical system components. The idea is to assign mode groups on different wavelength channels to increase the WDM spacing between signals propagating on the same group. In this way, the wavelength interleaving between groups allows to recover signals on different wavelengths with common and cheap filters.

In the described scenario, the GN model used in the previous simulations can not be implemented because the required hypotheses are not satisfied. So first of all, a section has been dedicated to the description of the used simulator based on MATLAB® tool for this particular optical transmission system.

4.1 Simulator description

The results discussed in this chapter have been obtained by exploiting an existing MATLAB® simulator previously validated by comparing its results with the ones obtained by the commercial tool OPTSIM™ [40]. It simulates the signal transmission, its propagation through the fiber and its detection. The general structure of the simulator and the fundamental optical component implemented are reported below. The simulator is very flexible, thanks to the introduction of many flags. Therefore, even though we will present some results obtained with given parameters and conditions, the simulations can be adjusted for different purposes.

The propagating signal is generated according to the chosen modulation format: OOK or 4-PAM. Subsequently, the quantization with Digital-To-Analog Converter (DAC) device is required to convert a digital signal into continues one. Then, it is transformed in an optical one implementing a specific laser function.

The laser selected for our simulations is a Vertical Cavity Surface Emitting Laser (VCSEL) based on the InP (Indium phosphide) material system, characterized by emission along the vertical direction and a very short cavity [40]. On the one hand, this device which emits in the so-called C band, is more accessible, cheaper and with lower power consumption than a common Distributed Feedback (DFB) laser. On the other, because its cavity is so short, it leads to a substantial frequency variation, i.e. higher chirp effect. However, we have decided to simulate the external modulation of the laser source. This choice implies the use of an external device (Mach Zehender interferometer) which works as a switch controlled by the information to be transmitted, and in the meantime, the light source is kept on. As a consequence, the electro-optical bandwidth and the chirp depend directly by the modulator, so what characterized the selected source is only the laser linewidth.

Then, the generated optical signal is injected into the fiber. In particular, the fiber propagation is simulated by considering only linear impairments: fiber attenuation and chromatic dispersion. Since the travelled distances are very short, nonlinearities can be neglected. The output of the fiber function is the field itself. The signal amplification during propagation leads to the addiction of the standard ASE noise.

Finally, before signal detection, the effects of intermodal crosstalk introduced by the co-propagation of multiple modes are taken into account. Each interfering signal is generated with its proper level of interfering power and a frequency shift to simulate different laser source, and then summed to the

propagating signal. The simulator can also be easily adapted to transmit each supported mode on a different wavelength channel. In this case, each interfering mode must have an additional frequency shift equal to the distance in frequency between its wavelength channel and the λ-value of the reference signal.

Once the propagating signal has travelled through the fiber, a DEMUX filter can be used to emulate the separation of the corresponding wavelength multiplexed signals. Then, the signal generated in transmission is received with direct detection according to the selected modulation format. In practice, the direct receiver is made of a Photodiode (PD) which acts as a square-law detector; the phase information of the electric field is not recovered. Thus, a DFE can be used to reduce the effect of chromatic dispersion (paragraph 4.1.1). At the end, the signal that exits from the PD requires a second quantization by the Analogic-To-Digital Converter (ADC).

4.1.1 DFE equalizer

In the hypothesis of direct detention, as mentioned before, the signal is strongly degraded by the effect of chromatic dispersion during fiber propagation. Thus, we have decided to exploit a DFE equalizer to mitigate this particular linear impairment.

A DFE is a nonlinear equalizer that consists of a tapped delay line that stores samples from the input signal and contains a forward filter and a feedback filter to reduce Intersymbol Interference (ISI) [41]. In particular, DFE is implemented in the simulator using the *comm.DecisionFeedbackEqualizer* system object™ which is sketched in Figure 4.1.

DFEs can be of two different types: symbol-spaced equalizer, when the number K of samples per symbol is equal to 1, or symbol-spaced equalizer when $K > 1$. The input sample rate is K/T, while the output sample rate is always $1/T$.

The filter has L forward weights and $N - L$ feedback weights. They can be updated using different adaptive algorithms. The most common is Least Mean Square (LMS) algorithm which creates weights as

$$w_{new} = w_{current} + (StepSize) \cdot u \cdot e^* \tag{4.1}$$

where $w_{current}$ is the vector of current weights, u is the input vector and e^* is the complex conjugate of the error $e = d - y$.

In each symbol period, the equalizer receives K input samples at the forward filter and one training sample at the feedback filter. The equalizer

then outputs a weighted sum of the forward and feedback delay lines' values and updates the weights to be prepared for the next symbol period.

As we will see in next paragraphs, this particular equalizer can be useful to improve the quality of the received signals both in the presence of chromatic dispersion and intermodal crosstalk.

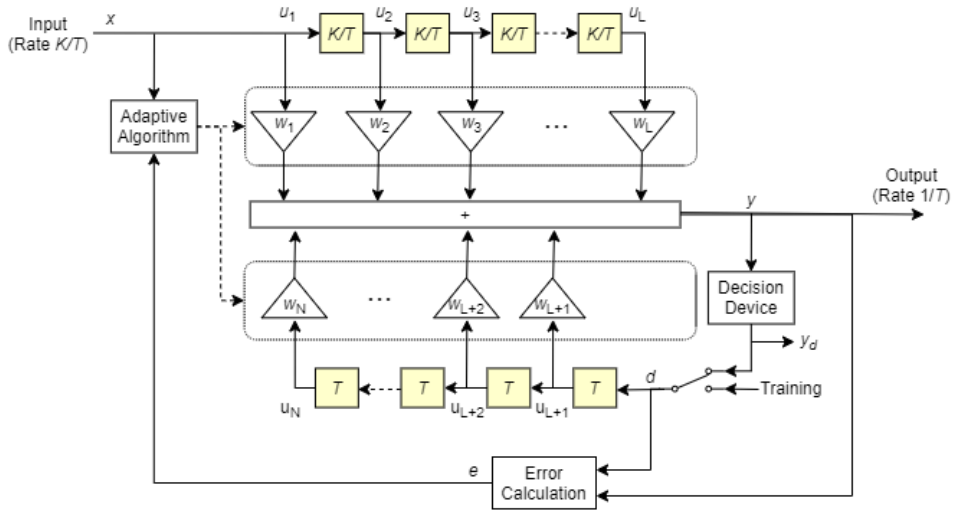

Figure 4.1. Schematic representation of a DFE equalizer [41]. At the top, the forward filter with L forward weights. At the bottom, the feedback weights with $N - L$ weights.

4.2 Performance analysis of MDM transmission systems for short-reach applications

In this section we analyze the performance which could be reach in a short-range application scenario exploiting MGDM. We propose several solutions to design high-capacity short transmission systems based on MDM propagation through the 9-LP-mode fiber. The reported results have been obtained through the simulator described in paragraph 4.1.

4.2.1 Simulation set-up

The general structure of the considered transmission system for these simulations is depicted in Figure 4.2. The MGDM propagation is possible thanks to 9-LP-mode fiber implementation in the transmission link (paragraph 2.2). In particular, we consider one only fiber span which is sufficient to design a system for point-to-point interconnection between intra and

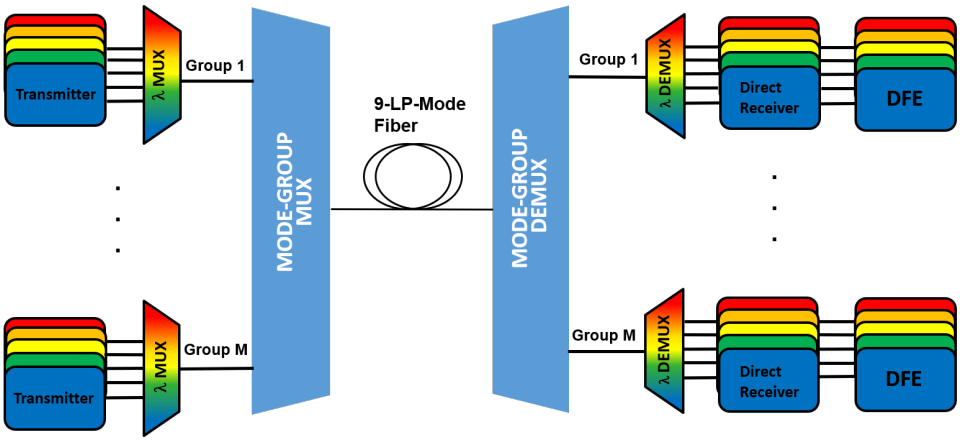

Figure 4.2. Schematic representation of short-range communication system architecture. At transmitter side: λ-MUX to combine wavelength channels, mode-group MUX to combine each supported group. Transmission line: 9-LP-mode fiber span. Receiver side: mode-group DEMUX to divide each supported group, λ-DEMUX to divide each wavelength channel, direct receiver and a potential implementation of a DFE equalizer.

inter-datacenters. In order to propose low-cost solutions, for this particular application, the direct receiver is preferred to the coherent one. This choice and the consequent lack of DSP in reception allows to excite only one mode inside a group in a single polarization. Therefore, the transmission capacity for each wavelength channel can be increased at most by a factor 5, which is the total number of supported groups. Thus, a mode-group MUX/DEMUX, corresponding to the 15-mode-selective MUX/DEMUX (paragraph 2.3.2), is required to combine/separate the five groups, composed by a single mode, into/from a single transmission line. This multiplexing/demultiplexing technology is available on the market and it is simpler than the 15-mode-selective MUX/DEMUX where all the 15 spatial modes must be multiplexed into the same transmission line and demultiplexed separately at the receiver; more precisely, in the multiplexing part, one arbitrary mode of each supported mode group is excited and after propagation in the 9-LP-mode fiber, due to the large intra-mode group coupling, all the modes of the same mode group need to be detected simultaneously.
General hypothesis of the simulated scenario:

- modulation formats: OOK and 4-PAM;
- VCSEL laser source with external modulation;
- linear fiber propagation with only attenuation and chromatic dispersion

effects (nonlinearities are neglected due to short distance traveled);

- direct detection and a potential using of a DFE;

The principal parameters used are:

- R_s symbol rate = 28 $Gbaud$;
- roll-off = 1;
- laser parameters typical of VCSEL and opportunely adapted to simulate external modulation: $alpha$ line enhancement factor = 0, adiabatic chirp coefficient $k = 0.83 \cdot 10^{13}$, modulation amplitude $ModAmpl = 17.99\ mA$, $Bias = 9\ mA$, f_p parasitic cut-off frequency = 35 GHz, f_r relaxation resonance frequency = 35 GHz;
- fiber linear effects parameters: α fiber attenuation = 0.22 dB/km and D chromatic dispersion = 16.7 $ps/nm/km$;
- N_{span} number of fiber spans = 1;
- DFE parameters: N_{samp} number of samples per symbols = 2, fw_{tap} number of forward taps = 9, fb_{tap} number of feed-back taps = 1, LMS adaptive algorithm with $StepSize = 0.01$;

To simulate the co-propagation of modes into the same core fiber, we have to take into account the precence of intermodal crosstalk. The values of crosstalk due to the presence of mode-group MUX/DEMUX are derived from Table 2.2 as follows. Since only one mode inside a group can be used, we have decided to select the mode with the higher crosstalk imposed on other modes of a different group. In this way, the worst possible combination of modes is considered. From this point of view, when we refer to a specific group, we are considering a generic mode belonging to that group. Table 4.1 reports the crosstalk values selected according this last consideration. The values of propagation crosstalk are assumed to be $-25\ dB/km$ between two first neighbouring group and $-40\ dB/km$ between two second neighbouring group (paragraph 2.2.4).

The main idea of the simulations is to evaluate the system performance in terms of BER by varying the value of the received power when multiple modes propagate into the fiber. Different span lengths have been simulated to understand the maximum reach with several groups combinations.

	A	B	C	D	E
A	N.A.	-19.5684	-28.6598	-29.9507	-36.9543
B	-20.4549	N.A.	-22.3318	-25.0898	-26.6983
C	-28.3349	-20.9869	N.A.	-20.7495	-25.858
D	-27.9723	-24.3285	-20.8584	N.A.	-19.9746
E	-27.6197	-24.1183	-22.9289	-18.2444	N.A.

Table 4.1. Worst values of B2B crosstalk with mode-group MUX/DEMUX.

4.2.2 Simulation results

The first step was to evaluate a single-mode transmission performance in the considered scenario using different fiber span lengths.

Figure 4.3 and Figure 4.4 show the case of OOK and 4-PAM modulation formats, respectively. As it is possible to see, without equalization, the maximum reachable distances are quite short. In specific, the propagation reaches at most 15 km with OOK and 5 km with 4-PAM. The system performance is limited by the chromatic dispersion, which can be partially compensated by a DFE. In fact, signal equalization allows reaching at least 25 km with OOK and 15 km with 4-PAM. As expected, distances covered with 4-PAM are lower than OOK due to higher intrinsic degradation.

In the case of OOK, received powers vary from -20 dBm to -14 dBm; instead, in the case of 4-PAM, they vary from -18 dBm to -10 dBm. Thus, in general, 4-PAM requires more power to obtain the same BER

Then, multimode propagation has been simulated considering several numbers of modes choosing the most suitable combination in terms of accumulated crosstalk:

- 5 modes: $A + B + C + D + E$ (only possible);
- 4 modes: $A + B + D + E$ combination allows to have each propagating mode with only one first neighbouring mode;
- 3 modes: $A + C + E$ combination allows to have each propagating mode with only second neighbouring modes;
- 2 modes: $A + E$ combination allows to have each propagating mode with lower node crosstalk (propagation crosstalk is negligible);

We have simulated the co-propagation of modes belonging to the chosen combinations with OOK and 4-PAM modulation formats without/with the use of the equalizer. For each combination, BER values are measured by

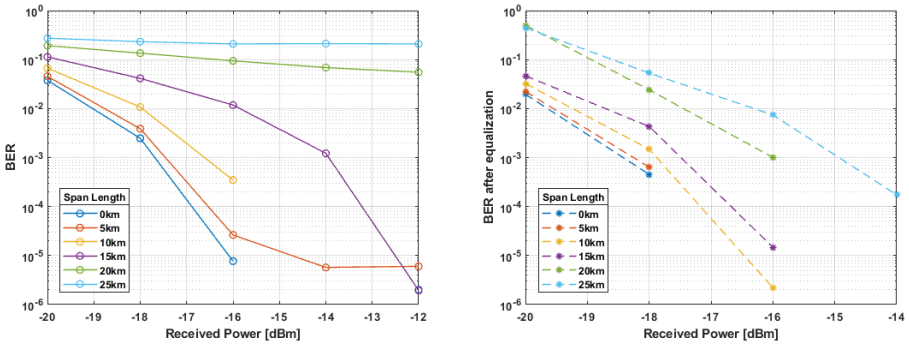

(a) BER without equalization *(b) BER after equalization*

Figure 4.3. Effects of chromatic dispersion on system performance in case of OOK modulation format: BER vs. received power without (a) and with equalization(b) for several fiber span lengths.

varying received powers. Each simulation of the selected mode number has been repeated by increasing the span length of 5 km, looking for the maximum reachable distance. Figure 4.5 shows an example of the obtained BER curves in the case of $A+C+E$ over 5 km span length. Each plot reports performance of each propagating group without equalization. As expected, according Table 4.1, group C has worst BER because it accumulates more crosstalk than others. However, in the case of OOK, BER results are pretty equal to which obtained for one mode. Instead, 4-PAM shows a worse deterioration due to the presence of crosstalk.

Always in the case of $A + C + E$: Figure 4.6 shows BER curves of only group C increasing the span length from 0 km to 20 km with OOK modulation. When distances are increased, performance decreases. In this case, for example, it is possible to reach a $BER = 3.8 \cdot 10^{-3}$ by propagating for at most 15 km. In addition, the power required to obtain this target BER increases in function of distances: -17.5 dBm and $-13dBm$ for 5 km and 15 km span lengths, respectively.

Figure 4.7 shows how OOK performance changes by increasing the number of propagating modes in the case of 5 km span length. Curves always refer to the mode with the worst total crosstalk within the reported combination. As it is possible to see, fixing the number of modes and the traveled distance, the use of the equalizer can improve performance. However, the DFE does not work well when the level accumulated crosstalk is too high and the received power is too low (see $A + B + D + E$ case). In all other cases, it is able to improve performance by almost an order of magnitude.

All these results have been elaborated and represented in terms of spectral

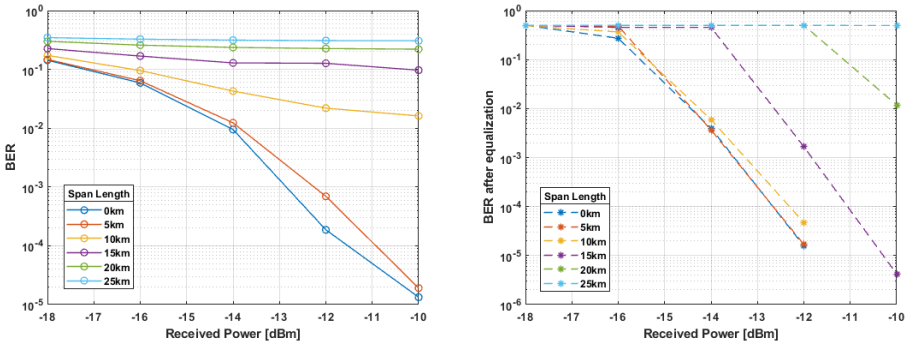

(a) BER without equalizer *(b) BER with equalization*

Figure 4.4. Effects of chromatic dispersion on system performance in case of 4-PAM modulation format: BER vs. received power without (a) and with DFE (b) for several span lengths.

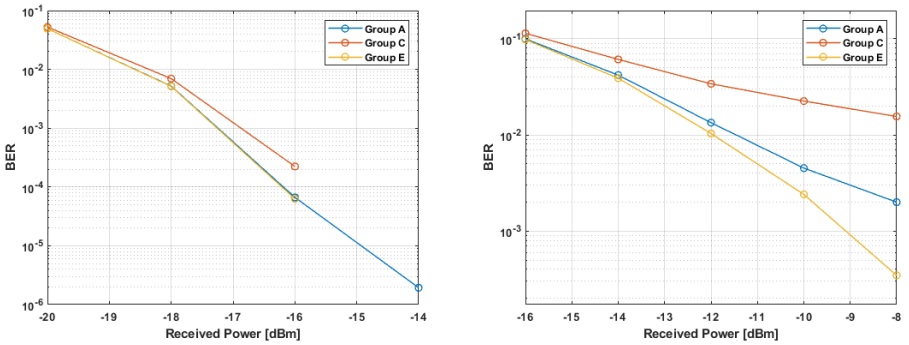

(a) BER with OOK *(b) BER with 4-PAM*

Figure 4.5. BER vs. received power with OOK (a) and 4-PAM (b) modulation format in case of co-propagation of $A - C - E$ groups over $5km$.

efficiency (Figure 4.8) and maximum achievable capacity (Figure 4.9), both for each wavelength, considering different FEC techniques. In particular, hard-FEC and soft-FEC are able to correct signals with at most $BER = 3.8 \cdot 10^{-3}$ and $BER = 2 \cdot 10^{-2}$, respectively. The former is characterized by 7% of overhead while the latter by 20%. On the one hand, soft-FEC can be typically used to increase transmission distances, but, on the other hand, it causes a slight decrease in the achievable data rates with respect to the traditional hard-FEC. For each WDM channel, in the case of single-mode transmission, the spectral efficiency is 0.5 $(bit/s)/Hz$ with OOK and 1 $(bit/s)/Hz$ with 4-PAM; in case of hard-FEC the net transmission capacity is 26.04 Gb/s with OOK and 52.08 Gb/s with OOK and 4-PAM, respectively; in case of

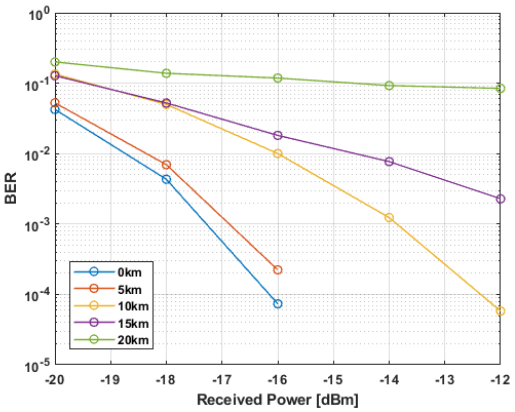

Figure 4.6. $A+C+E$ propagation: BER curves of group C in case of OOK modulation increasing span lengths.

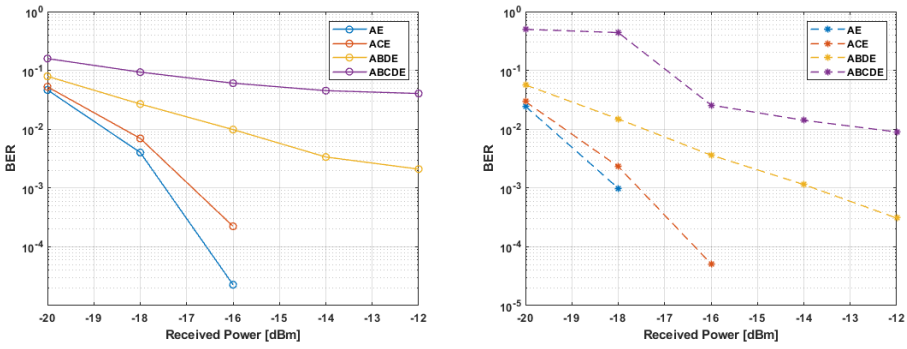

(a) BER without equalizer *(b) BER with equalizer*

Figure 4.7. BER vs. received power with OOK by varying the propagating mode number over $5km$: (a) case without equalizer and (b) case with equalizer.

soft-FEC, it is 22.4 Gb/s with OOK and 44.8 Gb/s with 4-PAM.

In case of very short distances (maximum 15 km):

- hard-FEC: OOK has slightly higher spectral efficiency and transmission capacity than 4-PAM;
- hard-FEC with equalization: 4-PAM has slightly higher spectral efficiency and transmission capacity than OOK;
- soft-FEC: 4-PAM has higher spectral efficiency and transmission capacity than OOK;
- soft-FEC with equalization: 4-PAM has higher spectral efficiency and transmission capacity than OOK;

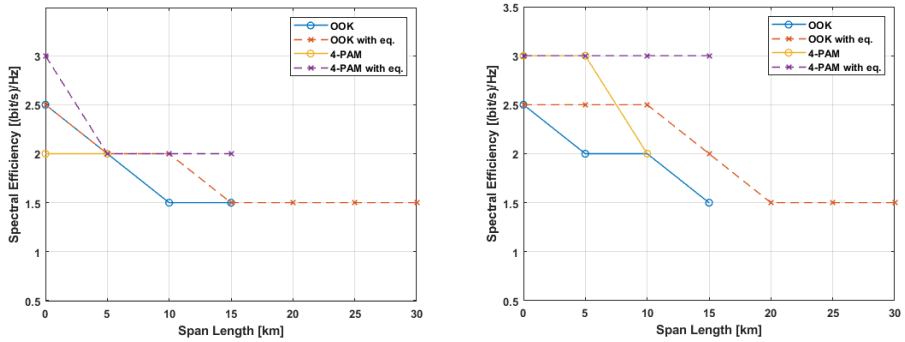

(a) Hard-FEC (b) Soft-FEC

Figure 4.8. Maximum achievable spectral efficiency (for each wavelength channel) vs. span length in case of hard-FEC (a) and soft-FEC (b). All possible simulated solutions are presented: OOK, OOK with eqalizer, 4-PAM and 4-PAM with equalizer.

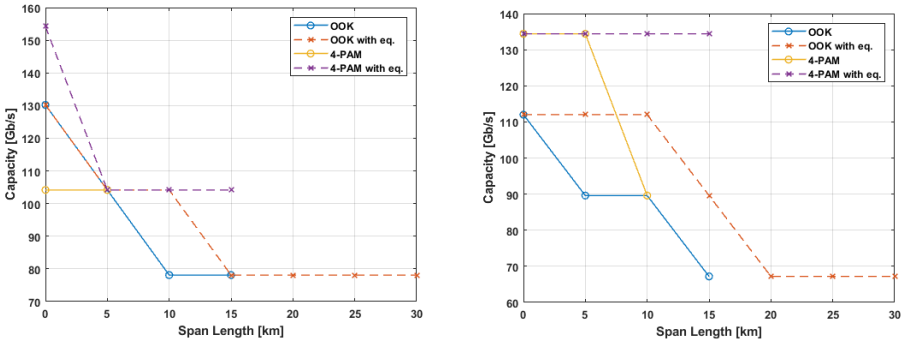

(a) Hard-FEC (b) Soft-FEC

Figure 4.9. Maximum achievable capacity (for each wavelength channel) vs. span length in case of hard-FEC (a) and soft-FEC (b). All possible simulated solutions are presented: OOK, OOK with equalizer, 4-PAM and 4-PAM with equalizer.

In case of distances from 15 km to 30km, multimode propagation is possible only in case of OOK modulation with equalization.

It can be said that the soft-FEC does not allow to reach longer distances due to crosstalk and dispersion limitations. However, it can be exploited to slightly increase system performance with 4-PAM in the case of span lengths from 0 km to 15 km.

In addition, Figure 4.10 shows the limit power values to obtain the maximum capacities in Figure 4.9 for the considered span lengths. More specifically, it shows how much the received power can reduce without losing

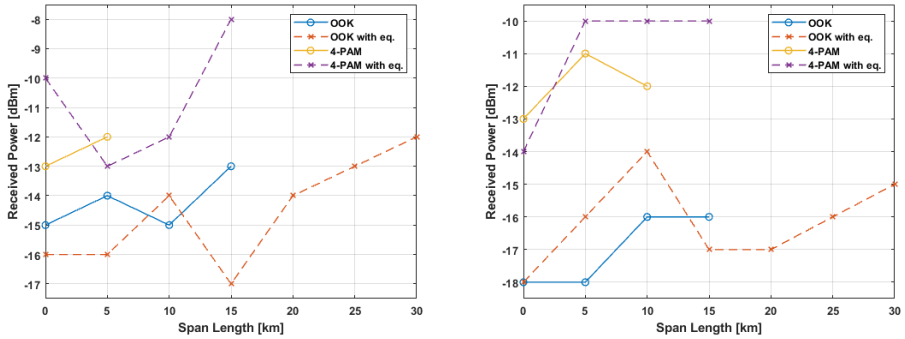

(a) Hard-FEC *(b) Soft-FEC*

Figure 4.10. Limit received power vs. span length in case of hard-FEC (a) and soft-FEC (b). All possible simulated solutions are presented: OOK, OOK with equalizer, 4-PAM and 4-PAM with equalizer.

performance. When capacities are constant, i.e. the number of modes is fixed, the limit on received powers increases. This is due to the fact that more power is required to cover longer distances. As expected, OOK modulation format always requires at least 2 dBm less than 4-PAM. Thus, it can be the right choice in order to reduce power consumption.

Finally, it can be helpful to know the maximum supported crosstalk to reach a given BER. For a fixed power received, BER is measured by varying total crosstalk, accumulated on propagating signal, from -30 dB to -10 dB. The procedure used for this type of simulation is different than before: for each considered value of crosstalk, the BER calculation is repeated for various signal realizations. This choice has been necessary due to the high variability of the results obtained. In fact, the coherent sum of a small number of interfering signals can vary depending on the realization. Figure 4.11 and Figure 4.12 show the case of OOK and 4-PAM, respectively (at -12 dBm). All the obtained BER values are distributed within the corresponding shaded area for each span length. Instead, the marked line is the most probable BER curve. Two different behaviours can be analyzed:

- Results without DFE: the variability of the values increases when the total crosstalk decreases; the range of values obtained is however, very narrow both for OOK and 4-PAM;
- Results with DFE: the variability is high when the total crosstalk is high for the considered modulation; the equalizer in these cases does not always improve performance and does not work correctly;

In general, by increasing the distance traveled, the total accumulated

crosstalk must be lower to get the same BER. For example, in case of OOK without equalization, having $BER = 3.8 \cdot 10^{-3}$ is possible at most with $-14\ dB$ (5 km span) and $-22\ dB$ (15 km span). The 4-PAM modulation requires even less crosstalk to reach the same BER value: at most $-28\ dB$ (5 km span). In addiction, it can be said that equalizer is able to reduce errors caused by crosstalk up to 30 km and 15 km for OOK and 4-PAM, respectively. However, the performance improvement in the case of 4-PAM is lower than OOK due to its higher intrinsic degradation.

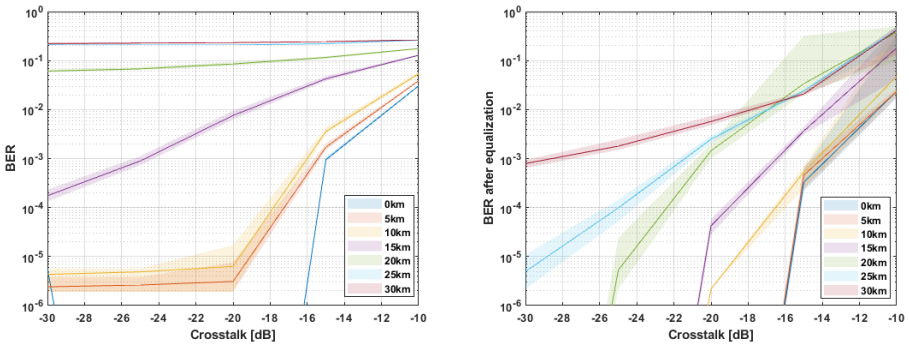

(a) OOK without equalizer *(b) OOK with equalizer*

Figure 4.11. BER vs. crosstalk by varying span length from $0km$ to $30km$ in case of OOK modulation (at $-12dBm$) without equalizer (a) or with equalizer (b).

4.2.3 Results discussion

In summary, MGDM propagation through the 9-LP-mode fiber can be used to increase transmission capacity in short-reach systems. Table 4.2 shows the best combinations of mode groups in terms of transmission capacity for each wavelength channel and maximum achievable distances in the hypothesis of hard-FEC.

In the case of OOK, it's possible to use at most 4 modes, instead, with 4-PAM only 2 modes could propagate together. However, both OOK and 4-PAM allow reaching capacities higher than 100 Gb/s on transmission distances between 0 and 15 km, always exploiting DFE in reception. In fact, the system performance is strongly limited by chromatic dispersion and intermodal crosstalk: the former limits the maximum reachable distances and the latter limits the maximum achievable capacities on a fixed span length. Thus, a DFE equalizer in reception can be useful to compensate for both the effect of dispersion and intermodal crosstalk. On the one hand, it can allow a

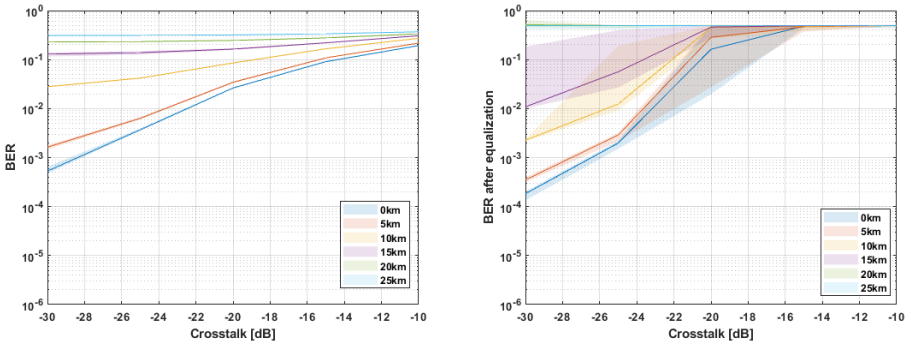

(a) 4-PAM without equalizer *(b) 4-PAM with equalizer*

Figure 4.12. BER vs. crosstalk by varying span length from $0km$ to $30km$ in case of 4-PAM modulation (at $-12dBm$) without equalizer (a) or with equalizer (b).

Mode groups	**Total capacity [Gb/s]**	**Reach [km]**	**DFE**
	OOK		
A+C+E	78.12	15	OFF
A+C+E	78.12	30	ON
A+B+D+E	104.16	5	OFF
A+B+D+E	104.16	10	ON
	4-PAM		
A+E	104.16	5	OFF
A+E	104.16	15	ON

Table 4.2. Total capacity (for each wavelength channel) and maximum reach for different combinations of groups with OOK or 4-PAM modulation in the case of hard-FEC.

higher number of co-propagating modes, i.e. higher capacities, for distances between 0 km to 15 km. On the other hand, it can be exploited to reach 30 km with 70 Gb/s in the case of OOK modulation. Without equalization, a capacity of 100 Gb/s is possible only over very short distances from 0 to 5 km. We have proposed different implementation solutions which can be used to increase the transmission capacity of short-reach point-to-point connections. Depending on the distances to be covered, it is possible to choose the best combination of modes, modulation formats and decide whether to implement an equalizer in reception.

4.2.4 Different implementation of MDM with λ interleaving for short-reach applications

This section is dedicated to a different implementation of the MDM technique to further reduce the overall system cost and complexity. The main idea is to propose a really cheap solution for short-range applications. In particular, the MMUX/ MDMUX can be used to separate signals on different wavelengths to exploit a more straightforward and cheaper WDM-MUX/ DEMUX.

4.2.4.1 Simulation set-up

A graphic representation of the system architecture is depicted in Figure 4.13.

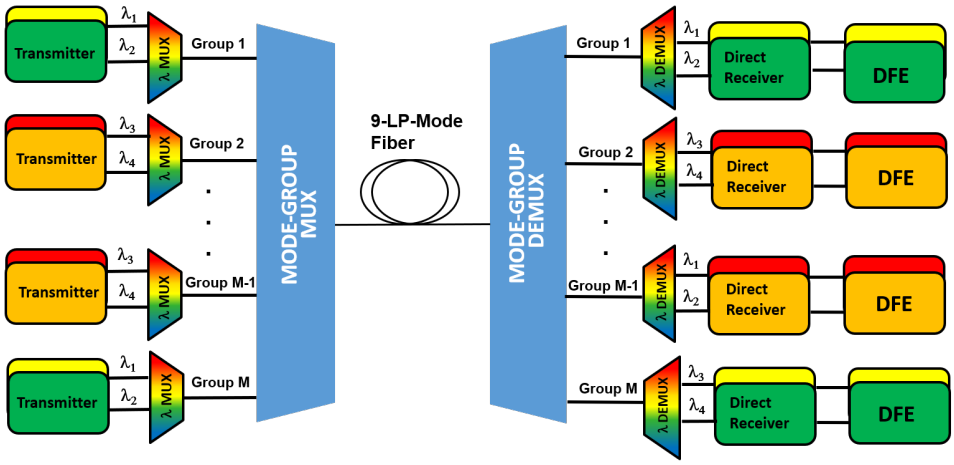

Figure 4.13. Schematic representation of short-range communication system architecture with mode groups on different wavelengths. At transmitter side: λ-MUX to combine wavelength channels, mode-group MUX to combine each supported groups. Transmission line: 9-LP-mode fiber span. Receiver side: mode-group DEMUX to divide each supported mode, λ-DEMUX to divide each wavelength channel, direct receiver and a potential implementation of a DFE equalizer.

The blocks of the presented structure are the same as the previous section, what changes is the use of WDM and MDM techniques. As it is possible to see, each group cannot put on the same wavelength channel. Different solutions have been investigated:

- Considering each group on different wavelength channels. In this way MDM is totally inefficient;

- Considering at least two or three groups on the same wavelength in order to increase system efficiency exploiting modes;

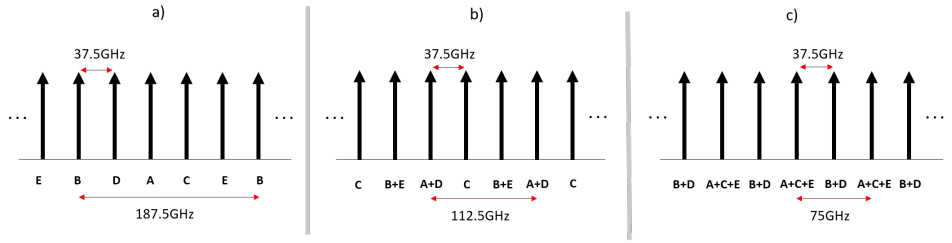

Figure 4.14. Three configurations implemented: a) Each supported group on a different wavelength; b) groups A, D together on the same wavelength channel and the same for groups B, E; c) group A, C, E multiplexed on the same wavelength channel and the same for groups B and D. The WDM spacing on each group is 187.5, 112.5 *and* $75GHz$*, respectively.*

In particular, we have considered a 37.5 GHz WDM channel spacing. Figure 4.14 shows the three cases of study:

a) Each supported group is on a different wavelength, so that WDM is spaced on each group by 187.5 GHz;

b) Groups A and D are together on the same wavelength channel. The same for groups B and E. Instead, Group C is alone. This solution supports a WDM channel spaced by 112.5 GHz;

c) Groups A, C and E are multiplexed on the same wavelength channel. The same for groups B and D. This can lead to WDM channel spaced by 75 GHz;

The WDM channel spacing obtained on each group with these three configurations allows to use more common AWGs than those 37.5 GHz spaced. For the first two options, a 100 GHz WDM MUX/ DEMUX is enough. Instead, the last one needs at least 50 GHz spacing. This two technologies are simulated applying a simple Gaussian filter with 100 GHz and 50 GHz width, respectively.

All others parameters and simulation assumptions are the same as before except for the roll-off value. In order to guarantee a symbol rate of 28 *Gbaud* with small wavelength crosstalk, we decide to fix roll-off equal to 0.34; this is the first value which does not allow overlapping channels.

Each simulation is done by considering each propagating mode centered in frequency $f = 0$ and interfering signals (on different mode and wavelength) with its proper interference power opportunely shifted in frequency.

4.2.4.2 Simulation results

The first step has been to evaluate the effect of dispersion on system performance, in the case of one propagating mode on a single channel and with the new roll-off value. Figure 4.15 and Figure 4.16 show the capabilities in terms of BER vs. received power by varying the span length in the case of OOK and 4-PAM modulation formats, respectively. The considered received powers vary from $-20\ dBm$ to $-12\ dBm$ for OOK and from $-16\ dBm$ to $-8\ dBm$ for 4-PAM. As expected, the obtained results are slightly worse than the case with roll-off equal to 1 reported in Figures 4.3 and 4.4. However, without equalization, dispersion limits the reachable distances at 15 km with OOK and 5 km with 4-PAM.

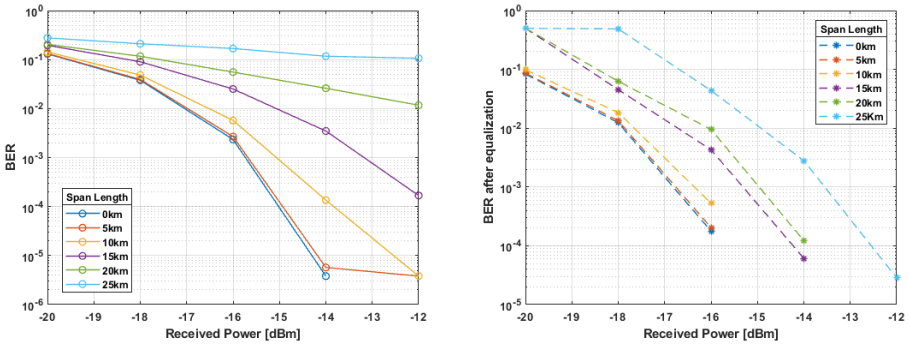

(a) BER without equalization *(b) BER after equalization*

Figure 4.15. Effects of chromatic dispersion on system performance in case of OOK modulation format and roll-off equal to 0.34*: BER vs. received power without (a) and with equalization (b) for several fiber span lengths.*

In a second step, we simulate the propagation of each mode group on a different wavelength channel with the modes configuration (a) proposed in Figure 4.14. In particular, Figure 4.17 shows the spectrum of the received signal on mode A before and after the 100 GHz filter.

The reference signal A is centred at frequency 0 while interfering signals are positioned at $+/-37.5\ GHz$ and $+/-75\ GHz$. Interfering signals that are at greater frequency distances have been neglected. As it is possible to see, the selected combination allows having modes with higher interfering power at 75 GHz distance from the reference signal so that, after filtering, their impact can be reduced. The effects of intermodal crosstalk are limited to modes on closest wavelengths. Because the interfering power of the closest modes is quite low, the obtained performance for each channel are very well equalized. Figures 4.18 shows the BER curves of the worst-mode by increasing

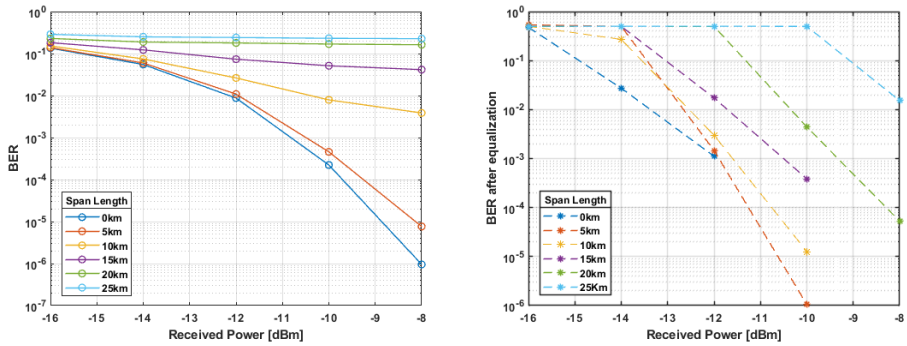

(a) BER without equalizer *(b) BER with equalization*

Figure 4.16. Effects of chromatic dispersion on system performance in case of 4-PAM modulation format and roll-off equal to 0.34*: BER vs. received power without (a) and with DFE (b) for several span lengths.*

the span lengths for OOK and 4-PAM cases. Comparing the obtained results with those shown in Figures 4.15 and 4.16, it can be said that the effect of intermodal crosstalk is practically null, i.e. the reachable distances are mainly limited by dispersion effect. The same simulations have also been done in the case of equalization. Table 4.3 summarizes the maximum reach with the hypothesis of hard-FEC or soft-FEC.

In these first simulations, as already mentioned, the single-channel gross transmission capacity remains equal to 28 Gb/s with OOK and 56 Gb/s with 4-PAM for each wavelength channel. Thus, to exploit the potentialities of MDM propagation, we have tried to increase the number of modes on a single wavelength.

We have analyzed the configurations (b) and (c) in Figure 4.14. Before reporting the obtained results for these particular cases, it can be useful to see the maximum reach with the combinations $A + D$, $B + E$, $B + D$ and $A + C + E$ without the interfering WDM channels. Table 4.4 summarizes the performances for the combinations $B + E$ and $A + C + E$ with hard/soft-FEC and with/without DFE. These results should be considered as a reference to evaluate how adjacent WDM channels affect the achivable performance. As it can be noted, the effect of intermodal crosstalk between modes on the same wavelength channel has a greater impact on 4-PAM modulation results. The signals are strongly degraded, and, therefore, it is almost impossible to reach distances with $BER = 3.8 \cdot 10^{-3}$.

A@λ C@λ+37.5GHz D@λ-37.5GHz E@λ+75GHz B@λ-75.5GHz		
Reach [km]	**FEC**	**DFE**
OOK		
15	Hard	OFF
20	Soft	OFF
30	Hard	ON
35	Soft	ON
4-PAM		
5	Hard	OFF
10	Soft	OFF
20	Hard	ON
25	Soft	ON

Table 4.3. Maximum reach obtained (with $R_s = 28Gbaud$ for each wavelength channel) with one mode for each channel wavelength with the hypothesis of hard-FEC or soft-FEC. All simulated cases are reported: OOK, OOK with equalization, 4-PAM and 4-PAM with equalization.

B+E@λ		
Reach [km]	**FEC**	**DFE**
OOK		
15	Hard	OFF
20	Soft	OFF
20	Hard	ON
30	Soft	ON
4-PAM		
5	Soft	OFF
10	Hard	ON
10	Soft	ON

A+C+E@λ		
Reach [km]	**FEC**	**DFE**
OOK		
10	Hard	OFF
15	Soft	OFF
15	Hard	ON
20	Soft	ON
4-PAM		
5	Soft	ON

Table 4.4. Maximum reach obtained (with $R_s = 28Gbaud$ for each wavelength channel) for the cases B+E (on the top) and A+C+E (on the bottom) without interfering WDM channels with the hypothesis hard/soft-FEC and with/without DFE.

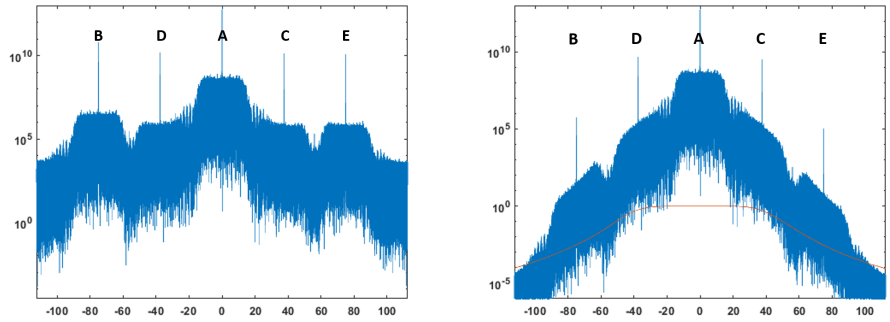

(a) (b)

Figure 4.17. Optical spectrum of the received signal before (a) and after (b) the Gaussian filter. Group A (reference signal) is centered in $f = 0$ and the interfering signals are: C at $\lambda + 37.5GHz$, D at $\lambda - 37.5GHz$, E at $\lambda + 75GHz$ and B at $\lambda - 75GHz$. The red line in figure (b) represents the shape of the $100GHz$ Gaussian filter.

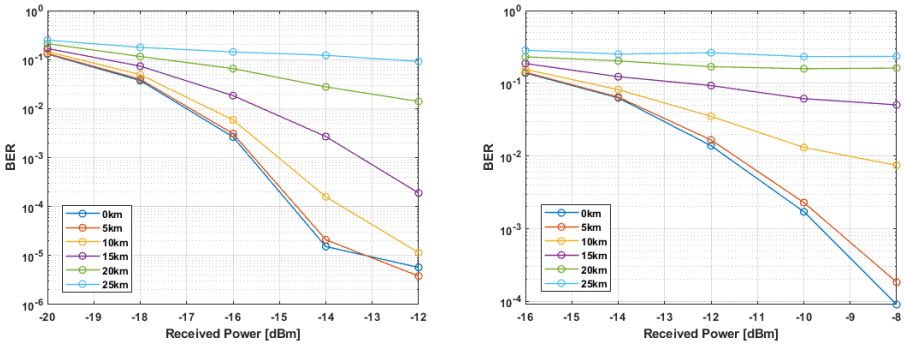

(a) BER with OOK (b) BER with 4-PAM

Figure 4.18. BER vs. received power with OOK (a) and 4-PAM (b) modulation format in case of each mode on a different wavelength (the worst-mode BER curves respectively over each distance have been reported).

As before, Figure 4.19 and Figure 4.20 show the optical spectrum of the reference signal A in the configurations (b) and (c) reported in Figure 4.14.

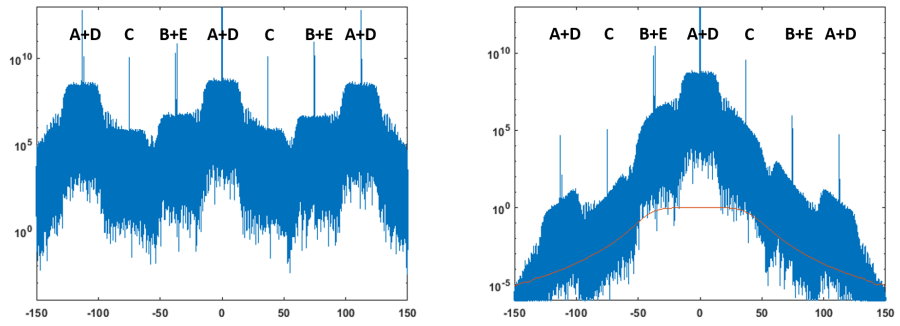

Figure 4.19. Optical spectrum of the received signal before (a) and after (b) the Gaussian filter. Group A (reference signal) is centered in $f = 0$ and the interfering signals are: D at the same frequency of A, C at $\lambda + 37.5GHz$, $B + E$ at $\lambda - 37.5GHz$, $B + E$ at $\lambda + 75GHz$, C at $\lambda - 75GHz$, $A + D$ at $\lambda - 112.5GHz$ and $A + D$ at $\lambda - 112.5GHz$. The red line in figure (b) represents the shape of the $100GHz$ Gaussian filter.

For the first case, a 100 GHz filter is still sufficient to limit the crosstalk caused by the same mode on a wavelength distant 112.5 GHz. For the second one, instead, it is necessary to use an 50 GHz AWG since the WDM spacing on each group is only 75 GHz. As shown, these simulations are made considering adjacent channels up to the wavelengths carrying the same mode as the reference signal. In fact, Figure 4.19 shows peaks at $+/-112.5\ GHz$ with the same power of the signal centered in $f = 0$. Similarly, Figure 4.20 exhibits these peaks at $+/-75\ GHz$.

Following the same procedure of the the previous simulations, we have been evaluated the maximum reach for OOK and 4-PAM modulation formats with or without the presence of the DFE equalizer. Table 4.5 and Table 4.6 summarizes the maximum reachable distances for the two analyzed configurations. If we compare the results with the single-channel cases reported in 4.4, it can be noticed that obtained values are almost identical. Thus, it is possible to affirm that, also in these cases, the 100 GHz and 50 GHz filters respectively, may be enough to separate WDM channels without additional intermodal crosstalk due to modes on closest wavelengths. These two configurations differ, in terms of reachable distances, only in the case of equalization: a maximum reach of 30 km with $A + D$, C, $B + E$ and up to 20 km with $A + C + E$, $B + D$.

A+D@λ C@λ+37.5GHz E+B@λ-37.5GHz		
Reach [km]	**FEC**	**DFE**
	OOK	
10	Hard	OFF
15	Soft	OFF
20	Hard	ON
30	Soft	ON
	4-PAM	
10	Soft	ON

Table 4.5. Maximum reach obtained (with $R_s = 28Gbaud$ for each wavelength channel) with A+D, C and B+E on different wavelength channels with the hypothesis of hard-FEC or soft-FEC. All simulated cases are reported: OOK, OOK with equalization, 4-PAM and 4-PAM with equalization.

A+C+E@λ B+D@λ+37.5GHz		
Reach [km]	**FEC**	**DFE**
	OOK	
10	Hard	OFF
15	Soft	OFF
15	Hard	ON
20	Soft	ON
	4-PAM	
5	Soft	ON

Table 4.6. Maximum reach obtained (with $R_s = 28Gbaud$ for each wavelength channel) with A+C+E and B+D on different wavelength channels with the hypothesis of hard-FEC or soft-FEC. All simulated cases are reported: OOK, OOK with equalization, 4-PAM and 4-PAM with equalization.

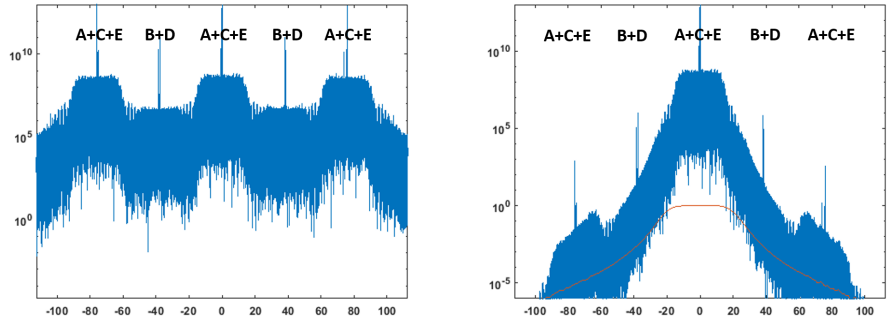

(a) (b)

Figure 4.20. Optical spectrum of the received signal before (a) and after (b) the Gaussian filter. Group A (reference signal) is centered in $f = 0$ and the interfering signals are: $C + E$ at the same frequency of A, $B + D$ at $\lambda + 37.5GHz$, $B + D$ at $\lambda - 37.5GHz$, $A + C + E$ at $\lambda + 75GHz$ and $A + C + E$ at $\lambda - 75GHz$. The red line in figure (b) represents the shape of the $50GHz$ Gaussian filter.

4.2.4.3 Results discussion

We have proposed three possible solutions, summarized in 4.7, that can be implemented in short-reach applications to reduce system costs according to the network requirements. The results reported are in the case of hard-FEC. As we have seen, the performance are mainly limited by chromatic dispersion and intermodal crosstalk between modes on the same wavelength channel. In fact, the presence of modes on adjacent channels slightly decreases the covered distances.

In particular, the first configuration with all modes on different wavelengths allows to reach 15 km without equalization. Instead, the last two configurations can be used to cover shorter distances, up to 10 km without equalization, but leading an improvement in system spectral efficiency. If we consider as reference the spectral efficiency of the configuration (a) in Figure 4.14, which is equal to $\frac{28\ Gbit/s}{37.5GHz}$ with OOK and $\frac{56\ Gbit/s}{37.5GHz}$ with 4-PAM, it can be incremented by a factor $5/3 = 1.67$ (in the case of $A + D$,C,$B + E$ where the WDM channel spacing for each group is 112.5 GHz) and $5/2 = 2.5$ (in the case of $A + C + E$ and $B + D$ where the WDM channel spacing for each group is 75 GHz). On the other hand, they can be used only with OOK due to high degradation of 4-PAM modulation format.

At the end, we can said that the reported configurations exploiting wavelength interleaving between groups can be promising solutions to design point-to-point short-reach interconnection with simpler and cheaper optical

MDM with λ-interleaving (hard-FEC)				
Mode groups	**Reach [km]**	**Spectral efficiency increment**	**AWG width [GHz]**	**DFE**
OOK				
A@λ C@λ+37.5GHz D@λ-37.5GHz E@λ+75GHz B@λ-75GHz	15	-	100	OFF
A@1 C@λ+37.5GHz D@λ-37.5GHz E@λ+75GHz B@λ-75GHz	20	-	100	ON
A+D@λ C@λ+37.5GHz B+E@λ-37.5GHz	10	5/3	100	OFF
A+D@λ C@λ+37.5GHz B+E@λ-37.5GHz	20	5/3	100	ON
A+C+E@λ B+D@λ+37.5GHz	10	5/2	50	OFF
A+C+E@λ B+D@λ+37.5GHz	15	5/2	50	ON
4-PAM				
A@λ C@λ+37.5GHz D@λ-37.5GHz E@λ+75GHz B@λ-75GHz	5	-	100	OFF
A@1 C@λ+37.5GHz D@λ-37.5GHz E@λ+75GHz B@λ-75GHz	20	-	100	ON

Table 4.7. Maximum reach obtained (with $R_s = 28Gbaud$ for each wavelength channel) with all studied cases of MDM with λ-interleaving (hard-FEC). The use of DFE, the increment in spectral efficiency and the AWG width are specified.

components: the required AWG at 37.5 GHz spaced in case of typical MDM can substitute with more common 100 GHz or 50 GHz filters according to the selected configuration. In specific, the case of $A+D$,C,$B+E$ (on different wavelengths) and the case of $A+C+E$,$B+D$ (on different wavelengths) could be a right trade-off between cost and efficiency of the system guaranteeing a 28 *Gbaud* transmission for each wavelength channel.

Conclusions

This thesis has studied the possible implementation of a MDM transmission system exploiting an innovative graded-index FMF that supports a total of 15 spatial modes, i.e. 9 LP modes. In particular, we have considered the propagation of the 5 supported mode groups as independent transmission channels to propose high-capacity solutions with low system complexity. Two different scenarios have been investigated: long-medium haul communication systems and short-reach applications.

We have firstly focused on medium-long haul transmission distances, in which MDM propagation is combined with the use of coherent detection. Thus, there is the possibility of exploiting PDM transmission in conjunction with WDM and MDM. To reduce the complexity of the ideal 30x30 MIMO equalizer necessary in case of full-MIMO approach, MGDM is adopted in order to support simpler MIMO DSP receivers for each supported modes group. This choice leads to additional limitations due to intermodal crosstalk between modes belonging to different groups.

An analytical simulator has been used to evaluate the real influence of the two crosstalk contributions on system performance: in-fiber contribution accumulated during propagation of multiple modes in the same fiber core and the contribution due to the presence of MMUX/MDMUX necessary at the transmitter, at the receiver and also in possible crossed nodes. This analysis shows the capabilities of MGDM in terms of reachable distances and maximum achievable capacities considering initially a span length typical of long-haul (80 km) and with high-speed modulation formats (4-QAM, 16-QAM and 64-QAM). We have noticed that only combinations with non first neighbouring groups can allow to reach at least the length of a span in a point-to-point connection with only MMUX at the transmitter and MDMUX at the receiver. Then, we have been analyzed the performance trend increasing the number of nodes at the end of each propagating span. When intermodal propagation crosstalk is totally negligible, the covered distances decrease linearly; otherwise the performance remain fairly constant

but always reaching shorter distances than previous cases. However, we have proposed different groups combinations ($A+D$, $A+E$, $B+E$) which allow to reach more than 500 Gb/s and 1 Tb/s per wavelength channel with 4-QAM and 16-QAM, respectively. With these combinations, it is possible to reach hundreds of kilometers both in the case of a point-to-point connection or a full-mesh network.

Finally, in support of FIRST project, maximum achievable capacities on some testable field trials in L'Aquila city have been evidenced. In particular, we have focused on 6 km and 16 km span lengths. Also in these particular cases, the usable combinations of groups to reach at least one span length are limited to modes with negligible propagation crosstalk. In a point-to-point network, the maximum achievable distances with $A + D$, $A + E$ and $B + E$ are higher than the 80 km span case; instead, in a full-mesh scenario, the distance covered are quite lower due to a higher number of crossed nodes. However, also in this case, tens of kilometers can be covered with more than 500 Gb/s and 1 Tb/s per wavelength channel with 4-QAM and 16-QAM, respectively.

In particular, among all the presented results, $A+D$ is the most promising solution which allows a right trade-off between high transmission capacity and low system complexity.

As second step, we have studied a possible implementation of MGDM transmission through the 9-LP-mode fiber for short-range applications. Here, we refer to point-to-point connections for communications inter and intra-datacenter.

In this scenario, simpler optical components have been considered: simple modulation formats such as OOK and 4-PAM, direct detection instead the coherent one, and a possible use of the DFE equalizer. Due to the lack of DSP at the receiver, only one mode for each supported group in a single polarization can be exploited to enhance system performance.

The capabilities have been evaluated in terms of BER by varying the received power for a different number of modes selecting the best combinations in terms MMUX/MDMUX crosstalk which has more impact than propagation crosstalk due to short transmission distances.

Depending on the distances to be covered and the capacities to be reached, it is possible to choose the best modulation format by implementing or not equalization in reception. As shown, DFE allows increasing the potential of the MDM system both with OOK and 4-PAM. In general, with equalization, 4-PAM results to achieve capacities of 100 Gb/s per wavelength over 15 km distances. On the other hand, OOK requires less power consumption and covers span lengths up to 30 km with 70 Gb/s per wavelength. However, it

can be said that MDM transmission results to be a promising solution over short distances: it's possible to cover up to 15 km reaching a transmission capacity of at least 100 Gb/s per wavelength, by exploiting low-cost optical components.

In the end, always in the context of short-range applications, we have tried to exploit MGDM to further reduce the cost of implemented optical elements: each group is put on a different wavelength reducing the WDM channel spacing. As a consequence, the possibility of implementing a simpler AWG is presented. Some simulations are reported pointing out system capabilities with a standard filter at 100 GHz. In order to limit intermodal crosstalk, each first neighbouring group is spaced at least twice the distance between wavelengths. In this case, MGDM cannot improve the transmission capacity, so the potentialities of this solution are presented in terms of maximum achievable distances. As shown, the only limiting factor is the chromatic dispersion. In fact, the width of the implemented filter is sufficient to eliminate the crosstalk effect between modes on different wavelengths.

In a second step, we have tried to increase system efficiency by adding one more group on the same wavelength. However, this second possibility sees a worsening of performance due to a greater incidence of intermodal crosstalk of modes on the same wavelength channel. However, this can be considered a very low-cost solution that allows increasing the spectral efficiency by a factor 5/3 and 5/2 implementing standard AWG at 100 GHz or 50 GHz, respectively, and reaching about 15 km without equalization.

In the future, all the obtained results could be experimentally verified in laboratory or, in the case of long-medium haul transmission systems, even by field trials in the already available MDM network in L'Aquila city.

Bibliography

[1] Allan W. Snyder and William R. Young. "Modes of optical waveguides". In: *J. Opt. Soc. Am.* 68.3 (Mar. 1978), pp. 297–309.

[2] D. Gloge. "Weakly Guiding Fibers". In: *Appl. Opt.* 10.10 (Oct. 1971), pp. 2252–2258.

[3] P. M. Morse and H. Feshbach. *Methods of Theoretical Physics, Part I.* New York: McGraw-Hill, 1953, p. 116.

[4] R. B. Adler. "Waves on Inhomogeneous Cylindrical Structures". In: *Proceedings of the IRE* 40.3 (1952), pp. 339–348.

[5] A. W. Snyder and J. D. Love. *Optical waveguide theory.* London: Wiley, Chapman, and Hall, 1983.

[6] A. W. Snyder. "Asymptotic Expressions for Eigenfunctions and Eigenvalues of a Dielectric or Optical Waveguide". In: *IEEE Transactions on Microwave Theory and Techniques* 17.12 (1969), pp. 1130–1138.

[7] N. S. Kapany and J. J. Burke. *Optical Waveguides.* New York: Academic, 1972.

[8] D. Marcuse. *Light Transmission Optics.* Princeton: Van Nostrand Reinhold, 1972.

[9] E. Snitzer and H. Osterberg. "Observed Dielectric Waveguide Modes in the Visible Spectrum∗". In: *J. Opt. Soc. Am.* 51.5 (May 1961), pp. 499–505.

[10] Clemens Koebele. "Mode-division-multiplexing as a possibility to cope with the increasing capacity demand in optical transmission systems". Theses. Institut National des Télécommunications, June 2012. URL: `https://tel.archives-ouvertes.fr/tel-00762642`.

[11] P. J. Winzer et al. "Penalties from in-band crosstalk for advanced optical modulation formats". In: *2011 37th European Conference and Exhibition on Optical Communication.* 2011, pp. 1–3.

[12] C. Koebele et al. “Nonlinear Effects in Mode-Division-Multiplexed Transmission Over Few-Mode Optical Fiber”. In: *IEEE Photonics Technology Letters* 23.18 (2011), pp. 1316–1318.

[13] B. Franz and H. Bulow. “Experimental Evaluation of Principal Mode Groups as High-Speed Transmission Channels in Spatial Multiplex Systems”. In: *IEEE Photonics Technology Letters* 24.16 (2012), pp. 1363–1365.

[14] P. Sillard et al. “Low-Differential-Mode-Group-Delay 9-LP-Mode Fiber”. In: *Journal of Lightwave Technology* 34.2 (2016), pp. 425–430.

[15] Y. Yung et al. “First demonstration of multimode amplifier for spatial division multiplexed transmission systems”. In: *2011 37th European Conference and Exhibition on Optical Communication*. 2011, pp. 1–3.

[16] Roland Ryf et al. “Mode-Equalized Distributed Raman Amplification in 137-km Few-Mode Fiber”. In: (Sept. 2011).

[17] Peter M. Krummrich. “Optical amplification and optical filter based signal processing for cost and energy efficient spatial multiplexing”. In: *Opt. Express* 19.17 (Aug. 2011), pp. 16636–16652.

[18] S. O. Arik, J. M. Kahn, and K. Ho. “MIMO Signal Processing for Mode-Division Multiplexing: An overview of channel models and signal processing architectures”. In: *IEEE Signal Processing Magazine* 31.2 (2014), pp. 25–34.

[19] P. Sillard, M. Bigot-Astruc, and D. Molin. “Few-Mode Fibers for Mode-Division-Multiplexed Systems”. In: *Journal of Lightwave Technology* 32.16 (2014), pp. 2824–2829.

[20] H. Liu et al. “Reducing group delay spread in a 9-LP mode FMF using uniform long-period gratings”. In: *2017 Optical Fiber Communications Conference and Exhibition (OFC)*. 2017, pp. 1–3.

[21] D. Marcuse. *Theory of dielectric optical waveguides*. 2nd ed. New York: Academic Press, 1991.

[22] D. Gloge. “Optical power flow in multimode fibers”. In: *The Bell System Technical Journal* 51.8 (1972), pp. 1767–1783.

[23] Robert Olshansky. “Mode Coupling Effects in Graded-Index Optical Fibers”. In: *Appl. Opt.* 14.4 (Apr. 1975), pp. 935–945.

[24] Emmanuel Perrey-Debain, Ian Abrahams, and John Love. “A continuous model for mode mixing in graded-index multimode fibres with random imperfections”. In: *Proceedings of The Royal Society A: Mathematical, Physical and Engineering Sciences* 464 (Apr. 2008).

[25] M. Salsi et al. “Mode division multiplexed transmission with a weakly-coupled few-mode fiber”. In: *OFC/NFOEC*. 2012, pp. 1–3.

[26] Pierre Sillard. “Few-Mode Fibers for Space Division Multiplexing”. In: Jan. 2016, Th1J.1. DOI: 10.1364/OFC.2016.Th1J.1.

[27] P. Genevaux et al. “Comparison of QPSK and 8-QAM in a Three Spatial Modes Transmission”. In: *IEEE Photonics Technology Letters* 26.4 (2014), pp. 414–417.

[28] Haoshuo Chen et al. “Integrated Mode Group Division Multiplexer and Demultiplexer Based on 2-Dimensional Vertical Grating Couplers”. In: *European Conference and Exhibition on Optical Communication*. Optical Society of America, 2012, Th.1.B.2.

[29] N. K. Fontaine et al. “Mode-selective dissimilar fiber photonic-lantern spatial multiplexers for few-mode fiber”. In: *39th European Conference and Exhibition on Optical Communication (ECOC 2013)*. 2013, pp. 1–3.

[30] Sergio G. Leon-Saval et al. “Mode-selective photonic lanterns for space-division multiplexing”. In: *Opt. Express* 22.1 (Jan. 2014), pp. 1036–1044.

[31] Guillaume Labroille et al. “Efficient and mode selective spatial mode multiplexer based on multi-plane light conversion”. In: *Opt. Express* 22.13 (June 2014), pp. 15599–15607.

[32] Jean-François Morizur et al. “Programmable unitary spatial mode manipulation”. In: *J. Opt. Soc. Am. A* 27.11 (Nov. 2010), pp. 2524–2531.

[33] N. Barré et al. “Broadband, mode-selective 15-mode multiplexer based on multi-plane light conversion”. In: *2017 Optical Fiber Communications Conference and Exhibition (OFC)* (2017), pp. 1–3.

[34] Andrea Carena et al. “Statistical Characterization of PM-QPSK Signals after Propagation in Uncompensated Fiber Links”. In: Oct. 2010, pp. 1–3.

[35] P. Poggiolini. “The GN Model of Non-Linear Propagation in Uncompensated Coherent Optical Systems”. In: *Journal of Lightwave Technology* 30.24 (2012), pp. 3857–3879.

[36] A. Carena et al. “Modeling of the Impact of Nonlinear Propagation Effects in Uncompensated Optical Coherent Transmission Links”. In: *Journal of Lightwave Technology* 30.10 (2012), pp. 1524–1539.

[37] P. Martelli and P. Boffi. “Crosstalk-Induced Penalty in Coherent Space-Division Multiplexing Transmission”. In: *2018 20th International Conference on Transparent Optical Networks (ICTON)*. 2018, pp. 1–4.

[38] P. Serena. “Nonlinear Signal–Noise Interaction in Optical Links With Nonlinear Equalization”. In: *Journal of Lightwave Technology* 34.6 (2016), pp. 1476–1483.

[39] Dongweon Yoon, Kyongkuk Cho, and Jinsock Lee. “Bit error probability of M-ary quadrature amplitude modulation”. In: *Vehicular Technology Conference Fall 2000. IEEE VTS Fall VTC2000. 52nd Vehicular Technology Conference (Cat. No.00CH37152)*. Vol. 5. 2000, 2422–2427 vol.5.

[40] Silvia Biazzi. “Analysis of the capabilities of DMT modulation in VCSEL-based metropolitan area network”. Theses. Politecnico di Milano, 2018/2019.

[41] Mathworks. *Adaptive equalizers*. Documentation. 2019. URL: `https://it.mathworks.com/help/releases/R2019a/comm/ug/adaptive-equalizers.html`.